/
Article / Book Information

( )	
Title(English)	Effect of chemical additives and electrode modification on carrier behavior in organic solar cells studied by using spectroscopic technique
( )	ALROUGY Ibrahim Mohammed
Author(English)	Ibrahim Mohammed Alrougy
( )	: , : , : 12035 , :2021 6 30 , : , : , , , ,Shyam Sudhir Pandey
Citation(English)	Degree:Doctor (Engineering), Conferring organization: Tokyo Institute of Technology, Report number: 12035 , Conferred date:2021/6/30, Degree Type:Course doctor, Examiner:,,,,,
( )	
Type(English)	Doctoral Thesis

Effect of chemical additives and electrode modification on carrier behavior in organic solar cells studied by using spectroscopic technique.

A Doctoral Thesis Presented by

Ibrahim Alrougy

Supervisor: Prof. Takaaki Manaka

Department of Electrical and Electronic Engineering,

School of Engineering,

Tokyo Institute of Technology

2020

Preface

The recent research focuses on improving the solar cell devices and especially organic solar cells (OSCs) via improving new techniques to guarantee high performance of this technology. As a result, the organic solar cells (OSCs) have been rapidly developed and approved. This in turn would interpret the progressive interest of analyzing the carrier behaviors and the prospected influence on the total performance. However, a detailed investigation of the carrier behaviors in bulk heterojunction (BHJ) has not been yet outlined. In other words, there is still an ambiguity of the carrier behaviors in BHJ and their role on improving the performance of OSCs is not thoroughly outlined in the open literature. This research comes to resolve this challenge. Therefore, a critical evaluation of the effects of chemical additives and electrode modification on carrier behaviors in BHJ films has been conducted. For the first time, this research entails a new methods of carrier behaviors of the electric-field-induced optical second-harmonic generation (EFISHG) measurement within laser wavelength of 1000 nm and 1080 nm to analyze the carrier behaviors. The current experimental research presented the prosperous of EFISHG measurements to modelling and analyze the carrier behaviors that effectively promote the performance of organic solar cells.

Table of Contents

Acknowledgements

List of Publications and Conference Presentations

Chapter 1
1 Overview

1.1 Introduction

Broadly speaking, there is a progressive demand of energy supply in the 21st century due to an exponential incline of population that noticed an increase from 1.5 to 7.3 billion for the last 100 years. In this regard, a noticeable depletion of the conventional sources of energy such as coal, oil and nature gas was pointed out. However, the massive consuming of fossil fuels causes a, serious emission pollutions that particularly one of the most challenges in several areas around the world such as China and India. These countries characterise by their high r population and speedy industry, and therefore it is fair to expect that pollution would passively impact the ecosystem and whole globe. Therefore, there was an intensive research to find alternative sources of energy. More specifically, the alarm of oil depletion encourages the evolution of solar cell technology for industrial and popular. Among all the developed technologies, solar cell is the most efficient developed one.

It has been confirmed that the average absorbed value of solar energy by land and water bodies suppress the total human energy consumption by more than 10,000. Therefore, the improvement of high-performance solar energy would be the subject for the upcoming research to sustain an efficient method of energy supply.

1.2 History of Solar Cells

Edmond Becquerel, a French scientist, was the first developer of the photovoltaic in 1839. He investigated that there is some materials can generate an electrical voltage when enlightening it[1]. In 1879, it is explored that selenium has a property of photoconductivity that can generate electricity without an intervention of thermal or mechanical sources [2]. Accordingly, an American explorer was succeeded in 1883 to manufacture the first light selenium absorber coated with a thin

layer of gold to produce solar energy of 1% efficiency [1-3]. This is followed by exploring the possibility of releasing electrons from a solid surface by subjecting ultraviolet (short wavelength light). This in turn observed for the first time the effect of photoelectric that elaborated by a German physicist in 1887.[2]. In 1904 and 1916, Albert Einstein in 1904 and Robert Millikan in 1916 were experimentally confirmed the theory of photoelectric effect. This in turn led to gain the Albert Einstein's Nobel Prize in 1921 [1-3].

Interestingly, the first practical milestone silicon cell which able to generate solar energy of 6% efficiency was produced by three scientists (Calvin Fuller, Daryl Chapin, and Gerald Pearson) in Bell Laboratories in 1954, It is revealed that the diffusion of boron into silicon via doping the semiconductor material can generate an appropriate carrier to transfer charge density [2,3]. The efficiency of the silicon solar cells was also promoted from 6% to 14% between 1950s to 1960s, In 1970s, the solar cell has been considered as a fundamental source of energy. However, the high cost of $150 per watt was a critical issue). Therefore, the mitigation of manufacturer's cost of silicon solar cell and improving its efficiency were affirmed as major concerns. Figure 1-1 depicts the efficiency energy chart endorsed by National Renewable Energy Laboratory. The essential physics of solar cell are thoroughly described in the upcoming section.
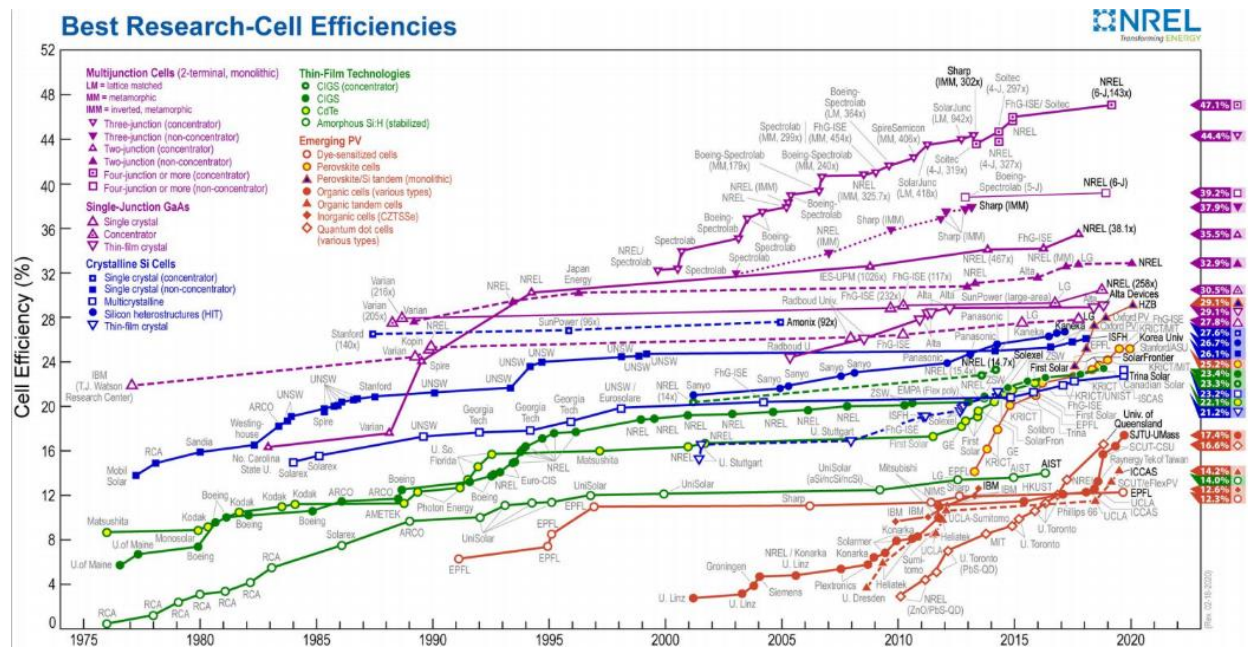
Figure 1-1. The energy efficiency chart by National Renewable Energy Laboratory [4]

1.3   Organic solar cells

Organic photovoltaic solar cells (OPV) are distributed into three groups namely, dye-sensitized solar cells (DSSCs), small molecule solar cells and polymer solar cells. Moreover, a combination of organic and inorganic materials in solar cells can be denoted as hybrid solar cell. In such type, the organic materials present the donor field while the inorganic materials present the acceptor field. The OPVs are efficient low-cost solar cells that low temperatures was used throughout its synthesizing. In 1991, O'Regan and Gratzel were produced the first DSSCs with an acceptable efficiency of 7.4% [5]. In 1994, this value was promoted to be 10% via the flourishing of technology. Interestingly, remarkable growths of efficiency of 10.4% and 11.1% were registered in 2001 and 2005, respectively [6,7]. The progress of solar cell efficiency was corresponding to the redox reaction by employment of a dye in electrolyte and a solid electron acceptor like titanium dioxide (TiO_2). In this regard, dye absorbs light and causing to gain electron kinetic energy that can be transferred the charge to the acceptor TiO_2. Furthermore, itself neutralization of dye occurs

9

via the addition of oxidized electrolyte. Then, the diffusion of oxidized electrolyte occurs to the next electrode to maintain a complete circuit. The above procedure was also used to produce polymer and small molecule cells. It is important to realise that polymer layers are basically solution processed compared to the small molecules that represented as spin-coated, spray paint or deposited under vacuum using organic molecular beam deposition that considered their properties. For the purpose of synthesizing the organic solar cell development, it is important to utilize an active layer of one coated thin film of small molecules like porphyrins or phthalocyanines [8]. The failure of some solar cell devices is attributed to the deficiency of the material or excessive concentration of impurities in contrast to inorganic semiconductors. The reduction of power efficacy is due to the interference between these impurities and the electrical features of the solar cells. Moreover, the exciton separation represents the most noticeable impediment in the early developed OPVs. Therefore, a new heterojunction structure of a double layer donor/acceptor between materials was developed to enhance charges separation. Accordingly, the new design permits to easily separate the excitons and effectively transfer if compared to Schottky cells [9]. In this regard, it is important to note that copper Phthalocyanine (CuPc) and perylenetetracarboxylic were used to synthesize the initial solar cell that generated power of less than 1% [9]. However, the power conversion efficacy was recently improved due to the production of low-bandgap organic materials. This involves the use of organic materials type C60 as the acceptor in OPVs. These materials characterise by its capacity to absorb shorter wavelengths besides a high level of mobility. These materials retain a high level of energy due to massive organic donors that permits to dissociate the excitons. Lately, the utilisation of new oligothiophene derivative of C60 allows to improve the power efficacy to hit 4.9% [10]. Moreover, the bulk heterojunction is the new generation of the heterojunction cells. The bulk heterojunction was

synthesized by spin coating of poly (2-methoxy-5-(2'-ethylyhexyloxy)-1, 4phenylene vinylene) (MEH-PPV) with dissolvable fullerene. However, the coating of the active layer of bulk heterojunction was simultaneously achieved instead of forming junction between layers. In this structure, the polymer and the fullerene separated into two domains that presented a marginal distance between two adjacent molecules. Interestingly, the power efficacy has been improved to 7.4% [11]. Nevertheless, it might be possible to mitigate this efficacy as a result to the establishment of different domains, which presents as a constraint in charge transfer. Therefore, the research efforts were paid in the last 10 years to enhance the charge transfer in the, there has been a great effort to improve the process of charge transport in the bulk heterojunction design. Specifically, polystyrene sphere was used to harvest a superior arrangement of these charges as a result to involving 3D structures of both the donor and the acceptor. The void spaces of the polystyrene spheres are originally filled with donors and acceptors that deduce a permanent transport of charges and improved power efficacy [12].

Organic tandem cells are another improved type of solar cells that invented by Hiram to et al in 1990 which specified with stuffing more layers to be put on the top of the first cell [13]. This design promotes a high degree of absorption that made the cell thinner and finally elaborates a bigger space to move the electrons and enhances the cell efficacy. Basically, the promotion of absorption property is due to the utilisation of two materials of metal-free phthalocyanine (sub cells) that are split by gold. The gold used prevents the build-up of charges between the adjacent sub cells. In 2013, a growth of power efficacy of 10.6% was noticed due to the inclusion of solution-processed polymers [13]. However, the shortcomings of fullerene acceptors are still valid despite the progress of efficacy of organic solar cells. These shortcomings include low chemical and photochemical stability, low photo-voltage with no light absorption in the close visible IR

region, scarcity of fullerene derivatives and finally an expensive recycling of fullerene [14-17]. Thus, there is a necessity to explore an adapted type of organic semiconductor to raise the efficacy and to improve the quality of fullerene acceptors. Detailed descriptions of the organic solar cell structures are represented in the upcoming sections.

1.4   Organic solar cells structure

1.4.1   Single layer organic solar cell

This type of solar cell contains two electrodes of different functions separated by a semiconductor layer. The first electrode has characteristics of high work function besides its apparent transparency if compared to the second electron that has low function. in this regard, the second electrode made from gold, silver, aluminum, or calcium including an aluminum layer at the top or lithium fluoride plugged by aluminum [18, 19]. A representative solar cell structure is figured out in Figure 1.2. (a) while Fig.1.2. (b) depicts the energy-band flow of an individual organic layer solar cell. The electric current between the two electrodes and via the active layer is generated due to the variation in the work functions that aids to discrete the exciton. This can be attributed to the formation of electron-hole pairs while a semiconductor absorbing a photon following the theory of Coulomb's electrostatic attraction) [18]. Nevertheless, one of the disadvantages of single solar cell is the very low the efficiency as a result to insignificant charge mobility via the semiconductor. More specifically, this leads to form a short exciton diffusion length of around 10 nm compared to the length of the absorbed light of around 100 nm. In other words, the generated electric current has no capacity to efficiently discard the exciton. Moreover, there is still a high probability of recombining the charges with holes without being transferred to the boundary between the cathode and semiconductor layer. Only 0.3% power efficacy was registered for such type of organic solar

cells [18]. To encounter such imperfection, an adapted structure of bilayer heterojunction (described below) was invented [19-21].
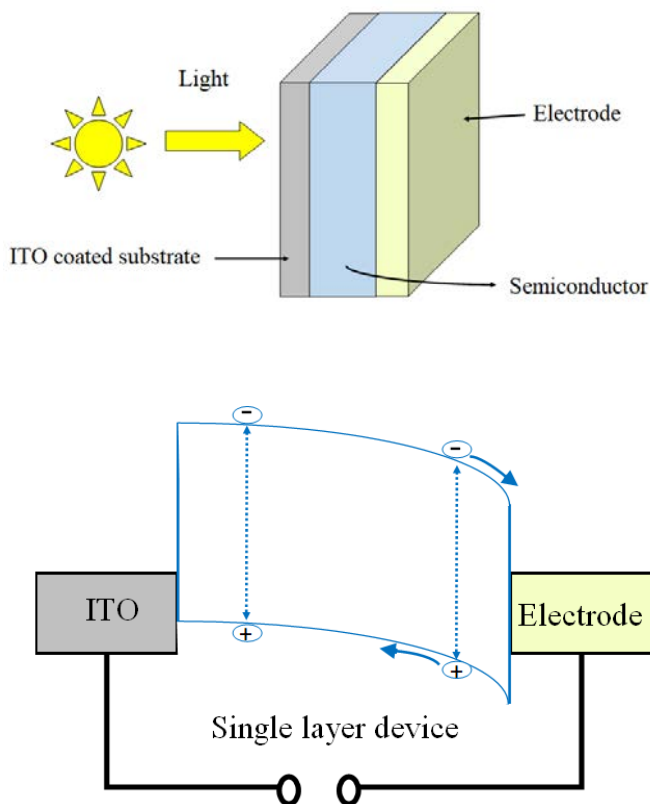
Figure 1.2: a) structure of a single layer solar cell b) energy band flow of a single layer solar cell

1.4.2   Bilayer organic solar cell

The invention of bilayer heterojuction has promoted the charge separation in solar cells and elaborated an effective model. this type characterises by emerging hole transport material and electron transport material. The performance of bilayer heterojuction was not exceeded 1% at the time of 1986. Tang was the inventor who synthesized it from two layers of copper phtalocyanine that work as the donor and an acceptor of perylene [22]. Afterwards, it is revealed that combining two layers in such structure would result in an intensive excitation. This is specifically meaning that the electron of the donor can be existed in the LUMO due to the donor's excitation. This would also accelerate the transferring of electrode from the donor to the LUMO of acceptor. More

importantly, a high energy should be provided to tackle the issue of the excitation energy and to push the electron towards separating the excitation into free charges [23]. An identical procedure can be employed to further enhance the transferring of the reverse hole from an acceptor. This implied that the excitation should be formed at a close point to the interface between the donor and the acceptor to successfully get the heterojunction inside the diffusion length of the excitation. Accordingly, it is easy to transfer the free charges to the electrodes after being apart from the excitation, with possible transfer of the holes from the donor and the electrons from the acceptor [24]. Therefore, this would reduce the level of combination and elucidates a remarkable merit of an efficient separating of holes and electrons. In this case, there is a condition of matching the electrodes to the donor HOMO and the acceptor LUMO [25]. The architecture of this solar cells has approved the generation of 3.6% PCE due to the existence of vacuum deposited copper pthalocyanine/C60 film [40]. However, a possibility of a limited excitations is still valid for this type which surely would limit the power generation performance as disclosed as a key disadvantage. Moreover, the existence of orthogonal solvents to process the solution of the layers would also consider as a disadvantage. Furthermore, the fabrication of bilayer heterojuction is mostly expensive and complicated method due to thermal evaporation steps used. However, Chang et al attempted to improve bilayer heterojuction using halogen-free solvents that predominantly growths the power generation efficacy to suppress 7% [26]. Undoubtedly, this means an improvement of the exciton diffusion length at the middle interface between the two layers. For the convenience of the reader, Figure 1.3 depicts a schematic diagram of the bilayer heterojuction and the energy flow diagram.
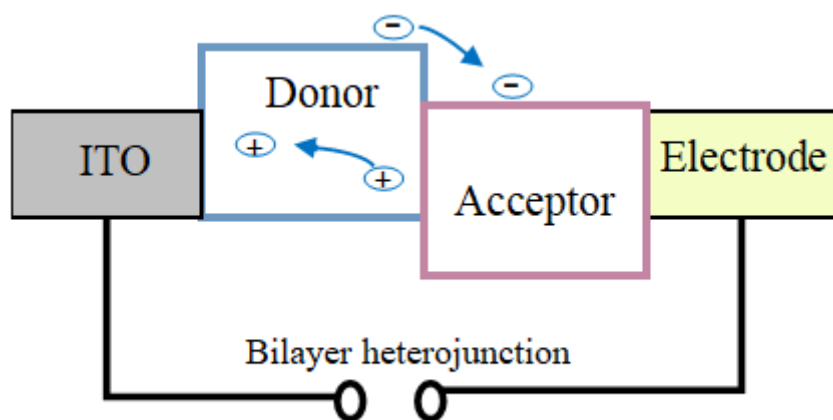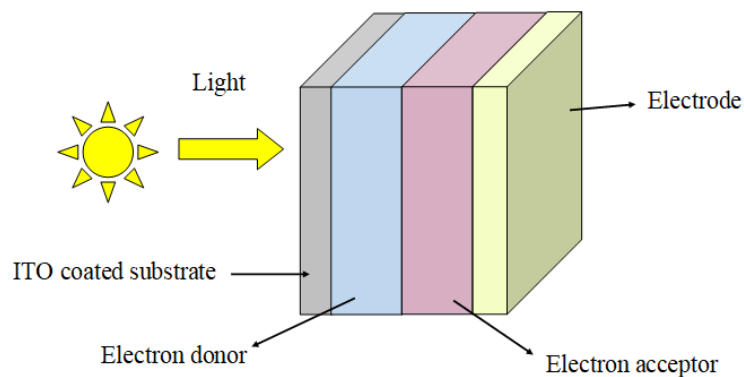
Figure 1.3: a) Device structure of an organic bilayer heterojunction solar cell b) the energy flow diagram of a bilayer heterojunction cell

1.4.3 Bulk Heterojunction (BHJ) organic solar cells

A step forward was elucidated due to the development of the bulk heterojunction (BHJ). In 1995,

Heeger and Friend have exceeded to improve this type of organic solar cells [27,28]. In this regard,

both the donating and the accepting materials are informally emerged that deduced a 3D structure

of consistent network. This type of solar cells is specified by the existence of a polymer

semiconductor. Moreover, the large interface area of BHJ is due to gaining a bicontinous network

which is normally coordinated on a nanometer that would create a high excitation case that reduce

the recombination and results in an elevated JSC. To justify the comparison between the bilayer

and BHH, the growth of an interface area is on the side of BHJ that secures a potential transfer of photoinduced charge. A comprehensive review of the photogeneration of charge in BHJ was attained by Durrant and his co-workers [29]. They affirmed that the excitation case has a capacity to endure an electron transferring from the donor (polymer) into the acceptor. This in turn would lead to the creation of an interfacial charge current that can be mitigated via the transferring of an electron hole from the acceptor. Based on the theory presented by Onsager theory, there is usually a possibility of the dissociation into free charges that is critically corresponding to the separation distance' ratio and the coulomb capture radius. A more favorable dissociation of charge transfer and improved excitation diffusion to the interface can be occurred   in case of existing a greater domain [30]. The most advantage of the charge transferring is the capability of growing its energy and therefore limiting the existed barrier, which is also related to the size of the solubilizing elements of the polymer. In other words, the design of molecules has a prominent influence on the charge transferring. A sufficient value of an interfacial area and a proper purification pathway should be provided to getting rid off any losses in the bimolecular recombination. Furthermore, the morphology has a fundamental impact on the power generation efficacy and therefore, it is vital to control it [31, 32]. To enhance the interface, a buffer layer was engaged to introduced to maximize the VOC besides preventing the charge transferring into the opposite electrodes [33]. Based on the argument above, it is mandatory to perceive the concepts of complicated structures of solar cells to gain high effective devices. In other words, the design of materials, the influencing operating conditions and the morphology are important for BHJ. Minely, the absence of solution in BHJ is another advantage where bilayer cells are requiring an orthogonal solvent to process compared to BHJ. However, the active layer in BHJ can be deposited using various techniques such as spin coating and doctor blading. Furthermore, the films drying has also a positive impact

16

on enhancing the morphology where the lack of morphological stability would degrade the efficacy of heterojunctions cells [25, 28, 34-39]. Interestingly, the thermal annealing is the most likely method deployed to justify the issues of the morphology. Furthermore, this method can be used to improve the phase segregation that would raise the efficacy [40-42]. In this line of research, there are various types of approaches to blend the morphology of BHJ including Atomic force microscopy (AFM), and Transmission electron microscopy (TEM), and Scanning electron microscopy (SEM). High resolution information is commensurate with AFM that can specify both the surface topography and the surface distribution of donor and acceptor [25]. The structure of BHJ is depicted in Figure 1.4. besides the energy path diagram.
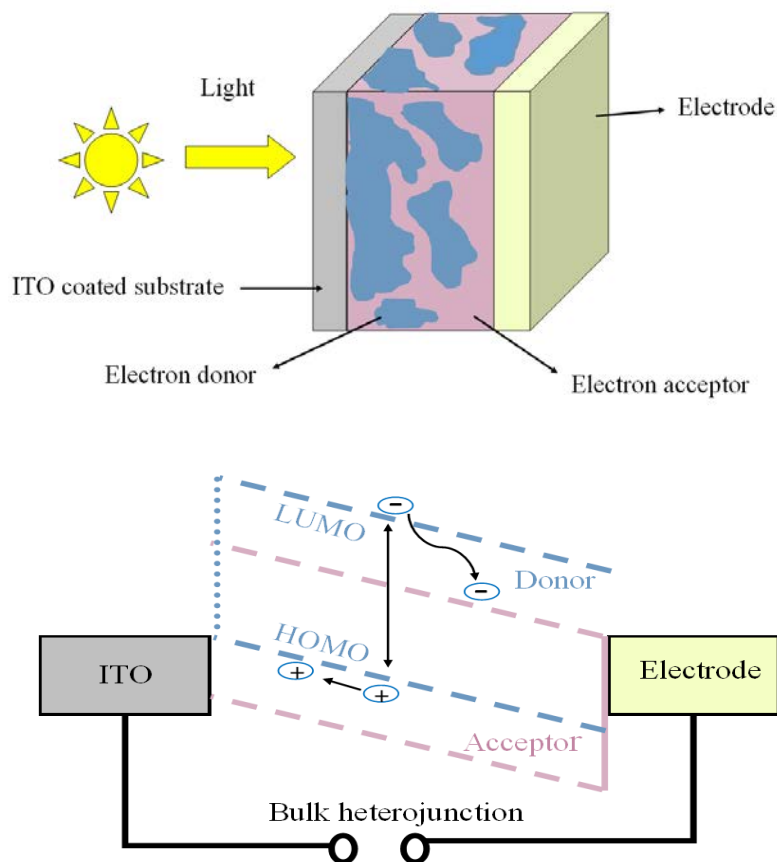
Figure 1.4: a) Device structure of an organic bulk heterojunction (BHJ) solar cell; b) energy band diagram of a BHJ cell

1.4.4 Tandem (multijunction) organic solar cells

The thermalisation losses of solar cells was significantly considered as a main issue. This issue was mostly resolved via the development of Tandem solar cell structures. A combination of two or more individual heterojunction organic solar cells has characterised Tandem type of multi junction solar cells as schematically represented in Fig.1.5. Various active layers can be found in this structure in each individual solar cell. More importantly, each active layer comprises both donor material and acceptor one [43, 44]. Therefore, it can be said that two sub cells are linked in a series configuration where one sub cell meets holes from the other. Mathematically, the summation of voltage of both sub cells can measure the total open-circuit voltage and therefore an equal current will flow via the sub cells based on the theory of Kirchhoff. However, the sub cell that has the lowest photocurrent should appropriately present the overall current. Moreover, both sub cells should produce the same photocurrent to maintain the lowest loss of thermalization. another structure of Tandem was also invented and called three-terminal (3T) that successfully able to diminish the losses of thermalization. However, the parallel connection is linked to a more complicated structure of Tandem [45]. Up to this point, it is fair to claim the feasibility of Tandem solar cells. Furthermore, the linkage of small and wide band gap polymers would gain an equal exposure of the invisible and infrared ranges of the solar spectrum. The active layers are normally segregated by a transitional contact in serial connection. This contact is organized by an electron transport layer that gathers electron from one sub cell to the other. Moreover, a hole transporting layer would collect holes from the adjacent sub cells. To quantify the lowest loss of voltage at the interfacial area, the opposite charges ought to come across at an intermediate point that characterises by an identical level of energy. More importantly, it is vital that the layers at the intermediate contact should avoid any damage of the 1st active layer at the time of deposition of

the 2nd layer throughout the solution processing. An alignment of the energy of the electron transport and hole transport layers to both the LUMO acceptor and the HOMO donor is important. Therefore, the voltage loss will be dropped at the intermediate interface between the electron transport and hole transport. In this regard, any alteration of the thickness of the two adjacent layers would be used to optimise the solar cells due to rearrangement of the current field [46- 48]. This is specifically carried out via the extraction of electrons from the front cell at the intermediate interface between the electron transport and hole transport to be rejoined with the holes gathered from the back cell. Therefore, hole transport layer is frequently used PEDOT: PSS and metal oxide (NiO, MoO3, V2O5, WO3 and ITO) while electron transport layer used ZnO, TiOx and Cs2CO [49-57]. Based on this information, the power generated efficacy of inorganic tandem solar cells hits 40% compared to only 11.1% for the organic tandem solar cells [58,13]. A schematic diagram of the organic tandem structure and the energy path are given in Figure 1.5.
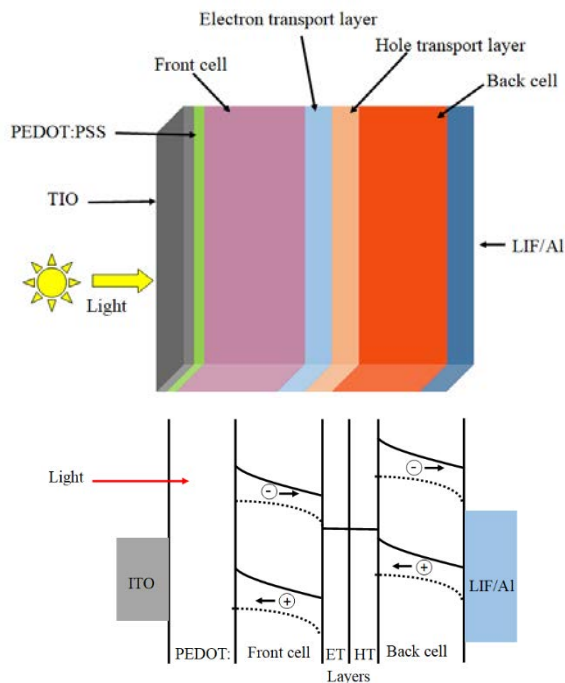
Figure 1.5: a) Device of an organic tandem solar cell; b) energy band diagram of organic tandem solar cell

19

1.5   Operational mechanisms in organic solar cells
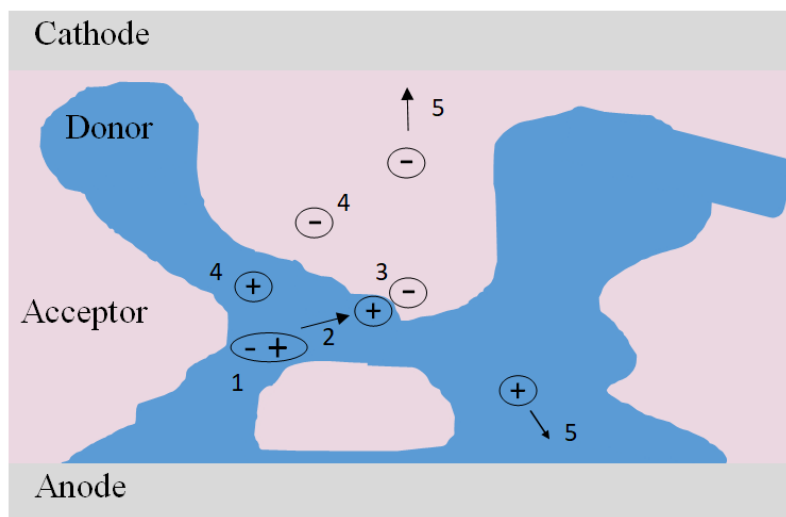
Figure 1.6. Operational mechanism in a BHJ. (1) An exciton is created by the absorption of a photon and (2) diffuses to a donor-acceptor interface. (3) Electron transfer from the donor to the acceptor via the CT state. (4) The CT state dissociates into a free hole and a free electron. (5) The charges are extracted at the electrodes

1.5.1   Optical absorption and associated exciton

The light absorption systems have two key properties. First of all, the wavefunction overlap between the ground state and the lowest excited state causes an intensive absorption [59] Secondly, the absorption is broad as a result to occur a considerable relaxation in the excited state. Within the typical first 100 nm of the active layer of organic solar cells, a massive number of photons can be absorbed. Specifically, the π-system lowers down to the bottom of the potential energy surface of the lowest excited state as a result to a great electron-vibration coupling. This in turn provided an equilibrium geometry of the excited state due to forming a Frenkel exciton [60-61] (Figure 1.6(1)). Basically, organic solar cells are denoted as excitonic solar cells in comparison to silicon type cells that forms free charges. To summarize, a high interfacial area of efficient dissociation

of BHJ can be created in case of providing an effective morphology of the donor and acceptor [28].
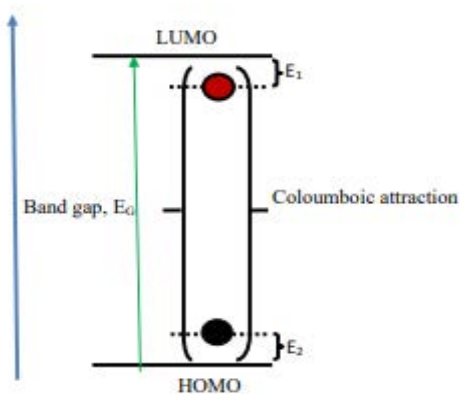
Figure 1.7: Exciton binding energy

1.5.2 Exciton migration

Figure 1.6. (2) presents the generation of free charges that requires a migration of excitons to a D/A interface. Basically, excitons are neutral individuals which are not affected by diffusion or existing of an electric field. A random motion drives the migration of the excitons into the interfacial area. The exciton diffusion length, accounts for 5 to 10 nm in almost all organic solar cells, is mathematically defined as $L = \sqrt{D}\ L = \sqrt{D\tau}$ where D is the diffusion coefficient and τ is the exciton lifetime [61-62]. The short length would plausibly interpret the high efficacy of BHJ if compared to bilayer structure.

1.5.3 Exciton dissociation at the donor-acceptor interface

The dissociation of the exciton (a doubted phenomenon) into electrons and holes is important to gain free charge after bringing in touch to the interfacial area. The dissociation is likely to be split into two procedures; first of all, after reaching an exciton into the interface, an electron is relocated

to the acceptor side causing a weakly bound electron hole pair denoted as a charge transfer (CT) state as represented in Figure 1.6. (3) [63-66]. The CT state is a transitional state between the exciton and the final Charge Separated state (CS) that noticed a week interaction of the coulombic if compared to the thermal energy. Various SM: PC71BM systems confirmed more than 90% of Internal Quantum Efficiencies (IQE) that specifies a high performance of charge separation. However, a challenging of explaining this high performance is valid due to assuming that the coulombic force between two opposite charges is within tenths of an electron volt. Therefore, a considerable driving force is vital to gain free charge that can be expected to be low one with realizing the dependence of both temperature and electric field. In other words, low driving force would plausibly gain due to approximately temperature and electric field independents. To clarify the state of charge generation, various mechanisms were explored:

First, the driving force that can be used to tackle with the exciton binding energy is the energy offset between the donor (LUMO) and the acceptor (HOMO). The practical value of energy offset is determined as 0.3eV. But realizing the energy offset is not enough to sufficiently drive the exciton dissociation. Hot is the oldest model developed that affirms a surplus of vibrational energy hold by the charges are capable to be separated throughout thermalization [67] [68]. However, this model recognize the dependence of the charge production on excitation energy and LUMO-LUMO offset [69-70]. Furthermore, the model was opposed by the theory of IQE that characterizes the independence between the charge production and energy (wavelength) [71]. Therefore, this issue was aided to form a new model of the charge delocalization, which informed the possibility of a spatial delocalization of both electron and holes [72-73]. This would enhance the distance between the charges and then reduces the binding energy of the charge transfer case. The outputs of this model were also confirmed that the donor phase is a main key of delocalization [74] with a

considerable intermolecular delocalization within fullerene [75-76]. Furthermore, increasing the level of interfacial mixing would be a plausible matter to increase charge segregation between donor and acceptor phases [77-78]. In this regard, a lower value of LUMO and a higher HOMO are associated with the more order phase. However, the mixed phase is inhibiting any recombination of the charge segregation [79]. Interfacial dipoles, interface molecule orientation, and entropy are another important parameter to justify the charge transfer [80], [81-82] and [83-85], respectively.
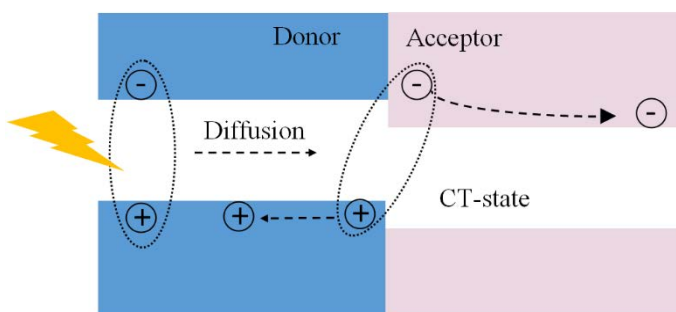
Figure 1.8: The CT state dissociates into a free hole and a free electron.

1.5.4 Charge transport and collection

The charge transport and segregation of charges is important, as presented in Figure 1.6(4), however, the tendency of movement into respective electrodes is existed in BHJ structure, as represented in Figure 1.6(5). In this regard, a high mobility can be found in an inorganic crystalline semiconductor between 102 to 103 cm^{2}V-1s^{-1}). However, organic crystalline semiconductor has a modest mobility that causes a high localization due to several factors including the weak electronic couplings, large electron-vibration couplings, and an insignificant disorder. However, in case of polymer solar cells, the overall charge transport is occurred throughout the main polymer chain [86]. Thus, the intermolecular charge transfer can allocate the overall charge transport for SM. Furthermore, the morphology of BHJ, determines amorphous to high crystalline materials, has a

direct impact on the charge separation and mobilities within a variable value range between 10-6

to 10.2 cm^{2}V-1s^{-1}). This in turn would the arguments of molecules' stacking in several studies. A

high mobility was noticed for rigid, symmetric, planar cores molecules that characterizes with a

high propensity of stacking to π-π [87]

1.6   Electrical characterization of organic solar cells

1.6.1   Equivalent circuit diagram of organic solar cells

A feasible discussion of the electrical properties of organic solar cells requires a full understanding

of the electrical model of a specified solar cell. Ideally, a diode parallel with a current source can

be used in the model. However, a series resistor Rs and a shunt resistor Rsh are important to be

involved in the model. Rsh denotes the recombination of charge carriers around the dissociation

area and Rs deems free transfer of charge carriers in the transport medium. A typical circuit for

solar cell is depicted in Figure 1.8. where Rs = 0 and Rsh = ∞ [88].
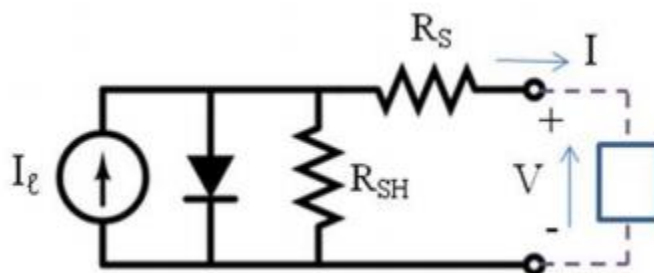
Figure 1.9: Equivalent circuit diagram of organic solar cells

Figure 1.8 specifies (I1) as the produced current from the event light while the diode signifies the

nonlinearity of the I-V curve. This is only conditioned by dropping the Rs below zero and equality

of the circuit`s I-V and diode with approximating to infinity for the Rsh. However, it is important

to note that the Rs of a solar cell is relevant to the conductivity of material, thickness of the active layer and impurity concentrations. Rsh can be measured from the reverse bias of the illuminated I-V. But Rs can also be measured from the slop of the illuminated I-V under high forwarded bias voltage (V >VOC). Overall, any growth of Rs would lessen circuit current. However, decreasing Rsh would influence the VOC and FF [89].

1.6.2   Current-voltage characterization

This section focuses on illustrating the essentials of electrical characterizations that are uniquely similar within all the organic and inorganic solar cells. The current-density to voltage (J-V) property is associated a dark place with low current in reverse bias and high current in forward bias. After directing a light, a growth of photocurrent in the solar cell is started considering that both the photocurrent and dark characteristic are originally reflect the J-V characteristic under lighting. In this regard, the J-V characteristic and photocurrent (Jph) are remarkably defined using the following equation of Shockley

$$J = J_0[\exp{(eV/nkT)}\text{-}1]\text{-}J_{ph}$$

J and Jo are the current density and the reverse saturation current density of the diode, e denotes the elementary charge, V is the utilized voltage, n is an ideal factor, k is the Boltzmann constant and finally T is operating temperature [90]. Basically, the photocurrent is directly related to the applied voltage while the diode's characteristics are joined to the lighting intensity. Figure 1.9. depicts the J-V plot for a normal solar cell in the dark place under the influence of lighting. In this aspect, the open-circuit voltage (VOC), short-circuit current density (JSC), fill factor (FF), and power conversion efficiency (PCE) are the key indicators that can be located from the J-V curve.
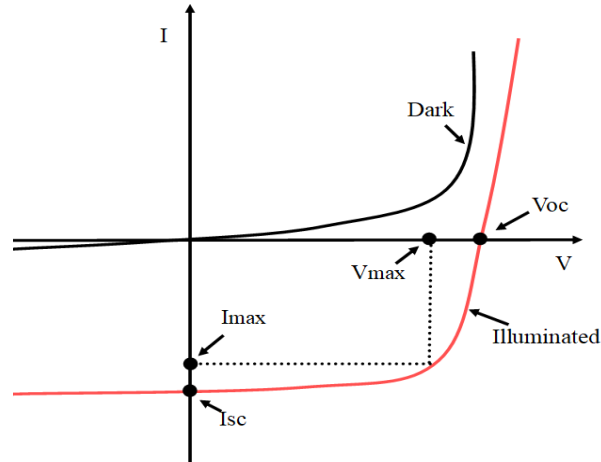
Figure 1.10: shows the J-V plot for a typical solar cell in the dark and under illumination
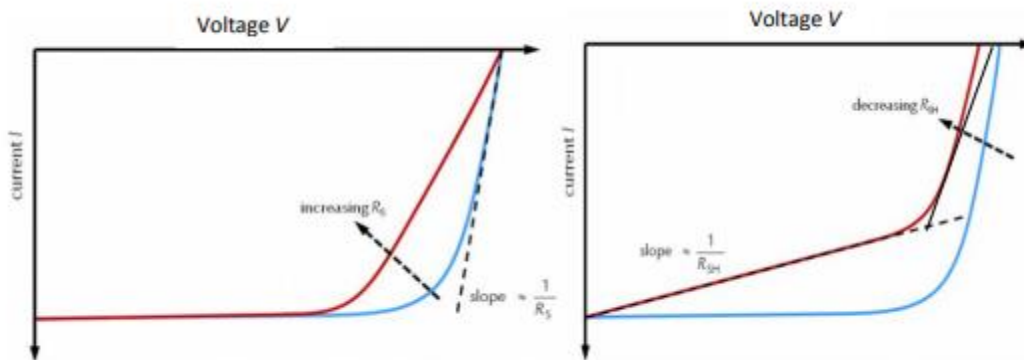
Figure 1.11: Effect of the series resistance RS and the shunt resistance RSH on the shape of an I-

V curve

1.6.3 Open-circuit voltage

VOC is considered as open circuit voltage occurs when J= 0. However, when power = current*voltage and J = 0, no possibility of generating power. The point at which the processes of production of photocurrent and dark current compensate one another is the open-circuit voltage [91].

1.6.4 Short-circuit current

the current density is considered to be short-circuit current density JSC when V=0 like VOC, due to occurring short-circuited as similar conditions were used being. Also, no power is generated in such case where the generation of power is related to JSC. Basically, the photocurrent density equals to the JSC (negative value). However, JSC treated as a positive sign where higher values of JSC are corresponding to higher values of Jph [92].

1.6.5 Fill-factor

The utilization of an ultimate power density Pmax occurs at specified conditions of maximum voltage Vmax and current density Jmax. therefore, JSC and VOC can be used to express the power generation via a solar cell. However, both JSC and VOC are bigger than Jmax and Vmax as a result to an increased in resistance and recombination losses and diode characteristic. The power generation (FF) is desired to have high values and can therefore be defined as

$$FF = \frac{J_{max} \times V_{max}}{Jsc \times V_{OC}}$$

The diode characteristic must be less than one to maintain high values of FF and also high values of JSC and VOC would mitigate FF [93].

1.6.6 Power conversion efficiency

This is an important parameter related to solar cells which defines the percentage irradiance IL (light power per unit area). The power conversion efficiency can be illustrated as

$$PCE = \frac{J_{max} \times V_{max}}{Plight} \times 100\,\% = \frac{FF \times J_{SC} \times V_{OC}}{P_{light}} \times 100\,\%$$

The above equation elucidates that all FF, JSC and VOC have a workable influence on PCE, where high values of PCE are favorable Furthermore, the calculation of area in J would also affect PCE. The domination of excellent power conversion efficiency is coupled to high space occupied by a cell. Also, a balance between PCE and operational cost is important. Furthermore, the power and

spectrum of the light source are identical parameters that have a contribution to measure the power conversion efficiency. This is because solar cells do not absorb and convert photons to electrons at all wavelengths with identical efficacy. The calculations and comparison of the performance of different photovoltaic solar cells mostly use AM1.5 G standard spectrum despite an expected variation of the spectrum with the location [94].

1.7   Motivation of the present study

As discussed earlier, the organic solar cells (OSCs) have gained an ascendingly attention that entirely deduced the proposition of many upgraded types of OSCs. Among them are the single layer, bilayer, bulk hetero-junction (BHJ) and tandem (multijunction). To quantify an efficient technology of OSCs, several technological institutes and industrial applications have deployed intensive research on OCSs. Therefore, various aspects of the OSCs were under investigation to be technically improved. The previous research of OSCs is therefore focused on two methods of improvements including the synthesized of efficient materials of OSCs and proposed new techniques. The scope of the research was to resolve the main concern of OSCs of low efficiency and short lifetime. Furthermore, another bath of research was focused on exploring different mechanism of OSCs and photovoltaic effect. Thus, several optimization methods were proposed to clarify and optimize the operation principle of OSCs.

Basically, the carrier processes of the OSCs such as separation of excitons into electron and hole pairs, lifetime of carriers, have a prominent role in delivering high performance. The basic carrier process of OSCs is characterized by generating excitons in the active layer by photo-illumination diffuse to the interface's donor-acceptor to be separated to electron and holes. Afterwards, electrons and holes are delivered to the opposite electrodes to produce photo-voltage. However, the carrier process in the real solar cell devices is more complicated. This is due to several causes

such as the uncertainty of interfaces, the existence of carrier traps, and the difficulty of the carrier pathway. in this aspect, several attempts were made to enhance the efficacy of OSCs. Interestingly, the improvement of morphology of active layers and charge extraction of the device are the most promising approaches. These concepts have paid the way to increase the open voltage besides delivering a short-circuit current of OSCs, and therefore the efficiency of OSCs was improved. However, a detailed evaluation of interfacial carrier behaviors is somehow not thoroughly outlined in the literature. In other words, a detailed analysis-based on a comprehensive study to improve the carrier behavior and the electrical phenomena using different organic layer is not addressed in the open literature. Up to the author's knowledge, there is still room to improve the operation of the OSCs to accommodate the requirements of an efficient technology.

The recent study intends to improve the energetic of the OSCs. The gathered charges at the interfacial area would considerably affect the potential distribution in OSCs as a result to the dielectric nature of organic materials and the Maxwell-Wagner effect. Thus, the direct probing of the electric field in OSCs would aid to perceive the carrier behaviors in OSCs and upgrade the OSCs efficiency.

To successfully carry out this research, a new approach of the electric field induced optical second harmonic generation (EFISHG) measurement was developed. The method developed was able to directly probe carrier transportations and electric field distribution in OSCs such as the organic electroluminescence devices, organic field effect transistors, and organic solar cells. Furthermore, the contribution of the Maxwell-Wagner effect interface charges is another advantage of the proposed technique. Interestingly, the EFISHG technique is an efficient tool to determine the influence of BHJ in OSCs.

This is mainly emphasized the motivation of this study to appraise the involvement of the dielectric nature in OSCs to the carrier transportation in terms of the EFISHG measurement. The BHJ was prepared in this research by the mechanism of chemical additives and surface treatment to enhance the performance efficiency. At first, the ability of EFISHG will be demonstrated to be applied in the OSCs. Secondly, the coupling of EFISHG with Maxwell-Wagner model will be modelled to approve the existence of charge accumulation at each interface of BHJ and the variation of charge accumulations. Lastly, the feasibility of analyzing the accumulated charges, that have a considerable effect on the performance of OSCs, will be approved. The experimental results of this research have confirmed the successfulness of the proposed coupling of EFISHG and Maxwell-Wagner effect to critically improve the performance of the OSCs.

1.8   Bibliography

1. US Department of Energy, "The History of Solar," Office of Energy Efficiency & Renewable Energy, https://www1.eere.energy.gov/solar/pdfs/solar_timeline.pdf, accessed on December, 2018.

2. Solar Power authority, "A History of Solar Cells: How Technology Has Evolved", https://www.solarpowerauthority.com/a-history-of-solar-cells/, accessed on December, 2018.

3. Martin A. Green. (2009) "The Path to 25% Silicon Solar Cell Efficiency: History of Silicon Cell Evolution", Prog. Photovolt: Res. Appl. 17:183-189.

4. National Renewable Energy Laboratory, February, 2020.

5. B. O'Regan and M. Gratzel, "A low-cost, high-efficiency solar cell based on dyesensitized colloidal TiO2 films", Nature, Vol.353, pp. 737-740, 1991.

6. M. Gratzel and K. Kalyanasundaram., "Artificial photosynthesis- efficient dyesensitized photochemical cells for direct conversion of visible-light to electricity", Current Science, Vol. 66, pp.706-714, 1994.

7. M. Nazeeruddin, F. Angelis, S. Fantacci, A. Selloni, G. Viscardi, P. Liska, S. Ito, T. Bessho and M. Gratzel., "Combined Experimental and DFT-TDDFT Computational Study of Photoelectrochemical Cell Ruthenium Sensitizers", Journal of the American Chemical Society, Vol.127(48), pp. 16835–16847, 2005.

8. G. Chamberlain, "Organic solar cells: A review", Solar Cells, Vol.8, pp. 47-83, 1983.

9. C. Tang, "Two-layer organic photovoltaic cell", Applied Physics Letters, Vol. 48, pp. 183-185, 1986.

10. D. Wynands, M. Levichkova, K. Leo, C. Uhrich, G. Schwartz, D. Hildebrandt, M. Pfeiffer and M. Riede., "Increase in internal quantum efficiency in small molecular oligothiophene: C60 mixed heterojunction solar cells by substrate heating", Applied Physics Letters, Vol. 97(3), 2010.

11. Y. Liang, Z. Xu, J. Xia, S.-T. Tsai, Y. Wu, G. Li, C. Ray and L. Yu., "For the Bright Future—Bulk Heterojunction Polymer Solar Cells with Power Conversion Efficiency of 7.4%", Advanced Materials, Vol. 22(20), pp. E135–E138, 2010.

12. S. Schumann, S. Bon, R. Hatton and T. Jones, "Open-cellular organic semiconductor thin films by vertical co-deposition using sub-100 nm nanosphere templates", Chemical Communications, pp. 6478-6480, 2009.

13. J. You, L. Dou, K. Yoshimura, T. Kato, K. Ohya, T. Moriarty, K. Emery, C. Chen, J. Gao1, G. Li and Y. Yang., "A polymer tandem solar cell with 10.6% power conversion efficiency", Nature Communications, Vol. 4, pp. 1-10, 2013.

14. G. Li, R. Zhu and Y. Yang, "polymer solar cells", nature photonics, Vol.6(3), pp. 153-161,2012.

15. Z. He, C. Zhong, X. Huang, W. Wong, H. Wu, L. Chen, S. Su and Y. Cao., "Simultaneous Enhancement of Open-Circuit Voltage, Short-Circuit Current Density, and Fill Factor in Polymer Solar Cells", Advanced Materials, Vol. 23(40), pp. 4636–4643, 2011.

16. Y. Liang, D. Feng , Y. Wu , S. Tsai , G. Li , C. Ray and L. Yu., "Highly Efficient Solar Cell Polymers Developed via Fine-Tuning of Structural and Electronic Properties", Journal of the chemical society, Vol. 131(22), pp. 7792–7799,2009.

17. E. Ahmed, G. Ren, F. Kim, E. Hollenbeck, and S. Jenekhe., "Design of New Electron Acceptor Materials for Organic Photovoltaics: Synthesis, Electron Transport, Photophysics, and Photovoltaic Properties of Oligothiophene Functionalized Naphthalene Diimides", Chemistry of materials, Vol. 23, 4563– 4577, 2011.

18. C. Deibel , and V. Dyakonov, "Polymer–Fullerene Bulk Heterojunction Solar Cells: review article", Reports on Progress in Physics, Vol. 73(9). pp. 1-68, 2010.

19. S. Lattante, "electron and hole transport layers: their use in inverted bulk Heterojunction polymer solar cells", Electronics, Vol. 3, pp. 132-164, 2014.

20. P. Kumar and S. Chand, "Recent progress and future aspects of organic solar cells", Progress in photovoltics: research and application, Vol. 20, pp. 377- 415, 2011.

21. T. Kietzke, "Recent advances in organic solar cells", Advances in optoelectronics, Vol.2007, pp. 1-15. 2007.

22. C. Tang, "Two- layer organic photovoltaic cell", Applied physics letters, Vol. 48(2), pp. 183-185, 1986.

23. E. Bittner, J. Ramon and S. Karabunarliev. "Exciton dissociation dynamics in model donor-acceptor polymer heterojunctions. I. Energetics and spectra", Journal of Chemical Physics, Vol. 122(21), pp. 214719-214719-9, 2005.

24. P. Peumans, A. Yakimov, and S. Forrest. "Small molecular weight organic thinfilm photodetectors and solar cells". Journal of Applied Physics, Vol. 93, pp.3693–3723, 2003.

25. H. Hoppe and N. Sariciftci, "Organic solar cells: an overview," Journal of Materials Research, vol. 19(7), pp. 1924–1945, 2004.

26. J. Chang, H. Wang, W. Lin, K. Chiang, K. Chen, W. Huang, Z. Huang, H. Meng, R. Hob and H. Lin. "Efficient inverted quasi-bilayer organic solar cells fabricated by using non-halogenated solvent processes", Journal of Materials Chemistry A, Vol. 2(33), pp. 13398-13406, 2014.

27. H. Son, F. He, B. Carsten and L. Yu. "Are we there yet? Design of better conjugated polymers for polymer solar cells", Journal of Materials Chemistry, Vol. 21(47), pp. 18934-18945, 2011.

28. G. Yu, J. Gao, J. Hummelen, F. Wudl, A. Heeger. "Polymer Photovoltaic Cells: Enhanced Efficiencies via a Network of Internal Donor-Acceptor Heterojunctions", Science, New Series, Vol. 270(5243), pp. 1789-1791, 1995.

29. T.Clarke, J. Durrant. "Charge Photogeneration in Organic Solar Cells", Chemical Reviews, Vol. 110(2665), pp. 6736-6767, 2010.

30. T. Holcombe, J. Norton, J. Rivnay, C. Woo, L. Goris , C. Piliego, G, Griffini , A. Sellinger , J. Brédas , A. Salleo and J. Fréchet. "Steric Control of the Donor/Acceptor Interface: Implications in Organic Photovoltaic Charge Generation", Journal of the American Chemical Society, Vol. 133(31), pp. 12106-12114, 2011.

31. G. Li, V. Shrotriya, J. Huang, Y. Yao, T. Moriarty, K. Emery and Y. Yang. "High-efficiency solution processable polymer photovoltaic cells by selforganization of polymer blends", Nature Materials, Vol.4, pp. 864 – 868, 2005.

32. W. Ma, C. Yang, X. Gong, K. Lee and A. Heeger. "Thermally Stable, Efficient Polymer Solar Cells with Nanoscale Control of the Interpenetrating Network Morphology", Vol. 15(10), pp. 1617–1622, 2005.

33. W. Cai, X. Gong and Y. Cao. "Polymer solar cells: recent development and possible routes for improvement in the performance", Solar Energy Materials and Solar Cells, Vol. 94(2), pp. 114-127, 2010.

34. H. Hoppe, M. Niggemann, C. Winder, J. Kraut, R. Hiesgen, A. Hinsch, D. Meissner, N. Sariciftci. "Nanoscale Morphology of Conjugated Polymer/Fullerene-Based Bulk-

Heterojunction Solar Cells", Advanced Functional Materials, Vol. 14(10), pp. 1005-1011, 2004.

35. C. Chochos, S. Choulis, "How the structural deviations on the backbone of conjugated polymers influence their optoelectronic properties and photovoltaic performance", Progress in Polymer Science, Vol. 36(10), pp. 1326-1414, 2011.

36. V. Kamm, G. Battagliarin, I. Howard, W. Pisula, A. Mavrinskiy, C. Li, K. Müllen andF. Laquai. "Polythiophene:Perylene Diimide Solar Cells – the Impact of Alkyl-Substitution on the Photovoltaic Performance", Advanced Energy Materials, Vol.1(2), pp. 297–302, 2011.

37. N. Miller , E. Cho , R. Gyse , C. Risko , V. Coropceanu , C. Miller , S. Sweetnam , A. Sellinger , M. Heeney , I. McCulloch , J. Brédas , M. Toney and M. McGehee. "Factors Governing Intercalation of Fullerenes and Other Small Molecules Between the Side Chains of Semiconducting Polymers Used in Solar Cells", Advanced Energy Materials, Vol. 2 (10), pp. 1208-1217, 2012.

38. X. Yang , J. Loos , S. Veenstra , W. Verhees , M. Wienk , J. Kroon , M. Michels and R. Janssen. "Nanoscale Morphology of High-Performance Polymer Solar Cells", Nano letters, Vol.5 (4), pp. 579–583, 2005.

39. M. Campoy-Quiles , T. Ferenczi , T. Agostinelli , P. Etchegoin , Y. Kim , T. Anthopoulos , P. Stavrinou , D. Bradley , J. Nelson . "Morphology evolution via self-organization and lateral and vertical diffusion in polymer:fullerene solar cell blends", Nature Materials, Vol. 7(2), pp. 158-164, 2008.

40. Y. Kim, S. Choulis, J. Nelson, D. Bradley, S. Cook and J. Durrant. "Device annealing effect in organic solar cells with blends of regioregular poly(3- hexylthiophene) and soluble fullerene", Applied physics letters, Vol. 86(6), pp. 063502-3, 2005.

41.] L. Nguyen, H. Hoppe, T. Erb, S. Günes, G. Gobsch and N. Sariciftci. "Effects of Annealing on the Nanomorphology and Performance of Poly(alkylthiophene):Fullerene Bulk-Heterojunction Solar Cells", Advance functional materials, Vol. 17(7), pp. 1071-1078, 2007.

42. G. Li, Y. Yao, H. Yang, V. Shrotriya, G. Yang and Y. Yang. "Solvent Annealing Effect in Polymer Solar Cells Based on Poly(3-hexylthiophene) and Methanofullerenes", Advanced Functional Materials, Vol.17(10), pp. 1636– 1644, 2007.

43. M. Riede , C. Uhrich , J. Widmer , R. Timmreck , D. Wynands , G. Schwartz , W. Gnehr , D. Hildebrandt , A. Weiss , J. Hwang , S. Sundarraj , P. Erk , M. Pfeiffer and K. Leo. "Efficient Organic Tandem Solar Cells based on Small Molecules". Advanced Functional materials. Vol.21, pp. 3019–3028, 2011.

44. D. Cheyns, J. Poortmans, H. Gommans, J. Genoe, and P. Heremans, "Stacked organic solar cells increase efficiency", SPIE Newsroom, May 11, 2007.

45. I. Etxebarria, A. Furlan, J. Ajuria, F. Fecherd, M. Voigt, C. Brabec, M. Wienk, L. Slooff, S. Veenstra, J. Gilot, and R. Pacios, "Series vs parallel connected organic tandem solar cells: Cell performance and impact on the design and operation of functional modules", Solar Energy Materials and Solar Cells, Vol. 130, pp. 495–504, 2014.

46. J. Drechsel, B. Männig, F. Kozlowski, M. Pfeiffer, K. Leo and H. Hoppe. "Efficient organic solar cells based on a double p-i-n architecture using doped wide-gap transport layers", Applied physics letters, Vol. 86, pp. 244102-3, 2005.

47. A. Hadipour, B. Boer and P. Blom. "Solution-processed Organic Tandem Solar Cells with embedded Optical Spacers", Journal of applied physics, Vol. 102 (7), pp. 074506, 2007.

48. R. Schueppe, R. Timmreck, N. Allinger, T. Mueller, M. Furno, C. Uhrich, K. Leo and M. Riede. "Controlled current matching in small molecule organic tandem solar cells using doped spacer layers", Journal of Applied Physics, Vol. 107(4), pp. 044503, 2010.

49. J. Gilot, M. Wienk and R. Janssen. " Double and triple junction polymer solar cells processed from solution", Applied physics letters, Vol. 90, pp. 143512, 2007.

50. M. Irwin, D. Buchholz, A. Hains,R. Chang, T. Marks. "P-Type semiconducting nickel oxide as an efficiency-enhancing anode interfacial layer in polymer bulkheterojunction solar cells". PNAS , Vol.105, pp.2783-2787, 2008.

51. F. Chen and C. Lin. "Construction and characteristics of tandem organic solar cells featuring small molecule-based films on polymer-based subcells", Journal of Physics D: Applied Physics, Vol. 43(2), pp. 025104, 2010.

52. G. Li, C. Chu, V. Shrotriya, J. Huang and Y. Yang. "Efficient inverted polymer solar cells", Applied physics letters, Vol. 88, pp. 253503, 2006.

53. A. Janssen, T. Riedl, S. Hamwi, H. Johannes and W. Kowalsky. " Highly efficient organic tandem solar cells using an improved connecting architecture", Applied physics letters, Vol. 91, pp. 073519, 2007.

54. K. Kenji, I. Norihiro,T. Nishimori and J. Sakai, "Open circuit voltage of stacked bulk heterojunction organic solar cells", Applied physics letters, Vol. 88(7), pp. 073514, 2006.

55. J. Gilot, I. Barbu, M. Wienk and R. Janssen. "The use of ZnO as optical spacer in polymer solar cells: Theoretical and experimental study", Applied physics letters, Vol. 91(11), pp. 113520, 2007.

56. J. Kim, S. Kim, H. Lee, K. Lee, W. Ma, X. Gong and A. J. Heeger. "New Architecture for High-Efficiency Polymer Photovoltaic Cells Using SolutionBased Titanium Oxide as an Optical Spacer", Advanced Materials, Vol. 18(5), pp. 572–576, 2006.

57. B. Lee, H. Kim, W. Jeong and J. Kim. "A transparent conducting oxide as an efficient middle electrode for exible organic tandem solar cells", Solar Energy Materials and Solar Cells, Vol. 94,pp. 542-546, 2010.

58. S. Sista, Z. Hong, L. Chenx and Y. Yang. "Tandem polymer photovoltaic cells—current status, challenges and future outlook", Energy & Environmental Science, Vol. 4, pp. 1606–1620, 2011.

59. Brédas, J.-L.; Norton, J. E.; Cornil, J.; Coropceanu, V., Molecular Understanding of Organic Solar Cells: The Challenges. Acc. Chem. Res. 2009, 42 (11), 1691-1699

60. Scholes, G. D.; Rumbles, G., Excitons in nanoscale systems. Nat. Mater. 2006, 5 (9), 683-696

61. Mikhnenko, O. V.; Blom, P. W. M.; Nguyen, T.-Q., Exciton diffusion in organic semiconductors. Energy Environ. Sci. 2015, 8 (7), 1867-1888.

62. Haugeneder, A.; Neges, M.; Kallinger, C.; Spirkl, W.; Lemmer, U.; Feldmann, J.; Scherf, U.; Harth, E.; Gügel, A.; Müllen, K., Exciton diffusion and dissociation in conjugated polymer/fullerene blends and heterostructures. Physical Review B 1999, 59 (23), 15346-15351.

63. Benson-Smith, J. J.; Goris, L.; Vandewal, K.; Haenen, K.; Manca, J. V.; Vanderzande, D.; Bradley, D. D. C.; Nelson, J., Formation of a Ground-State Charge-Transfer Complex in Polyfluorene//[6,6]-Phenyl-C61 Butyric Acid Methyl Ester (PCBM) Blend Films and Its Role in the Function of Polymer/PCBM Solar Cells. Adv. Funct. Mater. 2007, 17 (3), 451-457

64. Hwang, I. W.; Soci, C.; Moses, D.; Zhu, Z.; Waller, D.; Gaudiana, R.; Brabec, C. J.; Heeger, A. J., Ultrafast Electron Transfer and Decay Dynamics in a Small Band Gap Bulk Heterojunction Material. Adv. Mater. 2007, 19 (17), 2307-2312

65. Kanai, Y.; Grossman, J. C., Insights on Interfacial Charge Transfer Across P3HT/Fullerene Photovoltaic Heterojunction from Ab Initio Calculations. Nano Lett. 2007, 7 (7), 1967-1972.

66. Loi, M. A.; Toffanin, S.; Muccini, M.; Forster, M.; Scherf, U.; Scharber, M., Charge Transfer Excitons in Bulk Heterojunctions of a Polyfluorene Copolymer and a Fullerene Derivative. Adv. Funct. Mater. 2007, 17 (13), 2111-2116.

67. Arkhipov, V. I.; Emelianova, E. V.; Bässler, H., Hot Exciton Dissociation in a Conjugated Polymer. Phys. Rev. Lett. 1999, 82 (6), 1321-1324.

68. Peumans, P.; Forrest, S. R., Separation of geminate charge-pairs at donor–acceptor interfaces in disordered solids. Chem. Phys. Lett. 2004, 398 (1), 27-31.

69. Ohkita, H.; Cook, S.; Astuti, Y.; Duffy, W.; Tierney, S.; Zhang, W.; Heeney, M.; McCulloch, I.; Nelson, J.; Bradley, D. D. C.; Durrant, J. R., Charge Carrier Formation in Polythiophene/Fullerene Blend Films Studied by Transient Absorption Spectroscopy. J. Am. Chem. Soc. 2008, 130 (10), 3030-3042.

70. Shoaee, S.; Clarke, T. M.; Huang, C.; Barlow, S.; Marder, S. R.; Heeney, M.; McCulloch, I.; Durrant, J. R., Acceptor Energy Level Control of Charge Photogeneration in Organic Donor/Acceptor Blends. J. Am. Chem. Soc. 2010, 132 (37), 12919-12926.

71. Vandewal, K.; Albrecht, S.; Hoke, E. T.; Graham, K. R.; Widmer, J.; Douglas, J. D.; Schubert, M.; Mateker, W. R.; Bloking, J. T.; Burkhard, G. F.; Sellinger, A.; Fréchet, J. M. J.; Amassian, A.; Riede, M. K.; McGehee, M. D.; Neher, D.; Salleo, A., Efficient charge generation by relaxed charge transfer states at organic interfaces. Nat. Mater. 2013, 13, 63.

72. Murthy, D. H. K.; Gao, M.; Vermeulen, M. J. W.; Siebbeles, L. D. A.; Savenije, T. J., Mechanism of Mobile Charge Carrier Generation in Blends of Conjugated Polymers and Fullerenes: Significance of Charge Delocalization and Excess Free Energy. The Journal of Physical Chemistry C 2012, 116 (16), 9214-9220.

73. D'Avino, G.; Muccioli, L.; Olivier, Y.; Beljonne, D., Charge Separation and Recombination at Polymer–Fullerene Heterojunctions: Delocalization and Hybridization Effects. The Journal of Physical Chemistry Letters 2016, 7 (3), 536-540.

74. Feier, H. M.; Reid, O. G.; Pace, N. A.; Park, J.; Bergkamp, J. J.; Sellinger, A.; Gust, D.; Rumbles, G., Local Intermolecular Order Controls Photoinduced Charge Separation at Donor/Acceptor Interfaces in Organic Semiconductors. Adv. Energy Mater. 2016, 6 (6), 1502176.

75. Savoie, B. M.; Rao, A.; Bakulin, A. A.; Gelinas, S.; Movaghar, B.; Friend, R. H.; Marks, T. J.; Ratner, M. A., Unequal Partnership: Asymmetric Roles of Polymeric Donor and Fullerene Acceptor in Generating Free Charge. J. Am. Chem. Soc. 2014, 136 (7), 2876-2884.

76. Zusan, A.; Vandewal, K.; Allendorf, B.; Hansen, N. H.; Pflaum, J.; Salleo, A.; Dyakonov, V.; Deibel, C., The Crucial Influence of Fullerene Phases on Photogeneration in Organic Bulk Heterojunction Solar Cells. Adv. Energy Mater. 2014, 4 (17), 1400922.

77. Westacott, P.; Tumbleston, J. R.; Shoaee, S.; Fearn, S.; Bannock, J. H.; Gilchrist, J. B.; Heutz, S.; deMello, J.; Heeney, M.; Ade, H.; Durrant, J.; McPhail, D. S.; Stingelin, N., On the role of intermixed phases in organic photovoltaic blends. Energy Environ. Sci. 2013, 6 (9), 2756-2764.

78. Burke, T. M.; McGehee, M. D., How High Local Charge Carrier Mobility and an Energy Cascade in a Three-Phase Bulk Heterojunction Enable >90% Quantum Efficiency. Adv. Mater. 2014, 26 (12), 1923-1928.

79. Jamieson, F. C.; Domingo, E. B.; McCarthy-Ward, T.; Heeney, M.; Stingelin, N.; Durrant, J. R., Fullerene crystallisation as a key driver of charge separation in polymer/fullerene bulk heterojunction solar cells. Chem. Sci. 2012, 3 (2), 485-492

80. Arkhipov, V. I.; Heremans, P.; Bässler, H., Why is exciton dissociation so efficient at the interface between a conjugated polymer and an electron acceptor? Appl. Phys. Lett. 2003, 82 (25), 4605-4607

81. Ma, W.; Tumbleston, J. R.; Wang, M.; Gann, E.; Huang, F.; Ade, H., Domain Purity, Miscibility, and Molecular Orientation at Donor/Acceptor Interfaces in High Performance Organic Solar Cells: Paths to Further Improvement. Adv. Energy Mater. 2013, 3 (7), 864-872.

82. Tumbleston, J. R.; Collins, B. A.; Yang, L.; Stuart, A. C.; Gann, E.; Ma, W.; You, W.; Ade, H., The influence of molecular orientation on organic bulk heterojunction solar cells. Nat. Photonics 2014, 8, 385.

83. Gregg, B. A., Entropy of Charge Separation in Organic Photovoltaic Cells: The Benefit of Higher Dimensionality. The Journal of Physical Chemistry Letters 2011, 2 (24), 3013-3015.

84. Vithanage, D. A.; Devižis, A.; Abramavičius, V.; Infahsaeng, Y.; Abramavičius, D.; MacKenzie, R. C. I.; Keivanidis, P. E.; Yartsev, A.; Hertel, D.; Nelson, J.; Sundström, V.; Gulbinas, V., Visualizing charge separation in bulk heterojunction organic solar cells. Nat. Commun. 2013, 4, 2334.

85. Nan, G.; Zhang, X.; Lu, G., The lowest-energy charge-transfer state and its role in charge separation in organic photovoltaics. Phys. Chem. Chem. Phys. 2016, 18 (26), 17546-17556.

86. Holliday, S.; Donaghey, J. E.; McCulloch, I., Advances in Charge Carrier Mobilities of Semiconducting Polymers Used in Organic Transistors. Chem. Mater. 2014, 26 (1), 647-663

87. Coropceanu, V.; Cornil, J.; da Silva Filho, D. A.; Olivier, Y.; Silbey, R.; Brédas, J.-L., Charge Transport in Organic Semiconductors. Chem. Rev. 2007, 107 (4), 926-952.

88. A. Cheknane, H. Hilal, F. Djeffal, B. Benyoucef, and J. Charles, "An equivalent circuit approach to organic solar cell modelling", Microelectronics Journal, Vol. 39, pp. 1173–1180, 2008.

89. J. Zhang, S. Lee, and B. Sun, "Effect of Series and Shunt Resistance on OrganicInorganic Hybrid Solar Cells Performance", Electrochimica Acta, Vol. 146, pp. 845-849, 2014.

90. R. Pierret, Semiconductor Device Fundamentals. New York: Addison-Wesley Publishing Company, Inc., 1996.

91. J. Blakesley and D. Neher, "Relationship between energetic disorder and open circuit voltage in bulk heterojunction organic solar cells", Physical review B, Vol. 84, pp. 075210-12, 2011.

92. N. Nehaoua, , Y. Chergui, and D. Mekki, "Determination of organic solar cell parameters based on single or multiple pin structures", Vacuum, Vol. 84(2), pp. 326-329, 2009.

93. B. Qiab and J. Wang, "Fill factor in organic solar cells", Physical Chemistry Chemical Physics, Vol. 15, pp. 8972-8982, 2013.

94. U. Würfel, D. Neher, A. Spie and S. Albrecht, "Impact of charge transport on current–voltage characteristics and power-conversion efficiency of organic solar cells", Nature communications, Vol. 6, pp. 1-9, 2014

Chapter 2

2 Materials and Experimental Techniques

1.1 Introduction

Producing OPV devices consists of necessary parts where the material of the substance has an effect on processing each layer. If different materials are implemented in the device, there will be some alterations in the processing of active layers. In a lot of cases, even when the exact material is produced by various pathways, there would still be different requirements for processing. Therefore, it is important to carry out large amounts of investigations in order to find out the most suitable conditions for processing. Thus, the best performance is maintained for producing OPV devices. This chapter illustrates the full details of the material and experimental deposition techniques used in this research. Furthermore, the measurement techniques are thoroughly detailed. This is followed by illustration the reliant of this research titled as electric field induced second-harmonic generation (EFISHG). Finally, the Maxwell-Wagner model was presented to explain the physics behind charge accumulation on the interface due to the reliant on the microscopic characteristics of materials.

2.1 Material

2.1.1 Donor Material

Poly[2,6-(4,4-bis-(2-ethylhexyl)-4H-cyclopenta   [2,1-b;3,4-b′]dithiophene)   -alt-4,7   (2,1,3-benzothiadiazole)] (PCPDTBT), copolymer of cyclopentane dithiophene and benzothiadiazole, is a low band-gap polymer semiconductor mainly deployed for efficient OPV devices that have great charge-carrier characteristics. Thus, the polymer can better order and self-organize in the process of deposition causing an increase in the device's mobility [1-2]. Figure 2.1 shows the chemical

structure of the material. To approximate the HOMO level at 5.3 eV, LUMO level 3.6 eV and the bandgap 1.5 eV, both of optical and electrical characteristics of the PCPDTBT were applied [3-4].
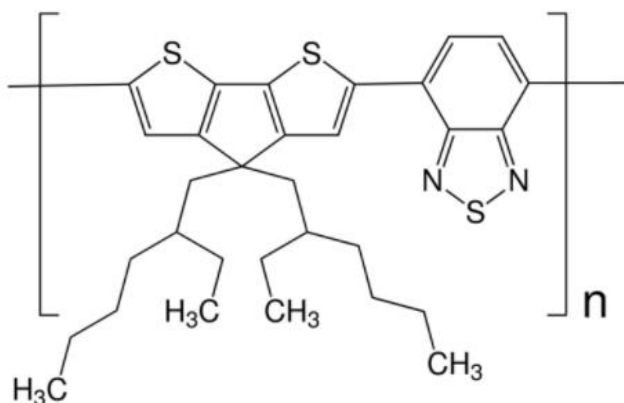
Figure 2.1: PCPDTBT structures

2.2   Accepter material

The familiar shortened form of fullerene derivative [6,6]-phenyl-C71-butyric acid methyl ester is known as PCBM. This type is tested mainly in organic solar cells [5]. In organic photovoltaic devices, PCBM is widely used as an electron acceptor, as well as it is a solubilized version of the buckminsterfullerene, C71. The fact that PCBM is soluble means that it dissolves in popular solvents that are used for donor polymers. In return, concurrent casting of both polymer and fullerene occur, as well as the production of a systematic bulk heterojunction. PCBM causes fast and coherent transfer of charge, as well as exciton dissociation when it is used in accordance with a donor polymer [6] whose electrons are highly mobile [7]. Presented in Figure. 2.2 is the chemical

structure of the material. In order to approximate the HOMO level at 6 eV, LUMO level 3.9 eV, both optical and electrical characteristics of the PC71BM were used.
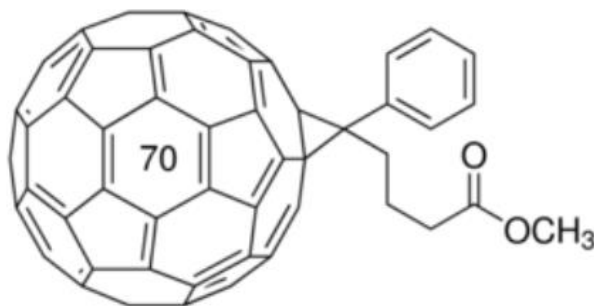
Figure 2.2: PC71BM structures

2.3   Transport material

Due to its hole conducting characteristics, Poly (3, 4-ethylenedioxythiophene) poly (styrenesulfonate) (PEDOT: PSS) is utilized in organic electronics. Before, it was used in transistors, buffers, or electrode materials as an active layer. That would occur in the middle of dielectric material and the gate electrode [8-10]. The most benefits of this material are the mechanical flexibility, satisfactory thermal stability, and great transparency. These characteristics enable it to be used in OSCs acting as an anode buffer layer [11-12]. The fact that its ionization potential is significant whilst its electron affinity is 2.2 eV, it is in the list of best hole-conducting buffers. In more details, its ionization potential is approximately equal to ITO work function and its electron affinity is low for stopping electrons [13]. Consisting of two isomers, it is a sole component polymer. One of the components is positive referred to (PEDOT), polythiophene polymer whilst the other is negative referred to (PSS), sodium polystyrene sulfonate polymer. For

the procedure ITO-anode contact, PEDOT: PSS mixture is involved [14-15]. The chemical structure of PEDOT-PSS is illustrated in Figure 2.3.
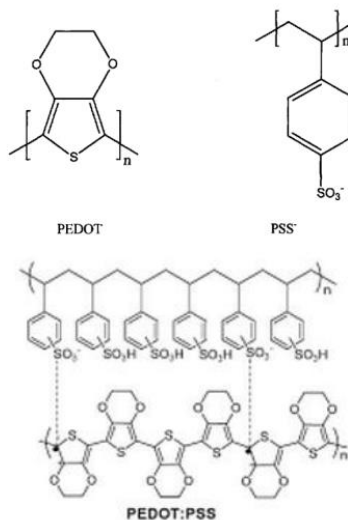
Figure 2.3: PEDOT, PSS and PEDOT: PSS structures

2.4   Deposition Techniques Used in This Investigation

2.5   Spin Coating

One of the quick and simple methods used to produce thin films is known as spin coating. The focus is placed on uniform thin organic films flat substrates. From various methods in the semiconductor manufacturing field, the most suitable developed technique is spin coating. Its applications are mostly noticed in organic insulators, photo resist, and semiconductors. Using spin coating method, the thickness of the films generated would be from nanometers to micrometers. Two factors affect the thickness of films; the material's concentration and the speed of the spin. As the speed of the spin increases, the layer of the film will be thinner. Throughout the operation, to ensure the layer is in a liquid form, either a lubricant or an oil is used. Moreover, to change the solid form into a liquid, a solvent is used [16].

2.6 Thermal Evaporation

A popular way of depositing metals like Aluminum, Gold and Chromium is thermal evaporation. This operation involves two stages where first the material is evaporated from a hot source, followed by condensing it on a cold plate. In order to come up with exact layers, the deposition process is done under high level vacuum system. Often, heating the material to its melting point followed by condensing it on a light substrate allows the generation of a thin film layer. Due to the variation between melting and condensing temperatures, a thin film layer is the result. However, both time and evaporation rate affect the film's thickness. It is important to maintain chamber's pressure below atmospheric pressure, so no reaction occurs between vapor and atmosphere. Typically, the pressure would be 10-6 Torr. The originality of the material decides evaporation temperature. Throughout the experiment, to control both film thickness and evaporation, a crystal monitor is found near the substrate. The reasons why thermal evaporation is widely used currently are due to both high wafer size and deposition rates [17].

2.7 Sample preparation

2.7.1 ITO

The first step is buying ITO-coated glass substrates from GEOMATEC. The glass substrate has dimensions of 10 cm × 10 cm consisting of a transparent ITO electrode of thickness 200 nm. The substrates were sliced into dimensions of 2.5 cm × 2.5 cm. Following this stage, for continuous 3 hours, at a temperature of 45 °C, shaping of the ITO via etching with $FeCl_2$ solution occurred. Ensuring there is no etching solution left in the modeled ITO-glass substrates, they were washed with distilled water. Further cleaning of the substrates occurred via ultrasonication where all of acetone, ethanol, and distilled water were used. This part was done twice, 10 minutes for each

solvent. For extra 3 hours, the substrates were placed in an oven to be dried at 80 °C. It is necessary to carry out UV-ozone treatment before any materials are deposited on the substrate.

2.7.2   Bulk Heterojunction (BHJ)

Fig. 2.4 (a) schematically shows the device structure of the BHJ based sandwich junctions and the experimental configuration. the BHJ films are designed with the device structure of ITO/BHJ/PEDOT:PSS/Au. In this aspect, the donor (PCPDTBT) with acceptor (PC71BM) are the main species of the active layer (BHJ). The amin solution was also made by solving 10 mg of PCPDTBT and 15 mg of PC71BM in 1 ml of chloroform. A glass plate was used substrate that decorated indium-tin-oxide (ITO) layer (10 Ω/sq). furthermore, 1500 rpm for 30 seconds was deployed as the spin-coating of the blended solution to deposit the film deposition onto the substrate. This in turn resulted a 150 nm thickness of the BHJ layer.

2.8   Hole transport layer

The following was made use of as a hole transport layer; P-type conducting polymer poly(3,4-ethylenedioxythiophene): polystyrene sulfonate (PEDOT:PSS). Under clear conditions, an ITO electrode had a PEDOT:PSS aqueous solution on top via spin-coating, keeping in mind that the solution was bought from Heraeus (Clevios, HTL solar). Then, ensuring a nitrogen atmosphere, the samples were annealed for a period of 15 minutes in an oven at 150 °C.

2.9   Electrode (Au, Ag)

In terms of evaporation, either electrodes Ag or Au were thermally evaporated via an evaporator. Respectively, evaporation rates for Au and Ag were 3~5 Å/s and 2~3 Å/s. Any electrodes that had a thickness of 100 nm were deposited as presented in Figure. 2.4 (b).

2.10 Encapsulation

To ensure no air damage occurs, the resultant samples were enclosed using a cover glass. For sticking the cover glass to the sample, a UV curable resin was the solution.
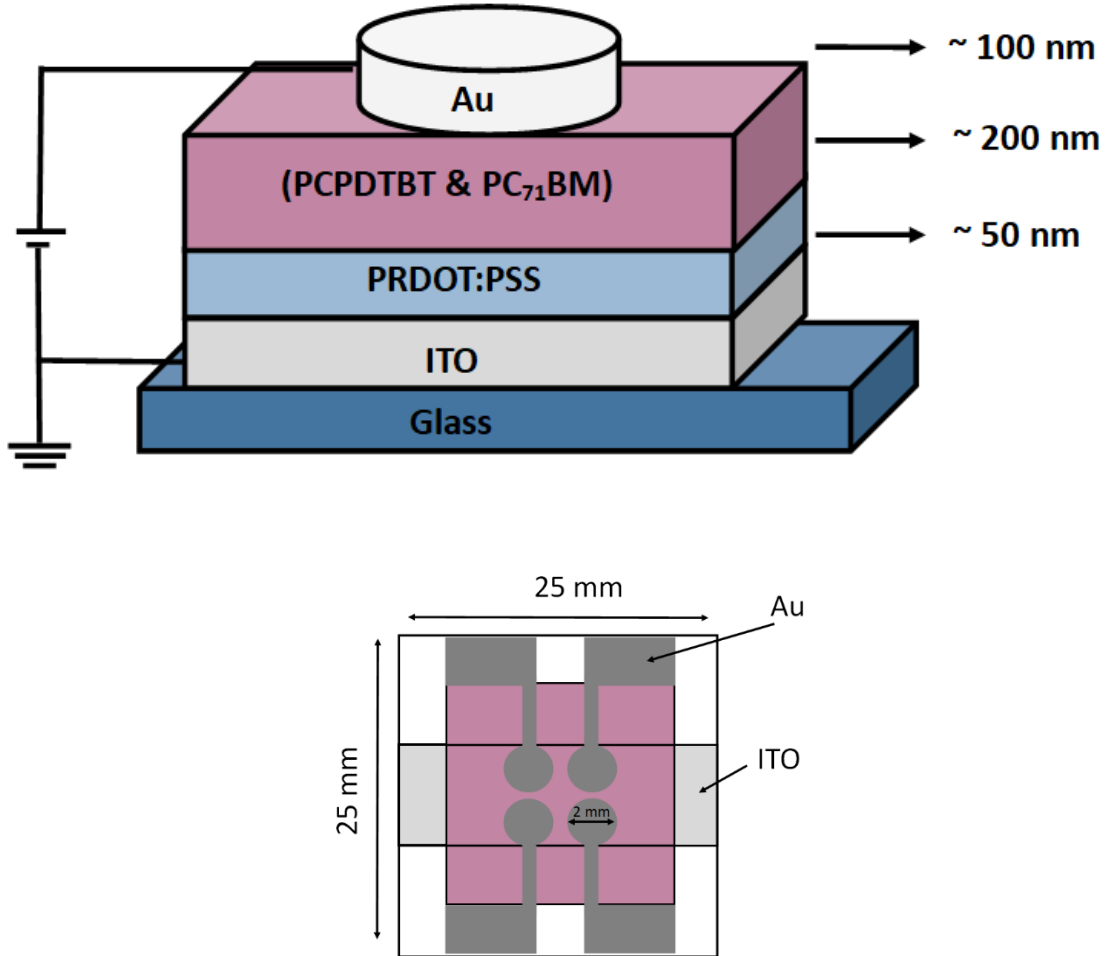
Figure 2.4: The structure of the solar cell sample. (a) Side view and (b) top view.

2.11 Measurement techniques

2.11.1 Characterization parameters of Organic solar Cells

As shown in Figure 2.5, using light illumination, a general solar cell current-voltage (I-V) is seen. The I-V properties in Figure 2.5 present photovoltaic factors being drawn out. Normally, the following points would be involved; short circuit current (Isc), open circuit voltage (Voc), and the maximum power (Pmax) of the device. In turn, these factors are used to come up with

the Fill Factor (FF). Figure 2.5 demonstrates FF as the proportion of the two rectangles and worked out via (Eq. 2.1).

$$FF = Pmax / Ptheoretical = = \frac{J_{max} \times V_{max}}{J_{sc} \times V_{OC}} \tag{2.1}$$

Using the proportion of maximum power (Pmax), the power conversion efficiency of the device (η) is found. It is decent to consider that the Pmax is produced due to incident optical power (Po). (Eq.2.2).

$$\eta = \frac{P_{max}}{Plight} = \frac{J_{max} \times V_{max}}{Plight} \times 100 \% \tag{2.2}$$
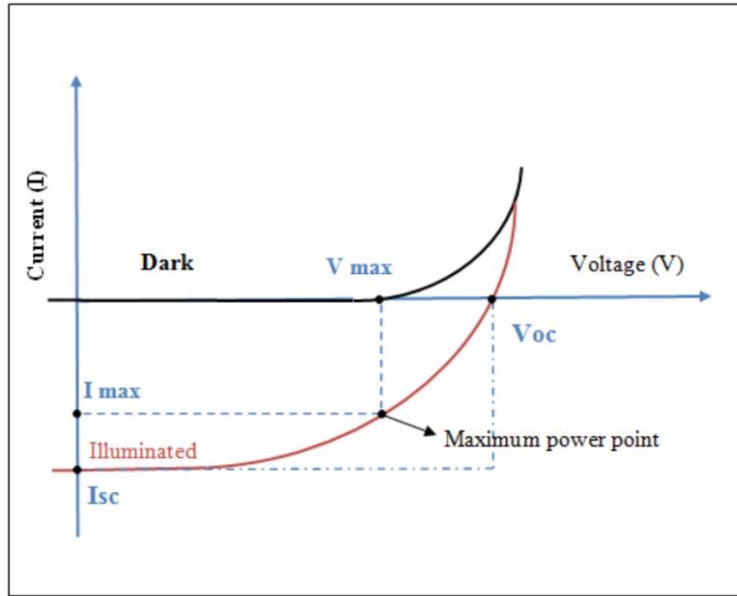
Figure 2.5: Typical I-V characteristics of a solar cell in dark and under illumination

2.11.2 Impedance spectroscopy (IS)

An analysis method used for minor signals is known as Impedance spectroscopy (IS). It is extensively used to characterize device factors [18]. When a minor AC signal is recognized by the device, ensuring multiple DC biasing circumstances, any parts of equivalent circuits are examined. In the year 1995, the first researchers trying impedance measurement on MEH-PPV were I.H. Campbell et al. [19] carried out experimental work and found that under a thin transparent, gold

had the positive contact whereas calcium had the negative one (Au/MEH-PPV/Ca). The reason is that capacitance does not depend on bias as all the polymer layer is consumed. In more details, when an increase is noted in a capacitance, it is because charging of the traps was perceived for a little forward bias. On the other hand, a decrease in capacitance is because neutralization of the traps was perceived for a higher forward bias. In the case of capacitance rise, an approximation of trap density is possible. A valued benefit of using impedance spectroscopy is that it is able to distinguish performance of interactions with a number of time constants. The work done by G. Yu et al. produced an accurate complicated admittance of polymer LECs [20]. The two gained advantages of using a pulsed driving scheme which involves the usage of both slow ionic response and rapid electronic response to monitor injection of the carrier. In conclusion, a distinguishable working strategy monitored the spread of ionic charges and the motion of electronic current. Another benefit of using impedance spectroscopy is its ability to differentiate between contributions of the interface from the bulk. This is especially when the equivalent circuit of device is familiar with the device physics. Consequently, this method was mainly used for the last ten years to characterize devices [21-22].

Throughout this study, Solectron 1260 impedance/gain-phase analyzer was used to carry out IS measurements where the frequency range was about 10 Hz -1 MHz ensuring pitch-black and under photo-illumination. Moreover, all the OSCs were short-circuited where a 10 mV AC voltage was used for the measurements. For IS measurements, it is necessary to use both equivalent circuit model and fitting techniques to analyze any findings. It is expected from the equivalent circuit model to accurately summarize and prototype all electrical characteristics for the device. Standardly, it would have both resistors and capacitors that demonstrate the outcome of multiple layers in the arrangement. To explain the data, comprehending the properties of AC is required.

For this current scenario, the final spectra were curve-fitted via the equivalent circuit of Maxwell-Wagner model. When it comes to the evaluation of organic devices, the physics is not fully comprehended so physical events taking place inside the device are not clear. However, OSCs consider any photovoltaic impact to be crucial. Regarding this, the aim is to discover a technique able to detect photovoltaic impact. However, analyzing organic photovoltaic impact requires more work to be done not only via IS measurement. Therefore, imbalance of the electric field in the organic layer needs to be known. Hence, more care is given to electric-field-induced second-harmonic generation (EFISHG) measurement. This type of measurement is able to probe electric field profile for organic devices considering carrier behaviors straight away [23-25]. Concluding, both EFISHG measurement with IS measurement should be used as a reliable direct image of interfacial phenomena associated with photovoltaic impact in OSCs is produced.

2.11.3 Electric-field-induced optical second-harmonic generation (EFISHG)

A conventional approach in the field of solar cells is called optical second harmonic generation (SHG). Whilst computing data, an intensive laser beams with the major wavelength being placed on the sample thus a second-harmonic signal is generated. As stated in the field of dielectric physics, materials consist of both electrons and positive charged cores. Moreover, any type of material that shows some insulating properties in electric fields produces polarization effects. Using Taylor series, polarization is enlarged in an electric field (involving external electric field, inner electric field such as generated by accumulated charge, electromagnetic wave electric field, etc.) as shown below:

$$P = P^{(1)} + P^{(2)} + P^{(3)} + \ldots = \chi^{(1)} : E + \chi^{(2)} : EE + \chi^{(3)} : EEE + \ldots \quad (2.3)$$

$P^{(1)}$, $P^{(2)}$ and $P^{(3)}$ denote the linear, quadratic, and cubic polarization in the electric field (E). $\chi^{(1)}$, $\chi^{(2)}$ and $\chi^{(3)}$ are the first-, second-, and third-order electric susceptibilities (or linear, first-, and second-nonlinear electric susceptibilities), respectively. Moreover, the operation ":" is an outlay of the scalar product between matrices. As greater susceptibility is more likely to be insignificant, higher order polarization has decreased effects. Up until the 1960s, higher order of polarization which is also known as nonlinear polarization was just discovered. At the same time, the strong laser was evolved in order to examine non-linear optics, keeping in mind the laser consists of a significant electric field, mainly 1 MV/cm.

This study focuses more on $P^{(2)}$ as it emphasizes second-order nonlinear optical phenomena. It is known that polarization vector is linked to the product of the two electric field vectors by electric susceptibility. Thus, it is a tensor of rank 3. The explanation behind this is that it consists of 27 parts and is still considered a 3×3×3 matrix. More clearly, by using laser light (a frequency of ω), any material that has inversion symmetry indicates that all of the 27 parts have disappeared. Hence, no second order polarization phenomenon occurs so no second harmonic generation (SHG) having a frequency of 2ω is noted. In contrast, any material that has non-inversion symmetry spots SHG. So, a material that has inversion symmetry cannot be used to spot SHG signal. As external electric field impacts the material's electronic spread, this study's lab has come up with a distinguished strategy known as electric field induced second-harmonic generation (EFISHG). As the electronic spread is altered, the symmetry is shown in Fig. 2.7. Furthermore, the presence of organic layers causes an EFISHG signal to be generated via laser irradiation. This process takes place due to combining electrons in molecules and electro-magnetic waves E(ω) in the existence of electrostatic local electric field E (0). The EFISHG intensity is specified as [25-26]

$$I\,(2\omega) \propto \left| \vec{P}\,(2\omega) \right|^2 \quad \vec{P}(2\omega) = \chi^{(3)}\,(-2\omega, 0, \omega, \omega) : E(0)E(\omega)E(\omega) \quad (2.4)$$

$\vec{P}$ (2ω) denotes the nonlinear polarization generated in the organic layers and $\chi^{(3)}$ is the third order nonlinear susceptibility tensor. The electrostatic local field in organic layers is given the symbol E (0) where the positive electric field E (0) points from the Au electrode to the ITO electrode. Besides, the electric field of incident laser beam is given the symbol E (ω). Essentially, the square-root of the SHG intensity is proportional to the electric field E (0) in organic layers as the equation supports. In this case, E (0) is derived from E0+Es, where E0 (E0 = $Q_m / \varepsilon_r \varepsilon_0$) is the electric field derived from charges $\pm Q_m$ on top and bottom electrodes of the OSCs. The E_s is the electric field originated from charges in organic devices, such as charges Q_s gathered at the double-layer interface. Accordingly, the charges $\pm Q_m$ on electrodes and charges Q_s at the interface are both probed by EFISHG measurement.
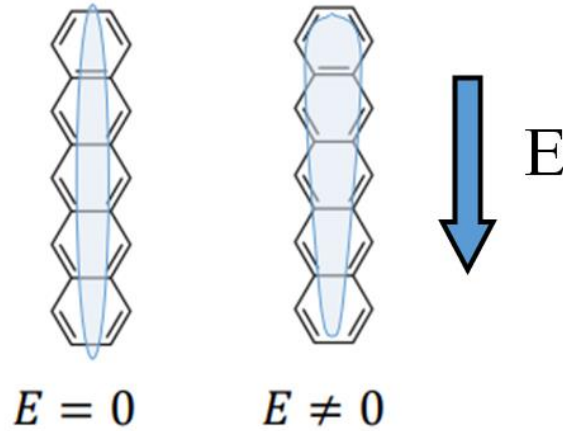

Figure 2.6. Sketch of distortion of electronic cloud for a pentacene molecule under external electric field.

2.12 Experimental methods

As depicted from Figure 2.7, an experimental structure for EFISHG measurement is performed. To offer probing light, a pulsed laser was the option. The light has a repetition rate of 10 Hz, a mean power of 1 mW lasting for 4 ns. In order for generation to take place, an optical parametric oscillator pumped with third-harmonic light of Q switched Nd:YAG laser were used. The incident angle at which the p-polarized pulsed laser beam emphasized on is 45°, ensuring the spot size was minor in comparison to the device area. By using both optical filters and monochromator, removal of reflected fundamental laser beam was possible. In terms of measurements, a photomultiplier tube (PMT) was used to spot SHG light given by the specimen. In addition, a digital multimeter was used to compute the intensity I (2ω). Presented in eq. (2.4) is the susceptibility tensor $\chi^{(3)}$ which is a substance dependent parameter as well as being a function of the optical frequency ω. To accurately probe layers of BHJ OSCs in an electric field, the variation in $\chi^{(3)}$ amongst materials enables this stage to take place. This happens where a suitable laser beam wavelength is chosen [15]. For almost all the studies, a laser beam of wavelength λ_ω=1080 nm was selected where the created SHG at a wavelength of $\lambda_{2\omega}$=540 nm was noted down. The reason behind this is to particularly compute the electric field in $PC_{71}BM$ layer. In terms of time resolved SHG measurements, OSCs were lightened using several states. Under a red illumination, photocurrent was the result keeping in mind a 50 ms illumination with an intensity of 10 mW/cm^2 accompanied with a 50 ms break. The cause is the LED being synchronized with the incidence laser beam. On the other hand, for short-circuit state, each interface of OSCs is supposed to have a gathering of extra charges Q_s. The Maxwell–Wagner effect causes this as well as exciton separation being triggered at the interface. It is necessary to consider that electric fields in OSCs will be altered when there is charge Q_s . In turn, the alteration in electric fields is probed by EFISHG.
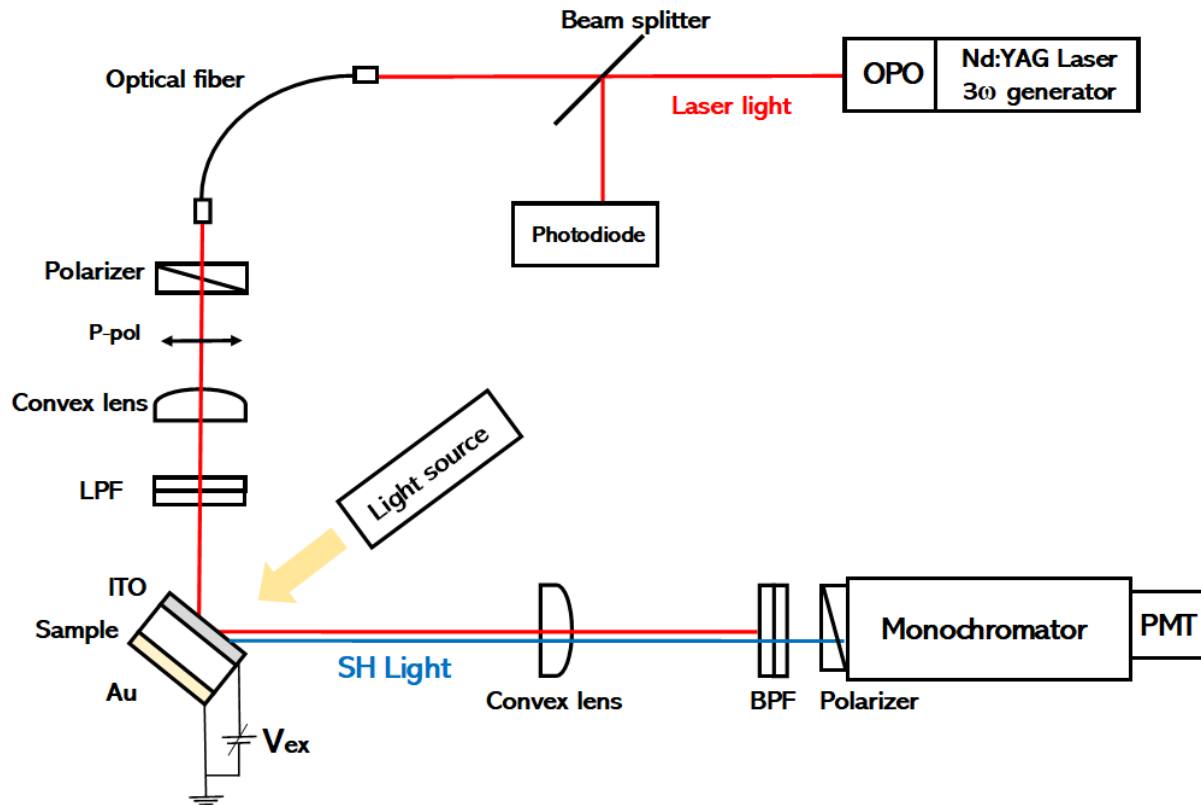
Figure 2.7: Experimental setup for EFISHG measurement

2.13 Maxwell-Wagner model

Mostly depending on the microscopic characteristics of materials, the MW model is the appropriate tool used to explain the physics behind charge accumulation on the interface [25, 27]. As the theory of Maxwell's electromagnetic field [27-29], an accumulation of charge Q_s is found at the interface right in the middle of two dielectric materials. These materials have non-similar relaxation times as stated by ($\tau=\varepsilon/\sigma$, where ε is the dielectric constant and σ is the conductivity) when current I(t) moves throughout the two-material interface [30]. To be more exact, $\nabla \bullet j = 0$ with $j = E\sigma \neq 0$ is accomplished as steady state current density j moves throughout the interface.

For this scenario, being originally from the interface, the below relation considers electric flux density D

$$\nabla \cdot D = \nabla \cdot (\varepsilon E) = \nabla \cdot \frac{\varepsilon}{\sigma} \mathbf{j} = Q_s \qquad (2.5)$$

As understood from the Maxwell-Wagner impact, an accumulation of Q_s is found at the interface as two adjoining materials each have a distinguished relaxation time [26]. In simpler words, this idea portrays the chance of Q_s accumulation taking place at the PCPDTBT-PC71BM interface once charge is being injected from a source electrode.

To fully comprehend charge accumulation and carrier transport in BHJ OSCs, an equivalent circuit was used as illustrated in Figure 2.8. This clearly presents interfacial charging and discharging processes taking place as an impact of Maxwell-Wagner theory. The modelling process of layers happens a paralleled circuit containing both a conductor (G1, G2) and a capacitor (C1, C2). In OSCs, organic thin films are identified using two macroscopic physical factors. Independently, these would be dielectric constant $\varepsilon_{1,2}$ and conductivity $\sigma_{1, 2}$. The mentioned relaxation time is derived from the ratio ε/σ where it represented extra charge carriers being distributed throughout the material. Once an elapsed time of $\tau = \varepsilon/\sigma$ occurs, a steady-state charge spread is confirmed. It is also important to realize that conductivity is proportional to carrier density n_0, and can be computed using $\sigma = \varepsilon n_0 \mu$. At thermodynamic equilibrium, the carrier density n_0 is known to be intrinsic carrier density of materials. The electro-magnetic field theory states that the overall current moving through an organic material is the total of both conduction and displacement current. For conduction and displacement currents, the current density j can be achieved from σE and dD/dt with D = εE, independently. In this case, the electric field is E and electric flux density is D. In a mean electric field, the drifts of carriers are used to explain charge transport in organic

films. This is where the square root of time dependency alongside the direction of the electric field is accomplished.
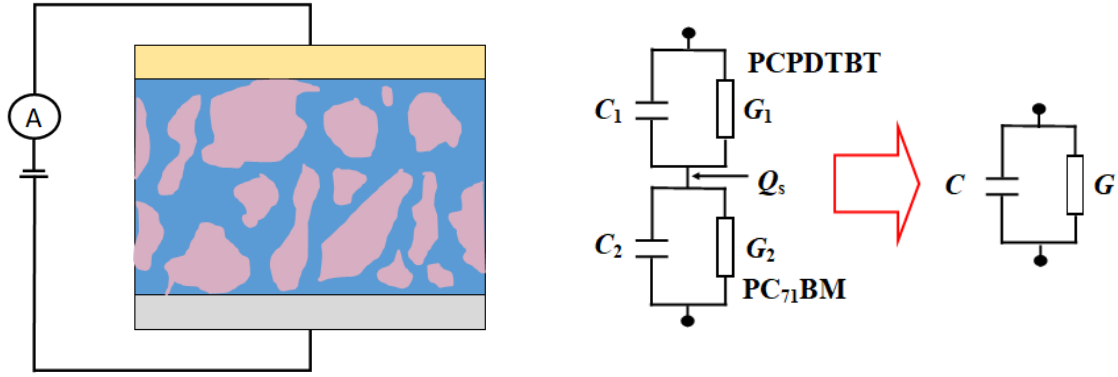
Figure 2.8. Model of BHJ for Maxwell-Wagner effect

As a result of relaxation time variation in the distinguished organic layers, the Maxell-Wagner effect notes that any extra charge accumulation takes place right in the middle interface of the two layers. Using the simplistic model of OSCs, charges density on both top and bottom electrodes can be computed (Q1 and Q2) as shown below:

$$Q_1 = -\frac{C_1 C_2}{C_2 + C_1} V - \frac{C_1}{C_2 + C_1} Q_s \qquad (2.6)$$

$$Q_2 = -\frac{C_1 C_2}{C_2 + C_1} V + \frac{C_1}{C_2 + C_1} Q_s \qquad (2.7)$$

For both Eqs. 1.2 and 1.3, the external voltage that is given to the two electrodes is called Vex whereas the charge density that is collected on the interface between the organic and insulator layer is called Q_s. If equivalent circuits are used, it is possible to determine charge density on the

interface Q_s. Noticed from Figure 2.8, organic and insulator layer has all G_1, C_2, G_2 and C_2 as unit conductance and capacitance.

$$Q_s = -\frac{G_2}{G_2+G_1} VC_1 - \frac{G_1}{G_2+G_1} VC_2 = -\frac{G_2 G_1}{G_2+G_1}(\tau_2 - \tau_1)V \qquad (2.8)$$

From a different perspective, the admittance Y of the double layer system is demonstrated as

$$Y = G + j\omega C = \frac{1}{Z} = \frac{1}{\frac{1}{G_1+j\omega C_1}+\frac{1}{G_2+j\omega C_2}} \qquad (2.9)$$

With
$$G = \frac{G_1 G_2}{G_1+G_2} + \frac{(G_1 G_2 - G_1 G_2)^2}{(G_1+G_2)^3} \cdot \frac{\omega^2}{1+\tau_{MW}^2 \omega^2} \qquad (2.10)$$

And
$$C = \frac{C_1 C_2}{C_1+C_2} + \frac{(C_1 C_2 - C_1 C_2)^2}{(C_1+C_2)^3} \cdot \frac{\tau_{MW}^2}{1+\tau_{MW}^2 \omega^2} \qquad (2.11)$$

where a response time $\tau_{MW} = \frac{1}{\omega_{MW}} = \frac{C_1+C_2}{G_1+G_2}$

Specifically, the Maxwell-Wagner effect shows the charge Q_s accumulation being linked to response time τ_{MW} at the interface right between layers 1 and 2 [31]. The equivalent circuit enables Q_s (t) to be discovered as

$$Q_s(t) = Q_s(\infty)[1 - \exp\left(-\frac{t}{\tau_{MW}}\right)] \qquad (2.12)$$

once employment of step external voltage V_{ex} takes place. This is where:

$$Q_s(\infty) = I_C\left(\frac{C_2}{G_2} - \frac{C_1}{G_1}\right) \text{ with } I_C = V_{ex}\frac{G_1 G_2}{G_{11}+G_2} \qquad (2.13)$$

All the way throughout the double-layer system, I_C is the conduction current moving around. As depicted by Eq. (2), $Q_s(t) = 0$ as $\frac{C_1}{G_1} = \frac{C_2}{G_2}$ ($\tau_1 = \tau_2$). However, it is required to consider that $Q_s(t)$ $\neq 0$ as $\frac{C_1}{G_1} \neq \frac{C_2}{G_2}$ ($\tau_1 \neq \tau_2$). In correspondence to this, if $\tau_1 = \tau_2$, both second terms of G and C

which are found in Eq. (1) are zero. However, they would be non-zero if $\tau_1 \neq \tau_2$. Hence, in IS spectrum, the Maxwell-Wagner type relaxation is present at angular frequency where $\omega_{MW} = \tau_{MW}^{-1}$. On the other hand, it is absent if $\tau_1 = \tau_2$. The plotting of both C (ω) and G (ω)/ω is presented in Figure 2.9 close to the frequency of ω_{MW}, where C_L and C_H are the capacitance in the limit $f \rightarrow 0$ and $f \rightarrow \infty$, independently. It is notable to consider the presence of dielectric relaxation in actual devices as a result to charging onto electrode with a response time $\tau_{MW} = R_0 C_t$. This occurs as C_t is the final series capacitance for the device as shown in Figure 2.9., $C_t = \frac{C_1 C_2}{C_1 + C_2}$. As a result, for a great frequency limit ($\rightarrow \infty$), an alteration in capacitance from C_H (=C_t) to zero happens.

In the preceding work, the Maxwell–Wagner (MW) model was favorably used to evaluate interfacial phenomena for bulk-layer organic devices. As an example, bulk layer organic light-emitting diode (OLED). The findings proved the evaluation's potentiality to rely on dielectrics physics technique [31-33]. In conclusion, these findings encouraged more research to be done for employing the MW model in evaluating carrier injection and transport processes in OSCs.
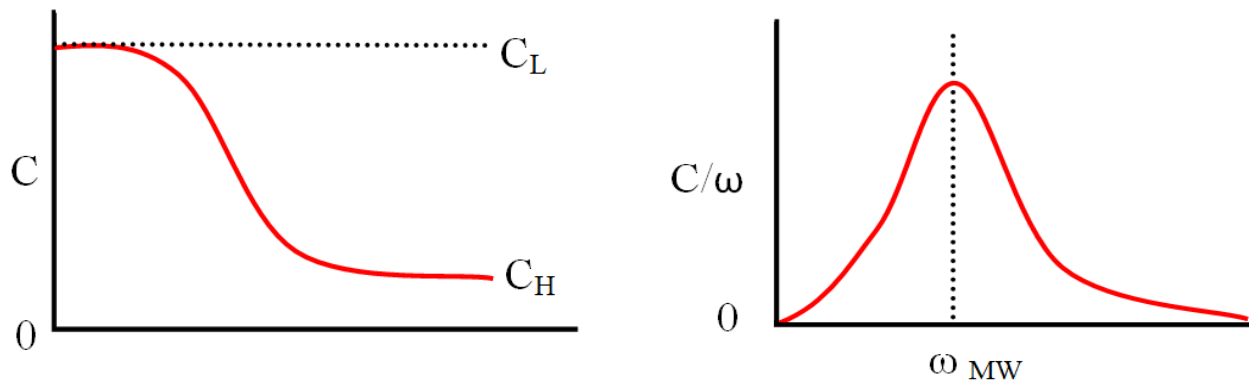
Figure 2.9. C (ω) and G (ω)/ω plots in frequency domain.

2.14 Summary

This chapter presented the necessary information of this research including the most important materials used to process each layer of the OPV device. Also, the full details of the experimental deposition techniques and measurement techniques are intensively described. To systematically elaborate the used measurements method, this chapter is critically analyzed the electric field induced second-harmonic generation (EFISHG). Lastly, the physical explanation behind the charge accumulation on the interface is referred to the Maxwell-Wagner model that successfully used in this research.

2.15 Bibliography

1. Pratyusha, T., Sivakumar, G., Yella, A., & Gupta, D. (2017). Novel ternary blend of PCDTBT, PCPDTBT and PC70BM for the fabrication of bulk heterojunction organic solar cells. Materials Today: Proceedings, 4(4), 5067-5073.

2. Fischer, F. S., Trefz, D., Back, J., Kayunkid, N., Tornow, B., Albrecht, S., ... & Brinkmann, M. (2015). Highly Crystalline Films of PCPDTBT with Branched Side Chains by Solvent Vapor Crystallization: Influence on Opto-Electronic Properties. Advanced Materials, 27(7), 1223-1228.

3. Ahmad, Z., Touati, F., Muhammad, F. F., Najeeb, M. A., & Shakoor, R. A. (2017). Effect of ambient temperature on the efficiency of the PCPDTBT: PC 71 BM BHJ solar cells. Applied Physics A, 123(7), 486.

4. Kowalski, S., Allard, S., & Scherf, U. (2012). Synthesis of Poly (4, 4-dialkyl-cyclopenta [2, 1-b: 3, 4-b′] dithiophene-alt-2, 1, 3-benzothiadiazole)(PCPDTBT) in a Direct Arylation Scheme. ACS Macro Letters, 1(4), 465-468.

5. Björström, C. M., Bernasik, A., Rysz, J., Budkowski, A., Nilsson, S., Svensson, M., ... & Moons, E. (2005). Multilayer formation in spin-coated thin films of low-bandgap polyfluorene: PCBM blends. Journal of Physics: Condensed Matter, 17(50), L529.

6. Kraabel, B., Hummelen, J. C., Vacar, D., Moses, D., Sariciftci, N. S., Heeger, A. J., & Wudl, F. (1996). Subpicosecond photoinduced electron transfer from conjugated polymers to functionalized fullerenes. The Journal of chemical physics, 104(11), 4267-4273.

7. Von Hauff, E., Dyakonov, V., & Parisi, J. (2005). Study of field effect mobility in PCBM films and P3HT: PCBM blends. Solar energy materials and solar cells, 87(1-4), 149-156.

8. Guerrero, A., Marchesi, L. F., Boix, P. P., Ruiz-Raga, S., Ripolles-Sanchis, T., Garcia-Belmonte, G., & Bisquert, J. (2012). How the charge-neutrality level of interface states controls energy level alignment in cathode contacts of organic bulk-heterojunction solar cells. ACS nano, 6(4), 3453-3460.

9. Chen, F. C., Chu, C. W., He, J., Yang, Y., & Lin, J. L. (2004). Organic thin-film transistors with nanocomposite dielectric gate insulator. Applied physics letters, 85(15), 3295-3297.

10. Khodagholy, D., Doublet, T., Quilichini, P., Gurfinkel, M., Leleux, P., Ghestem, A., ... & Malliaras, G. G. (2013). In vivo recordings of brain activity using organic transistors. Nature communications, 4(1), 1-7.

11. Haddock, J. N., Zhang, X., Domercq, B., & Kippelen, B. (2005). Fullerene based n-type organic thin-film transistors. Organic Electronics, 6(4), 182-187.

12. Cruz-Cruz, I., Tavares, A. C., Reyes-Reyes, M., López-Sandoval, R., & Hümmelgen, I. A. (2014). Interfacial insertion of a poly (3, 4-ethylenedioxythiophene): poly (styrenesulfonate) layer between the poly (3-hexyl thiophene) semiconductor and cross-linked poly (vinyl alcohol) insulator layer in organic field-effect transistors. Journal of Physics D: Applied Physics, 47(7), 075102.

13. Su, Z., Wang, L., Li, Y., Zhao, H., Chu, B., & Li, W. (2012). Ultraviolet-ozone-treated PEDOT: PSS as anode buffer layer for organic solar cells. Nanoscale research letters, 7(1), 465.

14. Han, Y. K., Chang, M. Y., Huang, W. Y., Pan, H. Y., Ho, K. S., Hsieh, T. H., & Pan, S. Y. (2011). Improved performance of polymer solar cells featuring one-dimensional PEDOT nanorods in a modified buffer layer. Journal of The Electrochemical Society, 158(3), K88.

15. Bello, A., Giannetto, M., Mori, G., Seeber, R., Terzi, F., & Zanardi, C. (2007). Optimization of the DPV potential waveform for determination of ascorbic acid on PEDOT-modified electrodes. Sensors and Actuators B: Chemical, 121(2), 430-435.

16. Hickmott, T. W. (1962). Low-frequency negative resistance in thin anodic oxide films. Journal of Applied Physics, 33(9), 2669-2682.

17. Petty, M. C. (2008). Molecular electronics: from principles to practice. John Wiley & Sons.

18. M. J. Ross and K. R William, Impedance Spectroscopy: Emphasizing Solid Materials and Systems, John Wiley & Sons, New York, 1987.

19. Campbell, I. H., Smith, D. L., & Ferraris, J. P. (1995). Electrical impedance measurements of polymer light-emitting diodes. Applied Physics Letters, 66(22), 3030-3032.

20. Yu, G., Cao, Y., Zhang, C., Li, Y., Gao, J., & Heeger, A. J. (1998). Complex admittance measurements of polymer light-emitting electrochemical cells: Ionic and electronic contributions. Applied physics letters, 73(1), 111-113.

21. Lin, J., Weis, M., Taguchi, D., Manaka, T., & Iwamoto, M. (2009). Carrier injection and transport in organic field-effect transistor investigated by impedance spectroscopy. Thin Solid Films, 518(2), 448-451.

22. Taguchi, D., Shino, T., Zhang, L., Li, J., Weis, M., Manaka, T., & Iwamoto, M. (2011). Direct probing of photovoltaic effect generated in double-layer organic solar cell by

electric-field-induced optical second-harmonic generation. Applied physics express, 4(2), 021602.

23. Chen, X., Taguchi, D., Lee, K., Manaka, T., & Iwamoto, M. (2011). Analyzing interfacial carrier charging in pentacene/C60 double-layer organic solar cells by optical electric field induced second-harmonic generation measurement. Chemical Physics Letters, 511(4-6), 491-495.

24. Chen, X., Taguchi, D., Shino, T., Manaka, T., & Iwamoto, M. (2011). Analysis of interface carrier accumulation and relaxation in pentacene/C60 double-layer organic solar cell by impedance spectroscopy and electric-field-induced optical second harmonic generation. Journal of Applied Physics, 110(7), 074509.

25. Maxwell, J. C. (1954). Treatise on Electricity and Magnetism, 2 vols., reprint by Dover. New York.

26. Manaka, T., Lim, E., Tamura, R., & Iwamoto, M. (2007). Direct imaging of carrier motion in organic transistors by optical second-harmonic generation. Nature photonics, 1(10), 581-584.

27. K. W. Wagner, Electrical Engineering (Archiv fur Elektrotechnik), 2, (1914) 371.

28. Pierret, R. (1996). Semiconductor Device Fundamentals, Addision-Wesley. Reading, Massachusetts.

29. Sze, S. M., & Ng, K. K. (2006). Physics of semiconductor devices. John wiley & sons.

30. Manaka, T., Lim, E., Tamura, R., Yamada, D., & Iwamoto, M. (2006). Probing of the electric field distribution in organic field effect transistor channel by microscopic second-harmonic generation. Applied physics letters, 89(7), 072113.

31. Lim, E., Manaka, T., Tamura, R., & Iwamoto, M. (2006). Maxwell–Wagner model analysis for the capacitance–voltage characteristics of pentacene field effect transistor. Japanese journal of applied physics, 45(4S), 3712.

32. Taguchi, D., Shino, T., Zhang, L., Li, J., Weis, M., Manaka, T., & Iwamoto, M. (2011). Direct probing of photovoltaic effect generated in double-layer organic solar cell by electric-field-induced optical second-harmonic generation. Applied physics express, 4(2), 021602.

33. Zhang, L., Taguchi, D., Li, J., Manaka, T., & Iwamoto, M. (2010). Probing of interfacial charging and discharging in double-layer devices with a polyimide blocking layer by time-resolved optical second harmonic generation. Journal of Applied Physics, 108(9), 093707.

Chapter 3

3 Spectroscopic study of EFISHG from PCPDTBT and PC$_{71}$BM thin films

3.1 Introduction

The bulk heterojunction (BHJ) organic solar cells are registered as the highly efficient type of solar cells and therefore remarkable efforts were paid from both academic and industrial sectors to improve its efficiency. BHJ holds a blended structure that comprises a combination of conjugated polymer and fullerene derivatives. More specifically, a donor of electron and acceptor of electron organic materials are forming the blended structure of BHJ that mixed to attain charge separation after photoexcitation [1]. Interestingly, the continuous research result to develop a novel structure of fabricated polymeric material and high-performance additives, interlayers and improved tiny donor materials. Therefore, the total power generation of organic solar cells of BHJ is significantly improved [2-7]. Statistically, the PCE of organic cells has been improved by 12% compared to conventional fullerene-based structures [9-10]. However, the fabrication of tiny molecule BHJ is not easy where a possibility of increased charge recombination with low fill factor are still valid for low material purity [11-12]. Thus, the morphology of pure materials and efficient blending procedure are important to fabricate organic solar cells.

The existence of blocking layer in organic solar cells would affect the charge transportation via the carrier that needs to be understood well. Moreover, another challenge of accumulated charges at the interfacial area would reason an altered electric field distribution due to the impact of Maxwell-Wagner (MW). This has entirely a notable effect on the power generation as a result to the dielectric nature of donor and acceptor organic materials. Thus, examining the electric

field would possibly pave the way to perceive the behavior of charge carrier to improve the efficiency of organic solar cells.

As stated above, the materialization of both donor and acceptor has a vital role to upgrade the generated charge transportation. consequently, several studies were derived to amend the morphology of organic solar cells that employed AFM, and TEM. However, primitive measurement methods used to explore the charge transportation between donor and acceptor layers are not professional tool. Therefore, to perceive the behavior of charge carrier and transfer phenomenon, it is crucial to locate a promoted electric field in both layers. This chapter intends to explore the charge transportation via the carrier in BHJ organic solar cells type poly [2,6-(4,4-bis-(2-ethylhexyl) - $4H$ – cyclopenta [2,1-b;3,4-b'] dithiophene) – alt - 4,7 - (2,1,3-benzothiadiazole)] (PCPDTBT) and [6,6] -phenyl C_{71} butyric acid methyl ester (PC$_{71}$BM), using a selective measurement of the electric-field-deduced optical second harmonic generation (EFISHG).

3.2   Fabrication process

3.2.1   Single layer of PC$_{71}$BM material

The fabrication a single layer of organic solar cells of PC$_{71}$BM requires a mixing of 10mg with 1ml of chloroform solvent. The prepared solution should be preserved in an ultrasonic bath for a period of three hours until a complete dissolving is accomplished with appearing of a bright red color. To systematically achieve that, spin-coating at 2000 rpm for 30 seconds at a thickness of about 100 nm was used to attain a full deposition. Afterwards, a low thermal evaporation rate of 1 A/s would guarantee the steady state deposition of an active electrodes thin layer of deposited silver of 0.12cm^2.
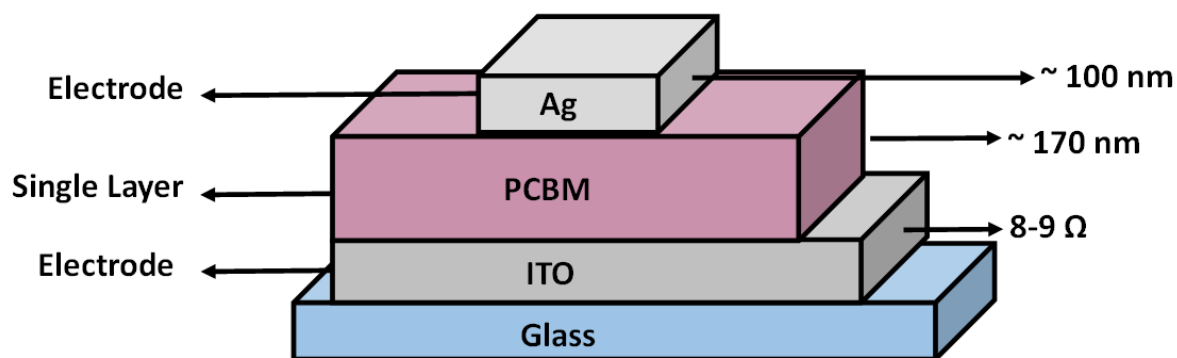
Figure 3.1. PC$_{71}$BM structure

3.2.2   Single layer of PCPDTBT material

The fabrication a single layer of organic solar cells of PCPDTBT necessitates a mixing of 20mg with 1ml of chloroform solvent. The prepared solution should be preserved in an ultrasonic bath for a period of more than three hours for a period time of three hours until a complete dissolving is accomplished with appearing of a bright green color. To systematically achieve that, spin-coating at 2000 rpm for 30 seconds at a thickness of 100nm was used to attain a full deposition. Afterwards. a low thermal evaporation rate of 1 A/s would guarantee the steady state deposition of an active electrodes thin layer of silver.
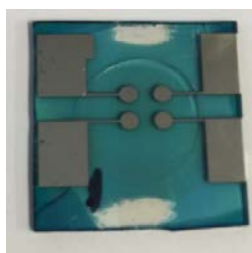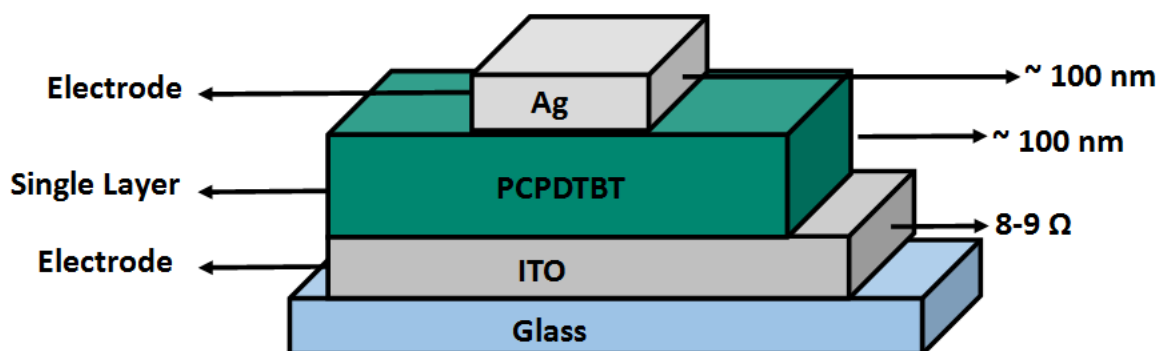
Figure 3.2. PCPDTBT Material Structure

3.2.3 Single layer of Bulk heterojunction structure

The experimental procedure of preparing organic solar cells of BHJ using both PCPDTBT: PC$_{71}$BM materials is presented in Figure 3.3. Moreover, Figure 3.3 depicts the equal RC circuit of the fabricated solar cells. However, the fabrication step should come after cleaning the Indium Tin Oxide (ITO) coated glass substrates using an ultrasonic bath of acetone, ethanol, and distilled water. The ITO coated glass was then left to be fully dried and then process by UV ozone to remove any organic residuals. This technique deduces 25 mg/ml concentration of mixed chloroform solutions of volume ratio of 1:1.5 of PCPDTBT and PC$_{71}$BM, respectively. However, thick films of PCPDTBT and PC$_{71}$BM BHJ are left on the top of Indium Tin Oxide and then dried at ambient temperature. This is also processed by post thermal annealing for one quarter of hour at 130 °C. Lastly, Au electrodes of 100nm thickness are formed on the surface of BHJ film of PCPDTBT and

PC$_{71}$BM with a thickness of 100 nm onto the surface of the BHJ film. The typical area used of the organic solar cells is approximately 3.1 mm^2.
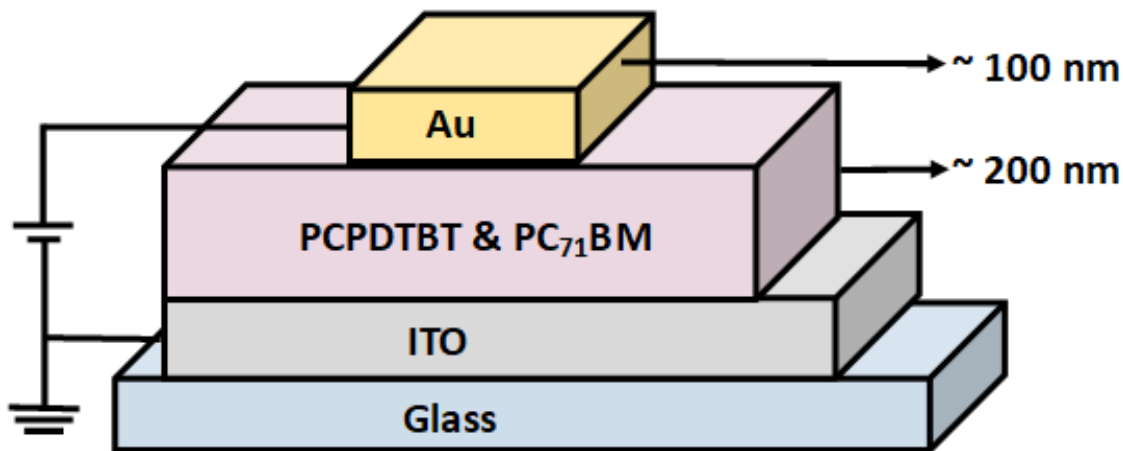

Figure 3.3. Structure of BHJ organic solar cells

3.3   Absorption spectra

The variation of three behaviors of optical absorption spectra of BHJ, PCPDTBT and PC71BM against the Ultraviolet (wavelength) are shown in Figure 3.4. This is implicitly depicted the three registered spectra of three structures. Occasionally, Figure 3.4 illustrates that the molecules of PCPDTBT structure are originally thrilled between 730-750 nm while PC71BM molecules are thrilled between 500–530 nm. Moreover, the BHJ materials are also thrilled and absorbed the light of wavelength between 730-750 nm. In this regard, 700 nm represents the peak position of the light absorption. Furthermore, these results confirm that PCPDTBT is the key material of light absorption due to its high eV of around 1.5.
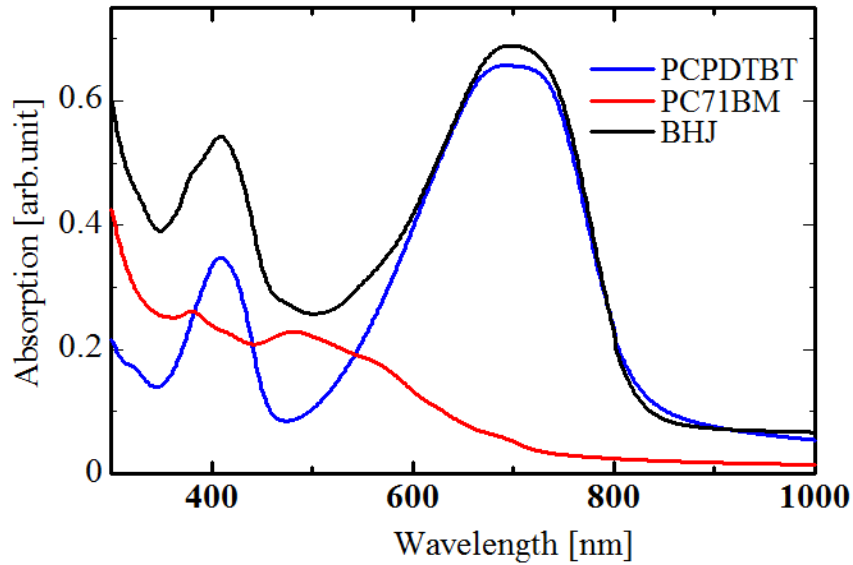
Figure 3.4. Absorption spectra of PCPDTBT, PC71BM, and BHJ

3.4 Electrical characterization

to evaluate the features of current-voltage (I-V) of any selected solar cell, it is important to measure the (I-V) in two fields of no incident light illumination and incident light illumination. Clearly, A PC controlled Keithley 2400 was deployed to calculate the I-V characteristics. The 1 sun illumination capacity was supplied via a tungsten halogen light source lamp of 50 mW directed into the solar cell. A light intensity meter was used to identify the capacity of the subjected light that already set to be 1.5 G of AM radiation equivalent to 100 mW/cm². In this regard, the bias voltage supplied to the Au electrode was applied to evaluate the I-V characteristics of the solar cells at the time of grounding the ITO electrode. The solar cells characterization comprises two bias scans under dark and light illumination fields. Each scan initiated from -1V and finished at +1V with considering a voltage step of 0.1V.

Figure 3.5. shows the characteristics of BHJ organic solar cells and the associated correlation between the J_{sc} and supplied voltage under dark and illumination fields. Specifically, BHJ works

as a photovoltaic cell of an open-circuit voltage of 0.41V, short-circuit current density of 2.71 mA/cm^2, and fill factor of 0.30.
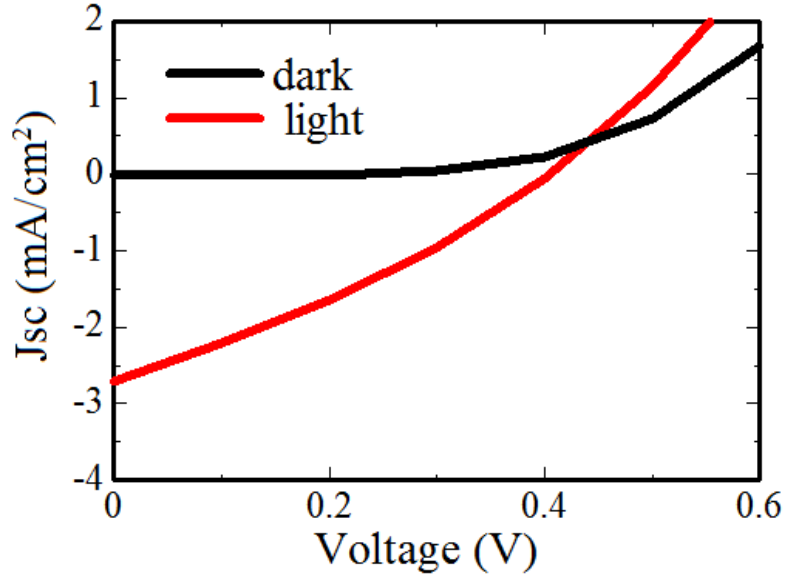
Figure 3.5. J-V characteristics of BHJ solar cells in dark and under illumination (1.5G, 100 mW/cm^2) fields

3.5 EFISHG Measurement

A probe laser beam was provided from a Q-switched Nd:YAG laser (pulse width 4 ns, and repetition rate 10 Hz) used with an optical parametric oscillator (OPO). The p-polarized probe laser was subjected at 45° to the BHJ layers [13],[14]. To measure the SH spectrum, the p-polarized probe laser wavelength was set between 800 nm to 1100 nm of wavelength. It is noteworthy to mention that a feasible laser wavelength should be applied to guarantee efficient EFISHG signals from PCPDTBT and PC71BM in the BHJ layer. This can be attributed to enhanced electromagnetic waves $\vec{E}(\omega)$ and coupling of electrons in the molecules occurred in an appropriate

wavelength of subjected laser. The second order polarization $\vec{P}_{2\omega}$ of the EFISHG is calculated from the below equation

$$I_{2\omega} \propto \left|\vec{P}_{2\omega}\right|^2 = \left|\varepsilon_0 \overleftrightarrow{\chi}^{(3)} : \vec{E}_0 \, \vec{E}_\omega \, \vec{E}_\omega\right|^2$$

ε_o, ω and $\overleftrightarrow{\chi}^{(3)}$ signify the fixed of the vacuum dielectric, the angular frequency of the laser light, and the third-order nonlinear exposure, respectively. $\vec{E}_{(0)}$ and $\vec{E}(\omega)$ represent the local electrostatic field, and the electric field of the laser.

$\vec{E}_{(0)}$ is measured using

$$\vec{E}(0) = \vec{E}\mathrm{p} + \vec{E}\mathrm{e} + \vec{E}\mathrm{s}$$

$\vec{E}\mathrm{p}$ is the internal electric field started by work function difference and other parameters, while $\vec{E}\mathrm{e}$ and $\vec{E}\mathrm{s}$ are the external electric field, and the space charge field, respectively [15]. Therefore, the EFISHG is initiated after constituting $\vec{E}_{(0)}$. The above equations affirmed the merits of the EFISHG method by selecting the appropriate material since $\overleftrightarrow{\chi}^{(3)}$ is a function of angular frequency of the laser light (ω), and allows to analyses the electric field of a targeted BHJ layer. This in turn can attribute the high utilization of EFISHG method. Therefore, this research intends to employ single-layer organic solar cells of the structure ITO/PCPDTBT/Al and ITO/ PC71BM /Al with an appropriate wavelength of laser light. Furthermore, this would be followed by measuring the EFISHG spectra of the PCPDTBT (donor) and PC71BM (acceptor) molecules. Monochromator was used to measure the SHG at the wavelength $\lambda_{2\omega} = \lambda_\omega/2$. To limit the impacts of wavelength necessity between the laser light and transportation of the optical system., a normalization of the SH intensity from the single-layer solar cells is carried out against the SHG spectrum of quartz powder [16].
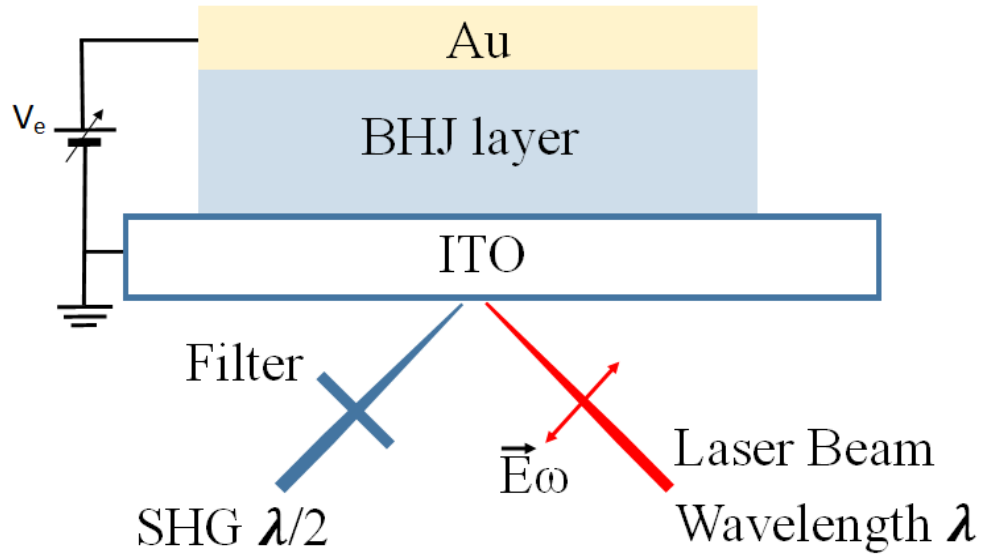
(a)
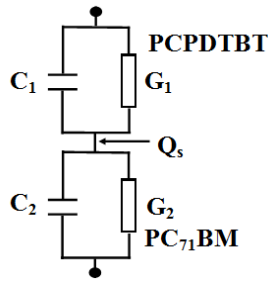
(b)

Figure 3.6. **S**tructure of BHJ solar cells. (a) The EFISHG measurement. (b) Maxwell-Wagner model

3.5.1 The EFSHG – Wavelength

The influence of SH wavelength of a single layer solar cells on the SH spectra intensity of for the donor (PCPDTBT) and receptor (PC71BM) at different voltage is represented in Figure 3.7. The electric field induced the generation of SHG signal and therefore the intensity of SHG is correspondingly varying with the square of supplied voltages. The electric fields in the donor

(PCPDTBT) and receptor (PC71BM) can be efficiently investigated using the laser wavelengths of 1000 nm and 1080 nm that are equivalent to 500 nm and 540 nm of SHG wavelengths, respectively. The EFISHG spectra detects peaks of SHG that affirmed the nonlinear exposure tensor $\bar{\chi}^{(3)}$ initiated at the SH peak wavelength. This is attributed to the electromagnetic coupling between the electric field of probing laser and electrons in the molecule. Accordingly, it can be said that SH peaks are directly related to the transfer of electrons from the ground state to the thrilled state of the molecule. This in turn would result various SH spectra for various molecules with a unique electronic structure for each molecule. This also aiding the enhancement of these molecules via the EFISHG.
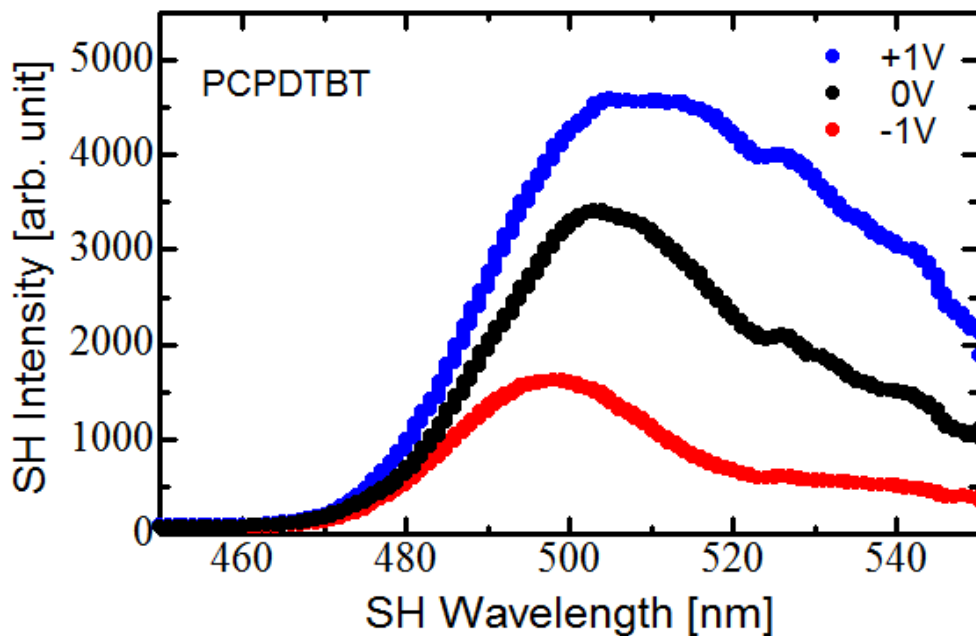
(a)
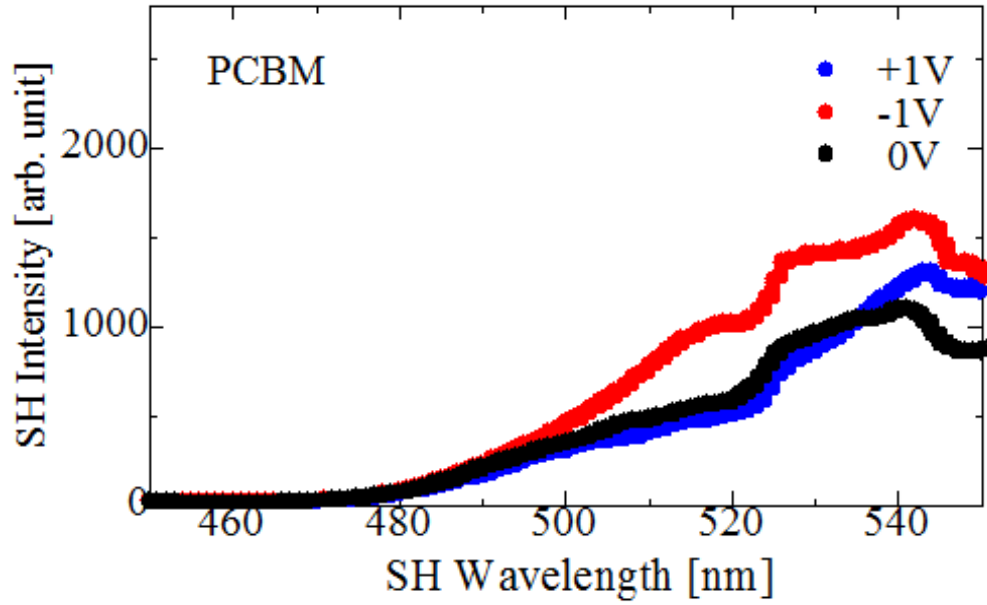
(b)

Figure 3.7. SHG spectra measurement (a) of the donor PCPDTBT and (b) of acceptor PC71BM.

3.5.2 The EFSHG – Voltage

Figure 3.8. depicts the influence of voltage variation on the SHG intensity for the suggested wavelength of 500 nm that equivalent to 1000 nm of laser wavelength and 540 nm that equivalent to 1080 nm of laser wavelength. A representative response EFISHG can be seen for the donor PCPDTBT at SH wavelength of 500 nm. An average electric field of the single layer solar cell can be estimated from

$$E_e = \left(|\vec{E}_e|\right) = V/d$$

d denots the layer thickness in the donor. Also, the SHG intensity $I_{2\omega}$ has a quadratic dependency on the electric field as pictured in the following equation

$$I_{2\omega} \propto \left|\vec{P}_{2\omega}\right|^2 = \left|\varepsilon_0 \overleftrightarrow{\chi}^{(3)} : \vec{E}_0 \vec{E}_\omega \vec{E}_\omega\right|^2$$

Furthermore, an enhancement of EFISHG from PC71BM (acceptor) can be shown with 450 nm of the SHG wavelength. Therefore, the registered results of Figure 3.8. can be used to conveniently probe the electric field in the donor (PCPDTBT) of PCPDTBT/PC71BM OSC. Therefore, the probe laser of wavelength 1000 nm is chosen within 500 nm wavelength to detect the SHG.
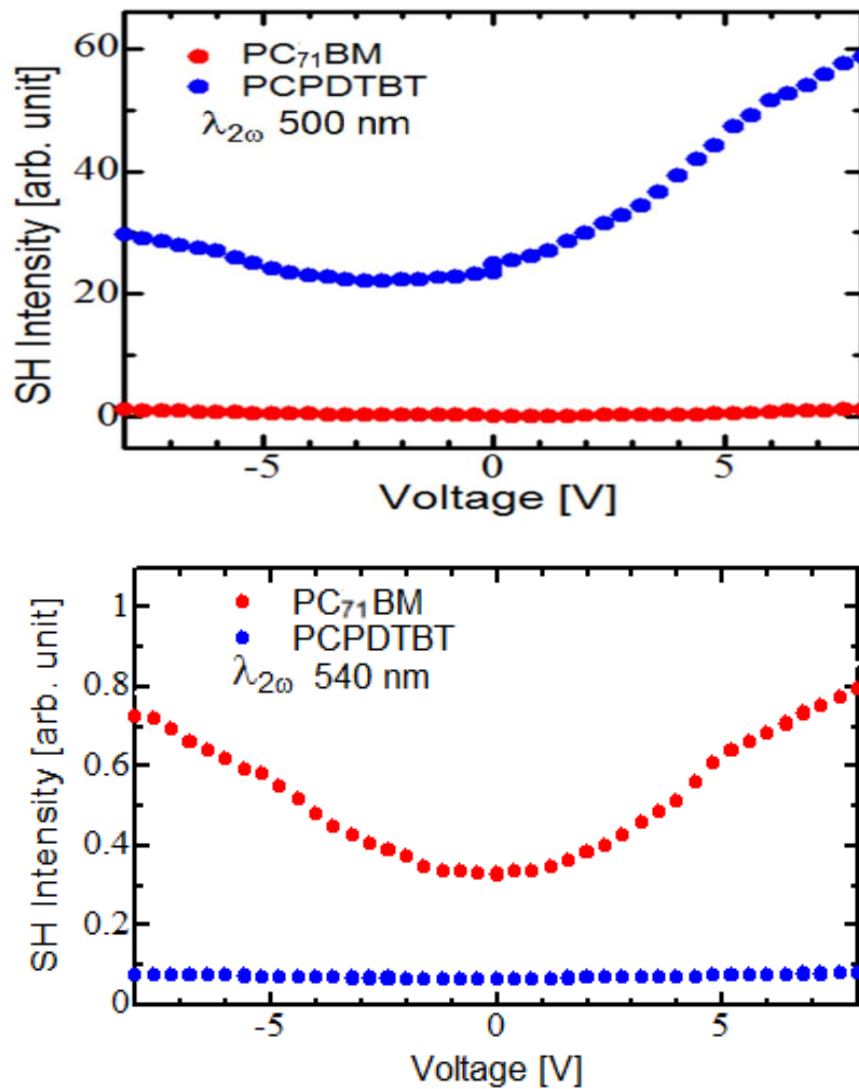

Figure 3.8. SHG intensity of PCPDTBT and PC71BM single-layer solar cells at a SH wavelength of 500 nm and 540 nm

3.5.3 Transient EFISHG response to observe carrier behavior

The variation of SH intensity for the ITO/PCPDTBT: PC71BM/Au OSC in dark environment against the operational time is plotted in Figure 3.9. for the range of Vex between +1 V and -1 V that subjected to the Au electrode in reference to the ITO electrode. Specifically, the SH intensity was generated after employing a Vex = +1 V, where an increase of SH intensity is produced at 500 nm with using of 1000 nm wavelength of laser light. However, a growth of SH intensity is noticed at 540 nm after deploying 1080 nm wavelength of laser light in the dark conditions. However, using a Vex = -1 V, negative voltage, causes a degradation of SH intensity.

It is vital to note that a non-zero electric field can be established in ITO/PCPDTBT: PC71BM/Au OSCs as a result to a change in functions of the ITO and Au electrode. Respectively, an electric filed Ee (t) is constituted in the donor and acceptor is initiated due to subjecting an external voltage. As described in Eq. 1, the electric field $E_{(0)}$ represents the sum of electric field (Ee), space-charge field (Es), and internal electric field (Ep). Therefore, the SH intensity in the BHJ layer is created in comparison to |Ep + Ee(t)|2. In this regard, the electric field is estimated from

$$Ee\ (t) = (Vex/d)\ (1-exp\ (-t/tRC))$$

d represents the thickness of BHJ layer while t_{RC} is the response time of the circuit calculated from

$$t_{RC} = R\ C$$

R is the sheet resistance of ITO 15 $\Omega/\square$ and C is the geometrical capacitance of the OSC). Clearly, the above equations show a direct relationship between the variation of the electric field and the polarity of the Ep. Results of Figure 3.9 affirm that the electric fields in the donor Ep1 and

in acceptor Ep2 are directed from Au to ITO electrode within 540 nm SH wavelength. Furthermore, the ignition of function difference causes an electric field in OSCs, that must be directed from Au (Ø= 4.5 eV) to ITO (Ø = 5.1 eV) electrode. This would interpret several resources of internal electric field including the charge transportation throughout the organic electrode interface and the surface of SHG from Au/organic and probably ITO. Thus, a black curve of the zero used voltage is presumed in Figure 3.9. that means no influence of the internal electric fields on the recent research.

The EFISHG is able to examine the electric field via the donor layer and also exposes carrier behaviors. In the dark conditions of no photo illumination, Eph will equal zero. Figure 3.9. illustrates a gradual reduction of SH intensity after t_{RC}. This is consequently associated with two carrier denoted by t_{RC} and tmw as depicted in Figure 3.9 where $t_{RC} = 5.5 \times 10^{-7}$ s for positive voltage of 1 V, and $t_{RC} = 6 \times 10^{-7}$ s with negative voltage. This is specifically referred as the response time for electrode charging via the external circuit. Furthermore, t_{MW} is represented as $\frac{C1+C2}{G1+G2}$ and approximately equals to 9×10^{-6} s with positive voltage and approximately equals to 5×10^{-6} s with negative voltage. t_{MW} specifically represents the response time for the Maxwell–Wagner-type interfacial charging.

The EFISHG response signifies the change of the electric field inside the donor layer, where the overall electric fields of the OSC ($E_{(0)}$) is estimated using Ep + Ee.

Therefore, the abolishment of the EFISHG response for the BHJ layer OSC is caused by the accumulation of electrons n at the interfacial area of the donor/receptor. Therefore, the signal of SHG would be decreased as declared in Figure 3.9 which informs the accumulation of electrons (Qs) at the interfacial area of the donor/receptor (PCPDTBT/PC71BM). For this case,

Qs = Es (C1+C2) × d1 ≈ 0.1 × 10-7 C/cm^2 with positive voltage of 1 V, and Qs = Es (C1+C2) × d1 ≈ 0.3 × 10-7 C/cm^2 with negative voltage of - 1 V.
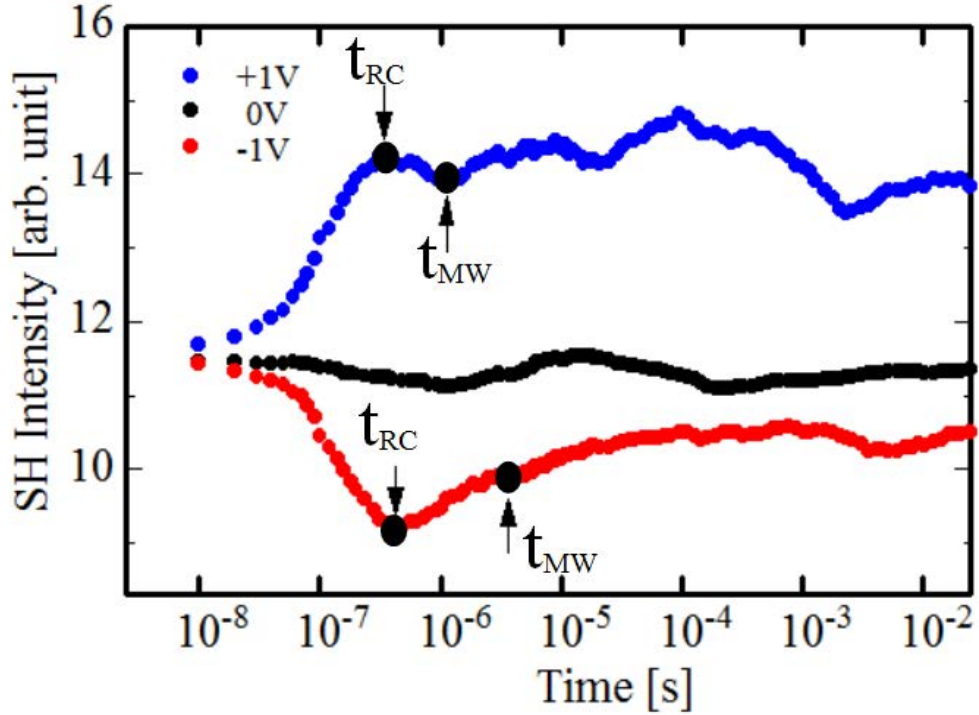
Figure 3.9. EFISHG measurement by deploying pulse voltages in the dark conditions

3.6   Conclusions

This chapter investigates the carrier behaviors in BHJ OSCs using EFISHG measurements. This showed that the circuit response time between positive and negative voltages are approximately identical. However, a significant difference was noticed for the response time of the Maxwell–Wagner-type interfacial charging between positive and negative voltages. This in turn specified the accumulation of electrons Qs in the interfacial area between the donor and acceptor. More specifically, the accumulated electrons in the donor side (PCPDTBT) is lesser than the electrons of the acceptor (PC71BM). This has a significant influence on the total efficacy of the bulk heterojunction OSCs.

3.7 Bibliography

1. Brédas, J. L., Norton, J. E., Cornil, J., & Coropceanu, V. (2009). Molecular understanding of organic solar cells: the challenges. Accounts of chemical research, 42(11), 1691-1699.

2. He, Z., Xiao, B., Liu, F., Wu, H., Yang, Y., Xiao, S., ... & Cao, Y. (2015). Single-junction polymer solar cells with high efficiency and photovoltage. *Nature Photonics*, *9*(3), 174-179.

3. Guo, X., Zhou, N., Lou, S. J., Smith, J., Tice, D. B., Hennek, J. W., ... & Chen, L. X. (2013). Polymer solar cells with enhanced fill factors. *Nature Photonics*, *7*(10), 825-833.

4. Silvestri, F., & Marrocchi, A. (2010). Acetylene-Based materials in organic photovoltaics. *International journal of molecular sciences*, *11*(4), 1471-1508.

5. Bruni, F., Sassi, M., Campione, M., Giovanella, U., Ruffo, R., Luzzati, S., ... & Brovelli, S. (2014). Post-Deposition Activation of Latent Hydrogen-Bonding: A New Paradigm for Enhancing the Performances of Bulk Heterojunction Solar Cells. *Advanced Functional Materials*, *24*(47), 7410-7419.

6. Ameri, T., Dennler, G., Waldauf, C., Azimi, H., Seemann, A., Forberich, K., ... & Brabec, C. J. (2010). Fabrication, optical modeling, and color characterization of semitransparent bulk-heterojunction organic solar cells in an inverted structure. *Advanced Functional Materials*, *20*(10), 1592-1598.

7. He, Z., Zhong, C., Su, S., Xu, M., Wu, H., & Cao, Y. (2012). Enhanced power-conversion efficiency in polymer solar cells using an inverted device structure. *Nature photonics*, *6*(9), 591-595.

8. Zhao, J., Li, Y., Yang, G., Jiang, K., Lin, H., Ade, H., ... & Yan, H. (2016). Efficient organic solar cells processed from hydrocarbon solvents. *Nature Energy*, *1*(2), 1-7.

9. Zhao, F., Dai, S., Wu, Y., Zhang, Q., Wang, J., Jiang, L., ... & Wang, C. (2017). Single-junction binary-blend nonfullerene polymer solar cells with 12.1% efficiency. *Advanced Materials*, *29*(18), 1700144.

10. Roland, S., Schubert, M., Collins, B. A., Kurpiers, J., Chen, Z., Facchetti, A., ... & Neher, D. (2014). Fullerene-free polymer solar cells with highly reduced bimolecular recombination and field-independent charge carrier generation. *The journal of physical chemistry letters*, *5*(16), 2815-2822.

11. Mukherjee, S., Proctor, C. M., Bazan, G. C., Nguyen, T. Q., & Ade, H. (2015). Significance of Average Domain Purity and Mixed Domains on the Photovoltaic Performance of High-Efficiency Solution-Processed Small-Molecule BHJ Solar Cells. *Advanced Energy Materials*, *5*(21), 1500877.

12. Taguchi, D., Shino, T., Zhang, L., Li, J., Weis, M., Manaka, T., & Iwamoto, M. (2011). Direct probing of photovoltaic effect generated in double-layer organic solar cell by electric-field-induced optical second-harmonic generation. *Applied physics express*, *4*(2), 021602.

13. Taguchi, D., Sumiyoshi, R., Chen, X., Manaka, T., & Iwamoto, M. (2014). Study of interface layer effect in organic solar cells by electric-field-induced optical second-harmonic generation measurement. *Thin solid films*, *554*, 51-53.

14. Taguchi, D., Shino, T., Chen, X., Zhang, L., Li, J., Weis, M., ... & Iwamoto, M. (2011). Analyzing photovoltaic effect of double-layer organic solar cells as a Maxwell-Wagner

effect system by optical electric-field-induced second-harmonic generation measurement. *Journal of Applied Physics*, *110*(10), 103717.

15. Y. R. Shen, The Principles of Nonlinear Optics, New York, Wiley-Interscience, p 575, 1984.

16. Ahmad, Z., Abdullah, S. M., Taguchi, D., Sulaiman, K., & Iwamoto, M. (2015). A way for studying the impact of PEDOT: PSS interface layer on carrier transport in PCDTBT: PC71BM bulk hetero junction solar cells by electric field induced optical second harmonic generation measurement. *Journal of Applied Physics*, *117*(16), 163101.

Chapter 4

4 Probing balanced carrier transport in PCPDTBT: PC$_{71}$BM BHJ films using 1,8-Diiodooctane (DIO) as an additive by using EFISHG

4.1 Introduction

This chapter aims to experimentally conduct the electric-field-induced optical second harmonic generation (EFISHG) measurement at the laser wavelength. In this aspect 1000 nm was deployed to explore the influence of 1,8-diiodooctane (DIO) additive on the charge transportation in bulk heterojunction (BHJ). The experiments were used a sandwich type device structure (ITO/BHJ/PEDOT:PSS/Au), where the BHJ layer is a blend of the [6,6] -phenyl C71 butyric acid methyl ester (PC$_{71}$BM) and regioregular poly [2,6-(4,4-bis-(2-Ethylhexyl) - 4H – cyclopentane [2,1-b;3,4-b'] dithiophene) – alt - 4,7 - (2,1,3- benzothiadiazole)] (PCPDTBT). The results affirmed an increase of around 25% of carrier transport characteristics in the PCPDTBT: PC$_{71}$BM layer due to DIO additive compared to without DIO solar device. This is also associated with a remarkable reduction of the accumulated charge on the interface between donor and acceptor phases and increased domain size.

4.2 General background

The application of effective cost industrial processes is progressively increased in the recent years to accommodate the demands of safe environment. In this regard, the polymer-based organic materials are the most potential solution to be engaged as a green source of energy [1-3]. Therefore, intensive researches were especially focused on organic solar cells applications to synthesize high performance BHJ films of an effective material of polymer donors [4-5]. Specifically, the research

intended to tackle the limitations of BHJ films that mainly comprise low charge transportation between the donor and acceptor [6]. This in turn has entailed an improvement of chemical structure of BHJ type PCPDTBT and PCBM to efficiently adsorb sunlight. However, the author believes that there is still a room to enhance the electron transportation that would raise the performance of associated BHJ film in solar cells. [6]. It is accepted that promoting the structural order of the BHJ is quite relevant to improve the carrier mobility of both donor and acceptor stages. However, it is important to realize that increasing the structural order would cause a reduction of interface between donor and acceptor phases that would also cause reduced of the recombination and exciton dissociation. In other words, larger domains form must be avoided [7-8]. The optimization of domains' size is vital to attain an improved performance of organic solar cells. [9-14] confirmed that the utilization of solvent additives would be an acceptable option to control the domains' sizes of donor and acceptor phases. The suppression of exciton recombination would be achieved by adding a some of solvent additive to form nano-size donor and acceptor domains [15].

To conduct this improvement, it has been decided to add 1,8- Diiodooctane (DIO) as a blending additive in the BHJ beside the requirements of optimising the domain size of the associated phases. Furthermore, $PC_{71}BM$ molecules was selected to be added to the BHJ due to its high capacity to be dissolved in DIO and form smaller domains of upgraded interface between donor and acceptor. Despite the shortage of studies to critically understand the influence of additive DOI (1,8-diiodooctane) and charge transportation, the performance of organic solar cells was meaningfully improved [9,16-17]. This is plausibly interpreted due to the enhancement of film morphology as it related to charge transportation. In this regard, the evaluation of charge transportation between the donor and acceptor phases is fundamentally evaluated using the electrical measurement without looking at critical details of carrier transportation [18-20]. However, the exciton and charge carrier

can also be evaluated using the optical measurements. Several researches were utilized two improved optical measurements methods of the electric-field-induced optical second-harmonic generation (EFISHG) and transient absorption spectroscopy (TAS). [21-22] pointed out the main discrimination between the utilized optical measurement methods where no details of gathered charge and carrier transportation can be given within TAS. However, the clarification of the exciton dynamics within the BHJ is a significant merit of TAS. On the other hand, the carrier charge transportation between donor and acceptor phases can be chased via EFISHG method after excitons dissociation. EFISHG is also characterized by high order of electromagnetic field that improves the interaction between laser beam and electrons. The electronic field can urge twofold frequency and deduce a nonlinear polarization oscillation. Moreover, the selection of proper wavelength of SHG light would aid to investigate the carrier behavior in the BHJ.

This study intends to utilize the optical measurement method of EFISHG to investigate the carrier behavior of (PCPDTBT) of [6,6] -phenyl C71 butyric acid methyl ester ($PC_{71}BM$) and regioregular poly [2,6-(4,4-bis-(2-Ethylhexyl) - 4H – cyclopenta [2,1-b;3,4-b'] dithiophene) – alt - 4,7 - (2,1,3-benzothiadiazole)]. Particularly, the influence of adding DIO in the BHJ layer will be appraised via studying of carrier behavior.

4.3   1,8-diiodooctane (DIO) material

As stated above, the improvement of OPV was realized via the addition of solvent additives of DOI [23], recent researches [24-32] are critically employed a wide set of additive solvents to the BHJ such as chloroform (CF), chlorobenzene (CB), and dichlorobenzene (DCB). The intention was to explore the influence of these additives on the domain size and purity besides allocating the best interface composition and crystallinity. The enhancement of morphology cannot be ignored in organic solar cells especially in the case of nominating numerous binary combinations or ternary

mixtures that corresponding to solvent additives. However, these methodologies were tackled with inherent issues for instance, there is a possibility of instable morphology, chemical degradation, and toxicity. Furthermore, there is a clear limitation of applying high boiling point additives as they characterized by low productivity [32-33]. Thus, the challenge of selecting a free additive of single solvent to promote PCEs is still existed [34-36]. This is actually compatible with the recent fabrication of non-halogenated single toxic solvents that probably influence the ecosystem [37-46].
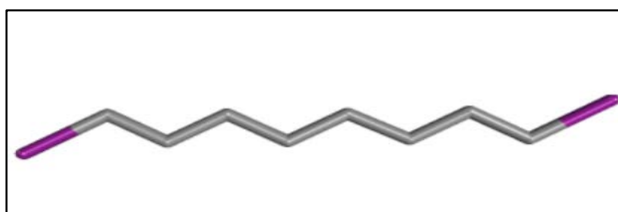

Figure 4.1. 1,8-diiodooctane (DIO) structures

4.4   Experimental Procedures

4.4.1   Sample preparation

Figure 4.2.(a) shows the schematic diagram of the experimental configuration and sandwich junctions structure of the BHJ. in this regard, ITO/BHJ/PEDOT:PSS/Au structure was used to fabricate the BHJ films. More specifically, a blended solvent of PCPDTBT (donor) and PC$_{71}$BM (acceptor) forms the active layer was introduced by solving 10 mg of PCPDTBT and 15 mg of PC$_{71}$BM in 1 ml chloroform. A continuous stirring of solution was kept for one hour fully dissolving. The formed BHJ films characterized by blending the solution with 3% of DIO. [47-48]. A substance of a patterned indium-tin-oxide (ITO) layer (10 Ω/sq) was used with a glass plate. Afterwards, spin coating of the blended solution within 1500 rpm and 30 seconds was employed

to successfully perform the film deposition onto the substrate. This results an active layer of 150 nm thickness of the BHJ film. After that, a spin coating of 3000 rpm for 60 seconds was used to full deposition of the PEDOT:PSS on the top of the BHJ film. This in turn deduced 50 nm thickness of PEDOT:PSS layer. Lastly, Au electrodes of 100 nm thickness were deposited onto the surface of the PEDOT:PSS layer that entailed an interfacial surface area of 3.1 mm^2. Furthermore, the incident photon to current efficiency (IPCE) was evaluated based on 400 to 900 nm wavelength.
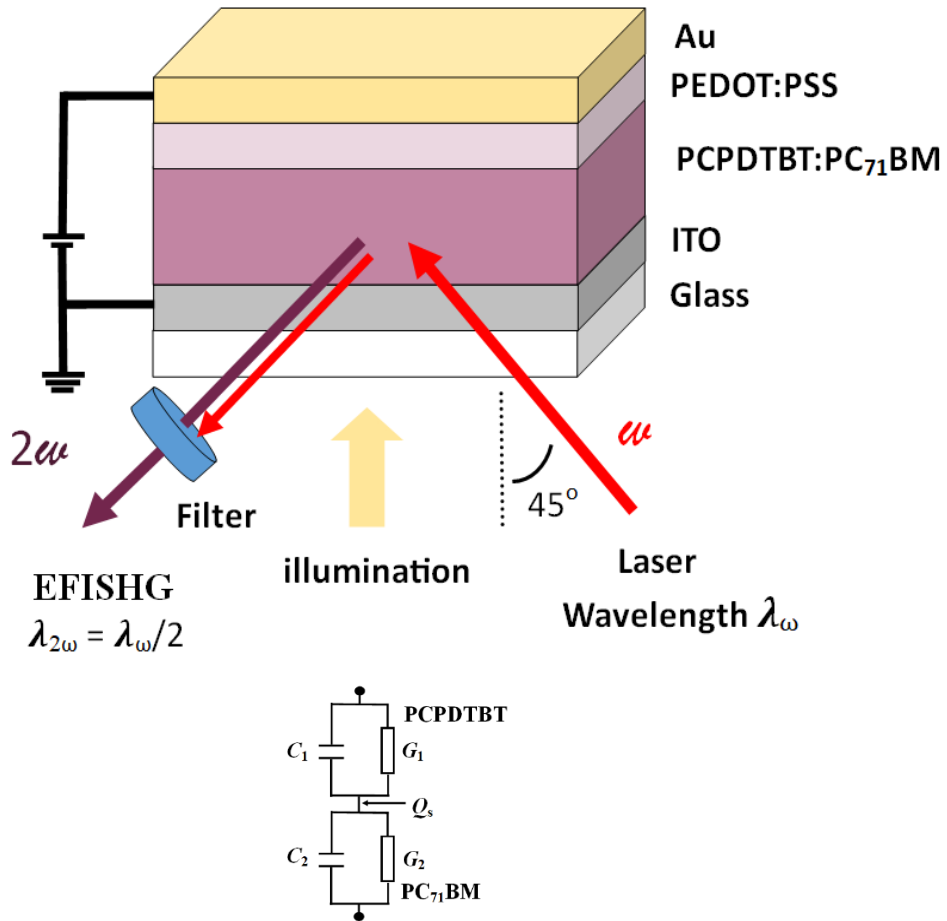

Figure 4.2. Schematic structure of BHJ solar cells. (a) The EFISHG measurement, (b) Equivalent circuit model for Maxwell-Wagner-type charging

4.4.2 EFISHG measurement

The EFISHG optical method was utilized to measure the SHG using a p-polarized pulsed laser

light of 10 Hz (repetition rate), 1 mW (average power) for 4 ns duration. The light laser was generated from an optical parametric oscillator pumped with the third-harmonic light of a Q-switched neodymium-doped yttrium aluminum garnet (Nd YAG) laser. The laser light was then imposed into the surface of the sample at an incident angle of 45°, as depicted in Fig. 1(a) [49-52]. Then, a photomultiplier tube was used to trace the generated SHG light from the selected sample. However, it is important to realise that type of material is strongly affected the nonlinear optical susceptibility, where the wavelength characterised the laser light [53]. The intensity of the SHG intensity ($I_{2\omega}$) is mathematically conveyed as,

$$I_{2\omega} \propto \left|\vec{P}_{2\omega}\right|^2 = \left|\varepsilon_0 \overleftrightarrow{\chi}^{(3)} : \vec{E}_{(0)} \vec{E}_{(\omega)} \vec{E}_{(\omega)}\right|^2 \qquad (1)$$

$\vec{P}_{2\omega}$ denotes the second-order nonlinear polarization. Also, $\varepsilon_{o,}$, ω and $\overleftrightarrow{\chi}^{(3)}$ are the dielectric constant of vacuum, is the angular frequency of the laser beam and the third-order nonlinear susceptibility of material. More importantly, the associated relationship between the wavelength and $\overleftrightarrow{\chi}^{(3)}$ aids to examine the carrier transportation between the donor and acceptor phases.

$\vec{E}_{(0)}$ and $\vec{E}_{(\omega)}$ are the local electrostatic field and the electric field of the laser, respectively. $\vec{E}_{(0)}$ is stated as $\vec{E}_{(0)} = \vec{E}_P + \vec{E}_e + \vec{E}_s$, where $\vec{E}_P$, $\vec{E}_e$ and $\vec{E}_s$ are the internal electric field, the external electric field, and the space-charge field, respectively [54-56]. In this aspect, the positive direction of the electric field was generated from PEDOT:PSS/Au to ITO via the BHJ layer. Therefore, the electric field $\vec{E}(0)$ attributes the generated EFISHG signal as given in Eq. (1). Since $\overleftrightarrow{\chi}^{(3)}$ spectrum is strongly dependent on the material type, it is fair to affirm that EFISHG method is correlated to material type which can be efficiently used to investigate the electric field of the used material for the used wavelength.

This study utilizes the BHJ type PCPDTBT:PC$_{71}$BM, where PCPDTBT has efficiently produced

the EFISHG signal at 1000 nm of laser wavelength which is equivalent to the SHG wavelength of 500 nm. However, $PC_{71}BM$ showed resonant enhancement of EFISHG at 1080 nm of laser wavelength [57]. In this regard, red illumination was used as the light source for the BHJ layer excitation (center wavelength 661 nm, intensity 100 mW/cm^2).

4.5 Electrical characterization

This study aims to control the morphology of BHJ film by adding DIO. This would increase the density of donor acceptor interface that commensurate with reducing the domain size and gathered charge throughout the interface. This is already figured in Figure 4.3. Undoubtedly, this means an improved efficiency of enhanced electronic field that induced the movement of electrons towards the ITO and holes towards PEDOT:PSS/Au electrode. The characteristics of the current density-voltage (J-V) is signified in Figure 4.4 considering both cases of with and without DIO under AM 1.5G solar illumination at one sun (100 mW/cm^2). In this regard, the performance metrics of two fabricated devices of samples (with and without DIO additive) are listed in Table 1. The operating conditions of both devices are identical including the spin-speed to control the film thickness, temperatures of the thermal treatments, and the ratio of donor and acceptor constituents. The results of these experiments concluded that the weight ratio of donor: acceptor solutions in chloroform of 1:1.5 was the optimal ratio to gain the optimal performance. Occasionally, [10] affirmed that adding 3 wt% of DIO to the solution would be an efficient option to enhance the nanoscale suitable phase separation. The highest Jsc of 5.03 mA/cm^2 was associated for a fabricated device of with DIO (Figure 4.4). On the other hand, the lowest Jsc of 4.45 mA/cm^2 was associated for a fabricated device of without DIO. Furthermore, an improvement of around 10% of Voc was also registered. Table 4.1 exhibits an improvement of 25% of solar cells device with DIO additive compared to without DIO. This is a considerable contribution since the fabricated organic solar cells devices of different electron transport layer (ETL) and hole transport layer (HTL) of DIO additive have

more than 5% of efficiency. [58]. Interestingly, this study investigated the performance of structure on the carrier behavior that recognizes the influence of additive DIO on the charge transport in the PCPDTBT: $PC_{71}BM$ layer. In this study, the PEDOT:PSS layer used to justify the hole transport toward the Au electrode. However, this study has excluded the effect of electron transport layer. The assessment of the electronic field and charge behavior using the SHG optical measurement method will be thoroughly presented in the upcoming sections.

Table 4.1. The performance of PCPDTBT: $PC_{71}BM$ blend films formed with and without DIO additive.

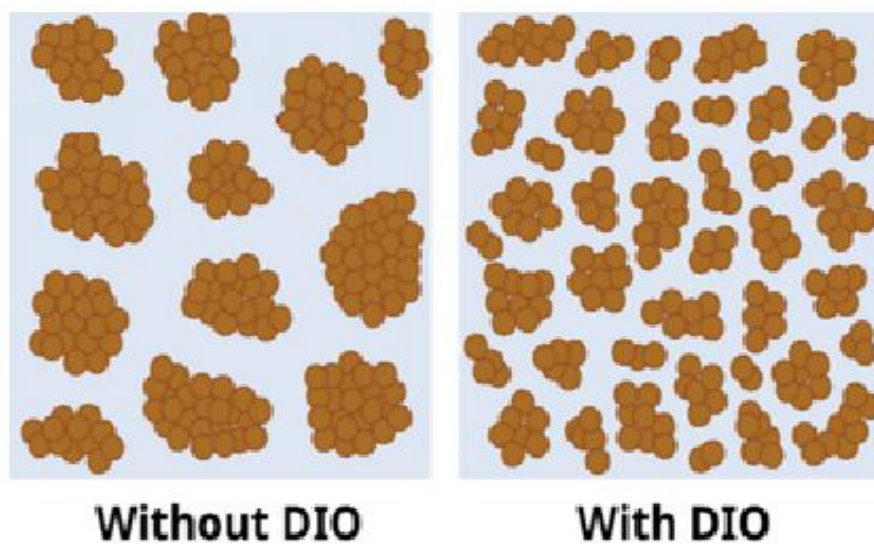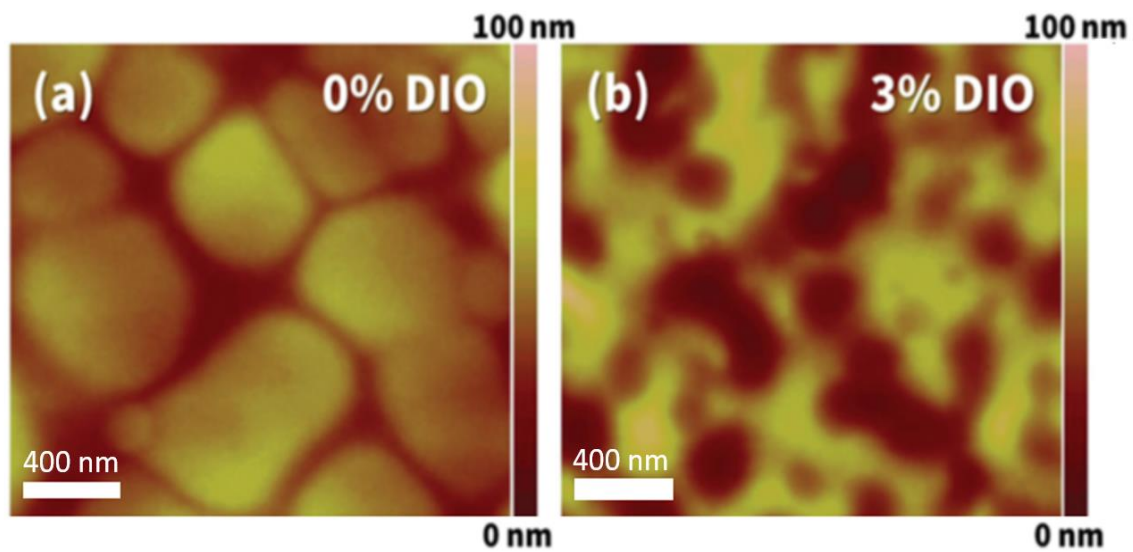|	Jsc (mA/cm^2)	Voc (V)	FF (%)	η (%)
Without DIO	4.45	0.50	29 %	0.67 %
With DIO	5.03	0.55	31 %	0.84 %

Figure 4.3. AFM images of BHJ films at different DIO concentrations in height mode
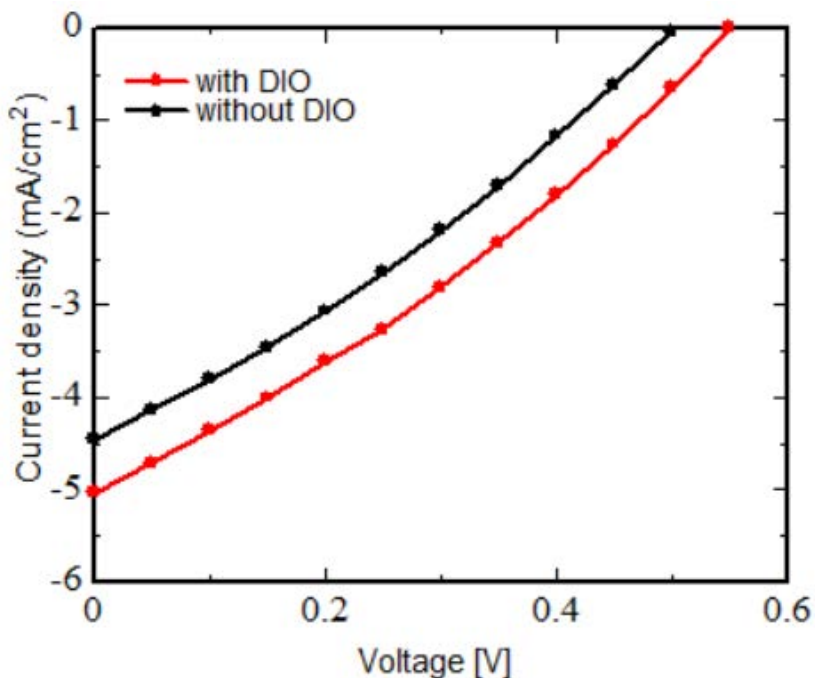
Figure 4.4. Current density-voltage (J-V) characteristics of BHJ sandwich structures with and without DIO

4.6 IPCE spectra

The IPCE spectra was measured in this study to evaluate the influence of with and without DIO additive. Figure 3(a) presents that the improvement of the IPCE with DIO additive between 400 to 900 nm of wavelength and AM 1.5G solar illumination that entailed an upgraded efficiency of 25%. Meaningfully, an enhancement of IPCE would confirm an enhancement of light absorption, and improved charge and exciton dissociation [59]. Moreover, Figure 4.5 asserts the improvement of IPCE due to DIO additive besides achieving a marginal influence on the absorption spectra (Figure 4.5). to summarize, the EFISHG was successfully used to explore the enhancement of IPCE due to the improvement of carrier behavior and accumulated charges at the donor-accepter interface.
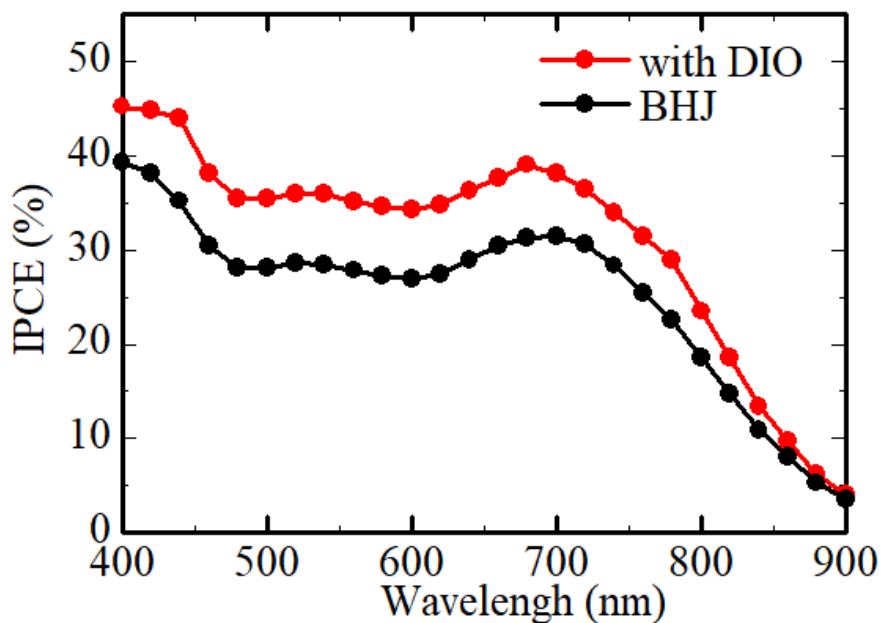
Figure 4.5. IPCE spectra of BHJ cells prepared with and without DIO

4.7   Absorption spectra

Evaluation of the absorption spectrum of the active layer is important to characterize the blend where the material type is correspondingly related to the absorbed light. To critically achieved this, the absorption spectrum was conducted for both with and without DIO devices since the deposited material would hinder the movement of photons to get the lower layer. Figure 4.6 illustrates the registered values of absorption spectra of with and without DIO devices. It is clearly noticed that there is no influence of adding DIO additive on the absorption spectra. Moreover, the thickness of active layer is not predominantly affected by adding DIO additive.
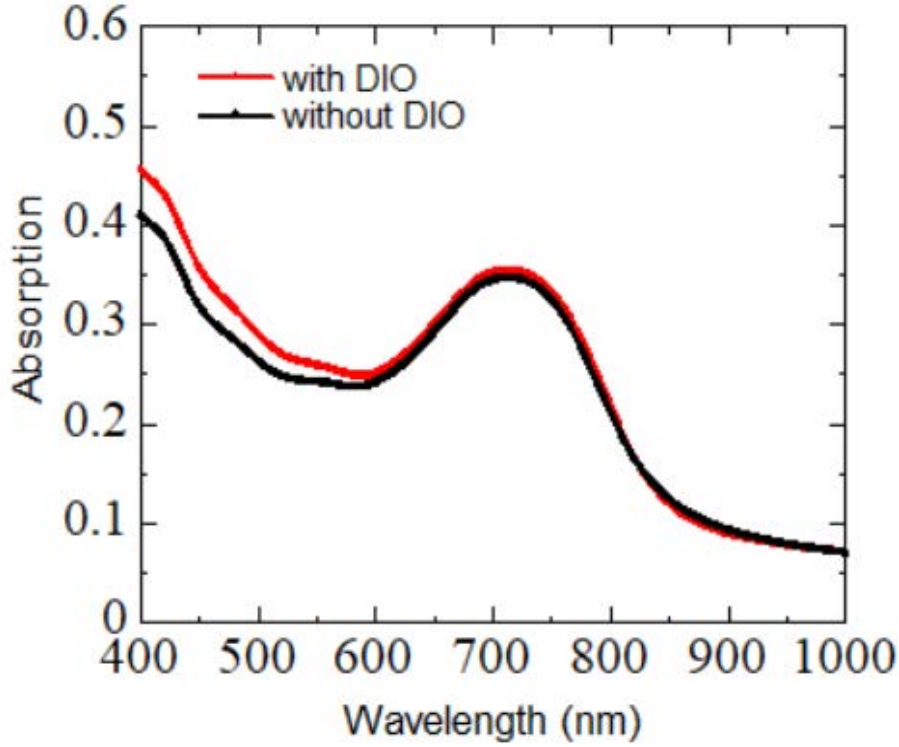
Figure 4.6. Optical absorption spectra of BHJ layer prepared with and without DIO.

4.8 EFISHG Measurement

4.8.1 Internal Field

Basically, the internal field ($\vec{E}_P$) between the PCPDTBT and PC$_{71}$BM stimulates the movements of holes and electrons generated in BHJ layer toward PEDOT:PSS/Au and ITO electrode, respectively. However, it is important to apply an external voltage to generate the internal electric field. As mentioned, the electric field $\vec{E}(0)$ in Eq. (1) consists of three components: the external electric field ($\vec{E}_e$), the space-charge field ($\vec{E}_s$), and the internal electric field ($\vec{E}_P$). In this regard, the EFISHG intensity measurements for two devices of with and without DIO are presented in Figure 4.7. with applying a range of +8 V to -8 V. This concluded an enhancement of EFISHG for PCPDTBT and PC$_{71}$BM for 500 nm and 540 nm of wavelength, respectively. According to Eq. 1, the EFISHG intensity is proportionate to the square of the local field ($I_{2\omega} \propto |\vec{E}_0|^2$). In this regard,

a minimum voltage of Ve=+0.6 V with DIO additive is enough to grow the SH intensity of PCPDTBT using 500 nm of SH wavelength. Occasionally, the positive value of voltage specifies the existence of the internal field directed from ITO to PEDOPT:PSS/Au electrode. The gained results are cooperative with the negative short-circuit current as depicted in Fig.2. Moreover, Fig. 4 indicates the improvement of the internal field as a result to DIO additive.
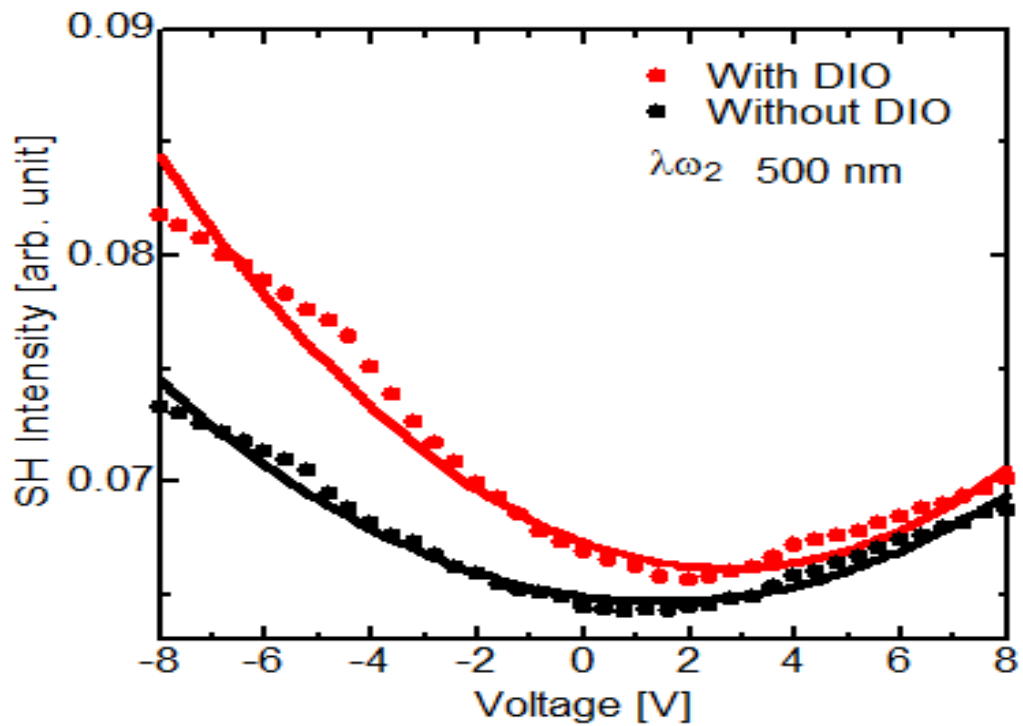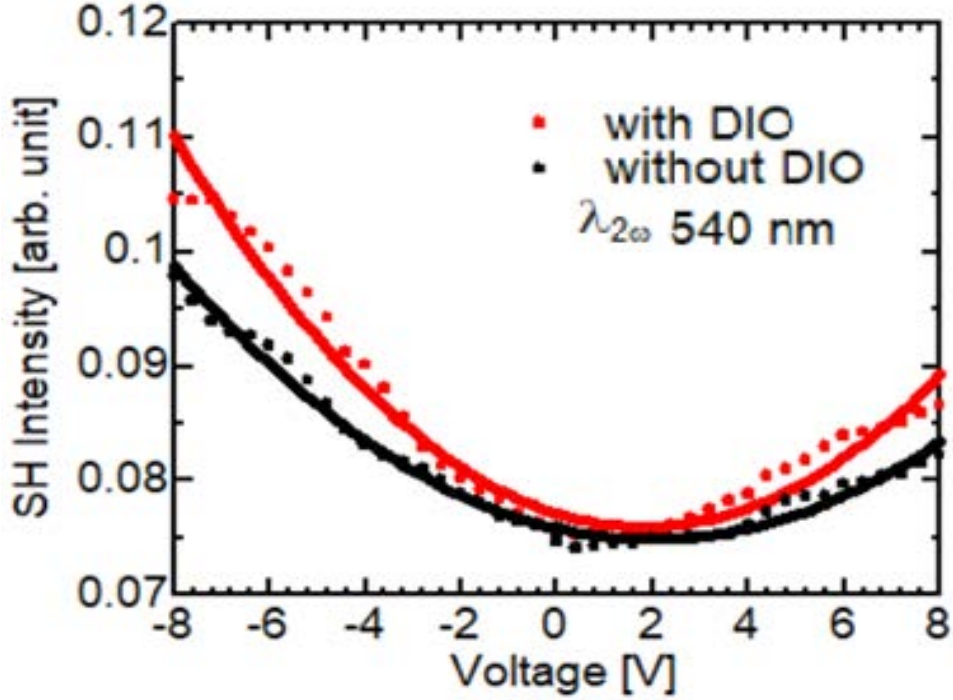
Figure 4.7. SHG intensity of BHJ film with and without DIO at SH wavelength of 500 nm and 540 nm

4.8.2 Carrier Behavior

The variation of SH intensity using EFISHG measurements against the operation time is illustrated in Fig. 5 for the sandwich structure BHJ devices with and without DIO additive between -3V and +3V. The variation of SH intensity is corresponding to the generated electrostatic field from electrode charges $\vec{E}_e$.

Firstly, the period between t=0 and response time of the equivalent circuit t_{RC} characterises by igniting the electrostatic field in the BHJ layer. t_{RC} is dominantly related to the capacitance C of BHJ layer and resistance of ITO. In this regard, the generated SHG is correlated as $|\vec{E}_P + \vec{E}_e(t)|^2$. Moreover, the experimental findings of EFISHG measurements throughout the time is consistently agree with Eq. 2.

$$\vec{E}_e\,(t) = (\tfrac{V_{ex}}{d})(1 - \exp{(\tfrac{-t}{t_{RC}})}) \qquad (2)$$

This elucidated that $t_{RC} = R_S\,C = 10^{-7}$s with the ITO resistance of $10^2\ \Omega$ and BHJ capacitance of 10^{-9} F. Also, these results are accommodating the ones presented in Table 2 at 1.2×10^{-7}s and 1.6×10^{-7}s of operating time. Figure 4.8 confirms a considerable change of SHG intensity at operating time around 10^{-7}. However, it is fair to assume fixed value of t_{RC} due to adding small amount of DIO that would not impact the film thickness. In other words, t_{RC} is assumed constant for the two devices of with and without DIO as depicted in Table 2.

Figure 4.2 (b) presents the estimation of charge accumulation at the donor and acceptor interface using an equivalent circuit model. The charging process is labelled as the Maxwell-Wagner effect. This study specifies the modelling of PCPDTBT (donor) as electronic source with conductance G_1 and capacitance C_1. Moreover, PC$_{71}$BM (acceptor) was modelling using conductance G_2 and capacitance C_2. Based on this model, the charges sourced from donor are moved at time constant $t_1 = \frac{C_1}{G_1}$, and received in acceptor at time constant $t_2 = \frac{C_2}{G_2}$. The constants are labelled as dielectric relaxation time. Eq. 5 is used to measure the accumulated charge along the interfacial area of donor and acceptor

$$Q_s(t) = Q_s \left(1 - exp\left(-\frac{t}{t_{MW}}\right)\right) \quad (3)$$

after applying dc voltage at t = 0. The time constant of the MW charging is given by $t_{MW} = \left(\frac{C_1+C_2}{G_1+G_2}\right)$. In the steady state, the amount of the accumulated charges are expressed by

$$Q_s = \frac{G_1 G_2}{G_1 + G_2}\, V\, (t_2 - t_1) \quad (4)$$

Since Q_s is the excess charge, it forms the space-charge field $\vec{E}_s$ in the BHJ layer.

Assuming that the BHJ layer is effectively modeled as a double layer of donor and acceptor, an effective space-charge field $\vec{E}_s$ is expressed as

$$E_s = -\frac{1}{d_1} \frac{Q_s}{C_1 + C_2} \qquad (5)$$

in donor and $E_s = +\frac{1}{d_2} \frac{Q_s}{C_1 + C_2}$ in the acceptor phase. Here, d_1 and d_2 are the effective thickness of donor and acceptor, Q_s is space charge, C_1 and C_2 are effective capacitance of donor and acceptor, respectively. Accordingly, assuming that donor is more conductive than acceptor [52,60], t_1 is smaller than t_2, and then $Q_s > 0$. As a result, the total electric field $\vec{E}_e + \vec{E}_s$ in donor will decrease as the interfacial charge Q_s accumulates, and the electric field in acceptor will increase meanwhile.

Table 2 summarizes the parameters such as relaxation times for the electrode charging t_{RC} and interface charge relaxations (Maxwell-Wagner time) t_{MW} estimated from the EFISHG measurements. The SHG measurement shows that the Maxwell-Wagner time constant t_{MW} decreases after adding DIO in the BHJ, from 2.4×10^{-7}s to 1.8×10^{-7}s at +3 V, and from 4.0×10^{-7}s to 2.8×10^{-7}s at -3 V. These imply that the relaxation time (t_{MW}-t_{RC}) decreases by DIO additive, because t_{RC} is the same for devices with and without DIO. Table 2 also represents the estimated space-charge field E_s and accumulated charge density Q_s in BHJ. EFISHG result indicates that the space charge field E_s is pointing in the opposite direction to the external field. At +3 V, E_s is reduced from -1.1×10^7 V/cm to -8.2×10^6 V/cm by adding DIO. At -3 V, E_s is decreased from $+5.7 \times 10^6$ V/cm to $+2.7 \times 10^6$ V/cm by adding DIO. As described in Eq. 5, reduction of the space charge field E_s originates from the decrease of the accumulated charge Q_s. Actually, the results showed that Q_s is decreased from 5.0×10^{-8} C/cm^2 to 3.9×10^{-8} C/cm^2 at

+3 V by adding DIO. The EFISHG results demonstrate that the relaxation time (t_{MW}-t_{RC}), the space charge field E_s, and interface charge Q_s are decreased by using DIO additive. This confirms that the size of the optimum domain produces the interface with similar relaxation times and leads to reducing the accumulate charge Q_s due to the MW-type charging. These effects contribute to the improvement of the device performance. It is noteworthy that the BHJ molecules bundle into large domains without DIO, a large average hopping distance between domains. An increased accumulated charge is caused by large domains. With DIO, the size of domains is reduced, and a smaller hopping distance is expected. The DIO contributes to a suitable internal field that drives the electrons toward the ITO electrode and holes toward the PEDOT: PSS/Au electrode and leads to improvement in efficiency performance.
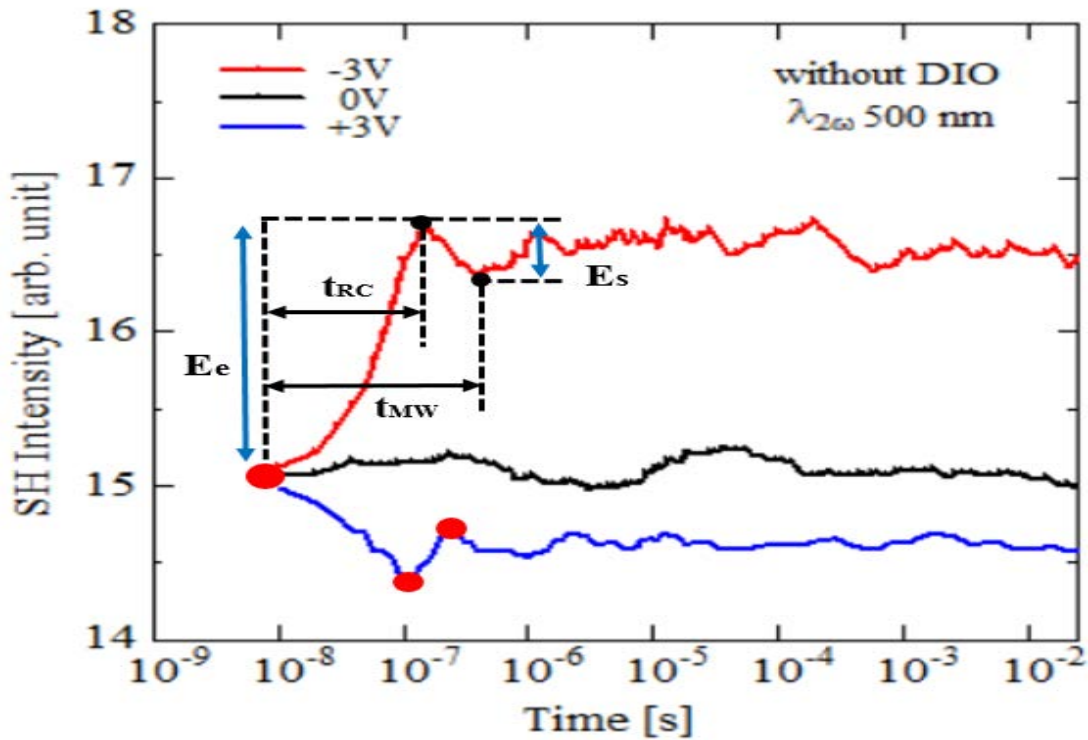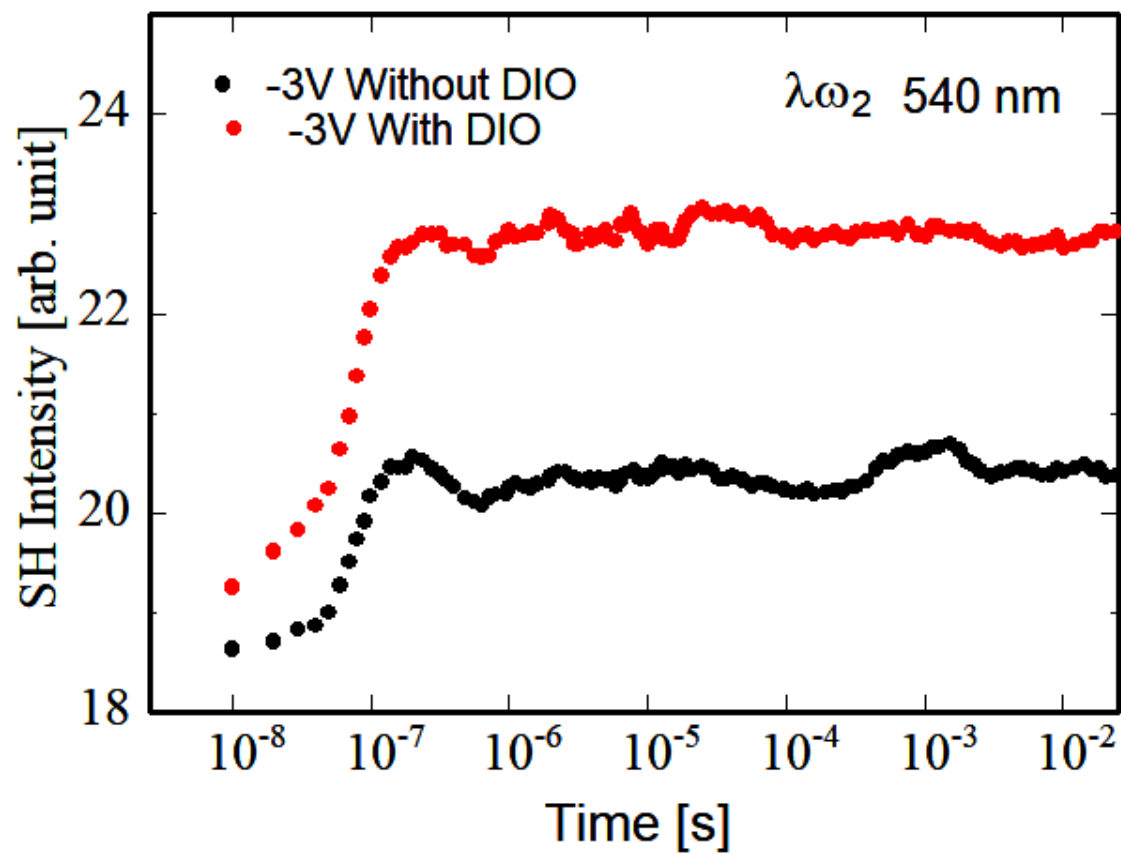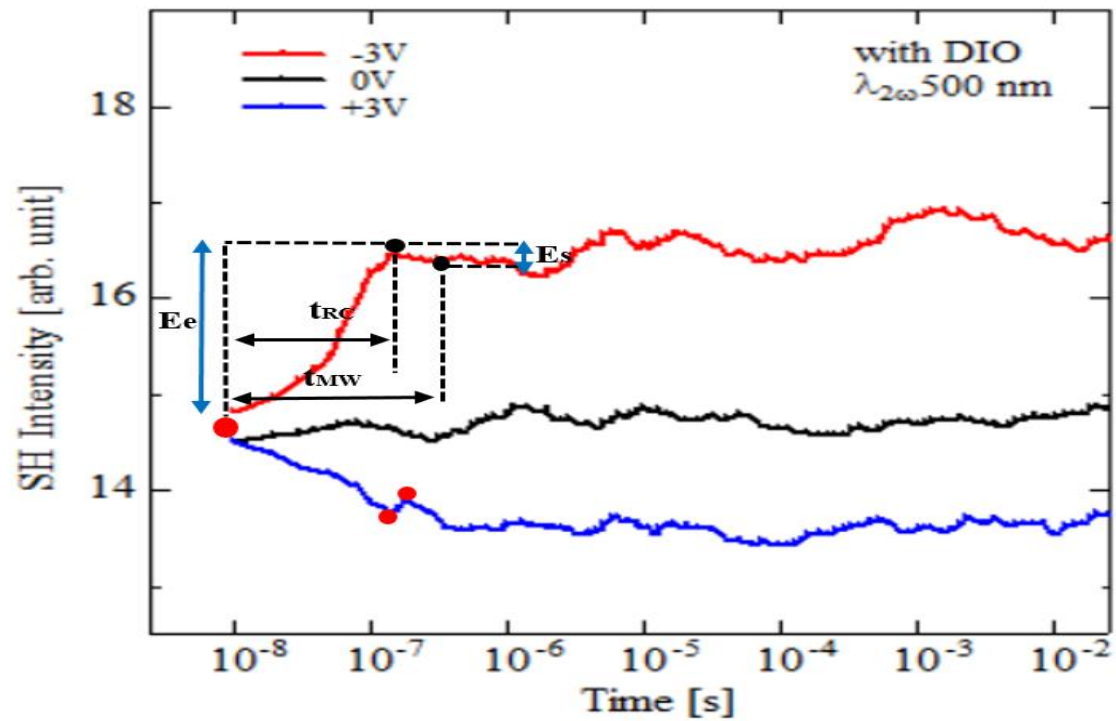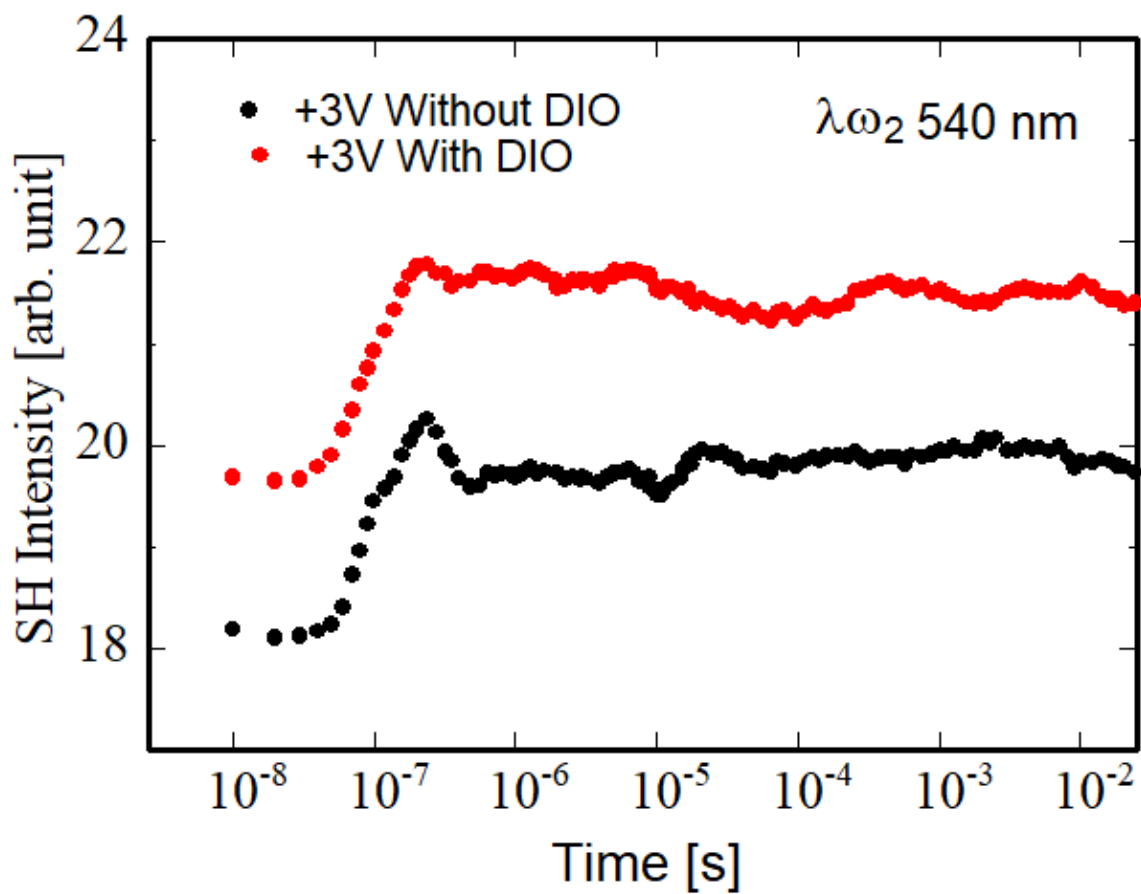
Figure 4.8. EFISHG measurement with applied voltage pulse in illumination condition. Relaxation times for the electrode charge t_{RC} and interface charge relaxations t_{MW}

Table 4.2. Comparison of SHG result for BHJ in sandwich structures without DIO and with DIO. Vex: External Voltages, t_{RC}: the circuit response time that is given by $t_{RC} = RC$, t_{MW}: The response time of Maxwell-Wagner charging, Es: The space charge field, Qs: The accumulated charge density

BHJ without DIO					
SHG	Vex	t_{RC}	t_{MW}	Es	Qs
500	+3 V	1.2×10^{-7} s	2.4×10^{-7} s	-1.1×10^{7} V/cm	5.0×10^{-8} C/cm^2
500	-3 V	1.6×10^{-7} s	4.0×10^{-7} s	$+5.7 \times 10^{6}$ V/cm	2.7×10^{-8} C/cm^2
540	+3 V	2.4×10^{-7} s	4.8×10^{-7} s	-6.0×10^{7} V/cm	5.5×10^{-8} C/cm^2
540	-3 V	2.0×10^{-7} s	6.4×10^{-7} s	$+1.0 \times 10^{7}$ V/cm	9.7×10^{-8} C/cm^2
BHJ with DIO					
SHG	Vex	t_{RC}	t_{MW}	Es	Qs
500	+3 V	1.3×10^{-7} s	1.8×10^{-7} s	-8.2×10^{6} V/cm	3.9×10^{-8} C/cm^2
500	-3 V	1.6×10^{-7} s	2.8×10^{-7} s	$+2.7 \times 10^{6}$ V/cm	1.3×10^{-8} C/cm^2
540	+3 V	2.4×10^{-7} s	3.6×10^{-7} s	-2.5×10^{6} V/cm	2.3×10^{-8} C/cm2
540	-3 V	2.4×10^{-7} s	6.4×10^{-7} s	$+5.7 \times 10^{6}$ V/cm	5.3×10^{-8} C/cm2

4.9 Conclusions

This chapter focuses on applying EFISHG measurement to evaluate the influence of adding 3 wt% DIO solvent to PCPDTBT: PC$_{71}$BM (BHJ). It is concluded that modifying the size of domains would vitally improve the performance of the BHJ layer. More specifically, the efficiency of BHJ was increased by around 25%. Interestingly, the SHG measurement is a feasible option to track the transportation of electrons and holes at the donor and acceptor and therefore aids to examine the associated electric field. However, it is important to justify the laser wavelength. Moreover, the internal electric field has improved by adding DIO. DIO additive has a considerable effect to decrease the relaxation time, interface charge and space charge field. Therefore, it is agreed that optimising of the domain size of interface is important to reduce the accumulated charge. This in turn would lead to enhance the performance of the PCPDTBT: PC$_{71}$BM based BHJ film.

4.10 Bibliography

1) He, Z., Xiao, B., Liu, F., Wu, H., Yang, Y., Xiao, S., ... & Cao, Y. (2015). Single-junction polymer solar cells with high efficiency and photovoltage. Nature Photonics, 9(3), 174-179.

2) Chen, J. D., Cui, C., Li, Y. Q., Zhou, L., Ou, Q. D., Li, C., ... & Tang, J. X. (2015). Single-junction polymer solar cells exceeding 10% power conversion efficiency. *Advanced Materials*, *27*(6), 1035-1041.

3) Li, S., Ye, L., Zhao, W., Zhang, S., Mukherjee, S., Ade, H., & Hou, J. (2016). Energy-level modulation of small-molecule electron acceptors to achieve over 12% efficiency in polymer solar cells. *Advanced materials*, *28*(42), 9423-9429.

4) Liu, Y., Zhao, J., Li, Z., Mu, C., Ma, W., Hu, H., ... & Yan, H. Aggregation and morphology control enables multiple cases of high-efficiency polymer solar cells, Nat. Commun. 5 (2014) 5293. *Yu, L. Huang, D. Yang, P. Fu, L. Zhou, J. Zhang, et al., Efficiency exceeding*, *10*, 10660-10665.

5) Zhao, J., Li, Y., Hunt, A., Zhang, J., Yao, H., Li, Z., ... & Yan, H. (2016). A difluorobenzoxadiazole building block for efficient polymer solar cells. *Advanced Materials*, *28*(9), 1868-1873.

6) Dou, L., You, J., Hong, Z., Xu, Z., Li, G., Street, R. A., & Yang, Y. (2013). 25th anniversary article: a decade of organic/polymeric photovoltaic research. *Advanced materials*, *25*(46), 6642-6671.

7) Markov, D. E., Amsterdam, E., Blom, P. W., Sieval, A. B., & Hummelen, J. C. (2005). Accurate measurement of the exciton diffusion length in a conjugated polymer using a heterostructure with a side-chain cross-linked fullerene layer. *The Journal of Physical Chemistry A*, *109*(24), 5266-5274.

8) Shaw, P. E., Ruseckas, A., & Samuel, I. D. (2008). Exciton diffusion measurements in poly (3-hexylthiophene). *Advanced Materials*, *20*(18), 3516-3520.

9) Arca, F., Loch, M., & Lugli, P. (2014). Enhancing efficiency of organic bulkheterojunction solar cells by using 1, 8-diiodooctane as processing additive. *IEEE Journal of Photovoltaics*, *4*(6), 1560-1565.

10) Zusan, A., Gieseking, B., Zerson, M., Dyakonov, V., Magerle, R., & Deibel, C. (2015). The effect of diiodooctane on the charge carrier generation in organic solar cells based on the copolymer PBDTTT-C. *Scientific reports*, *5*(1), 1-8.

11) Heeger, A. J. (2014). 25th anniversary article: bulk heterojunction solar cells: understanding the mechanism of operation. *Advanced Materials*, *26*(1), 10-28.

12) Chen, L. M., Hong, Z., Li, G., & Yang, Y. (2009). Recent progress in polymer solar cells: manipulation of polymer: fullerene morphology and the formation of efficient inverted polymer solar cells. *Advanced Materials*, *21*(14-15), 1434-1449.

13) Deibel, C., & Dyakonov, V. (2010). Polymer–fullerene bulk heterojunction solar cells. *Reports on Progress in Physics*, *73*(9), 096401.

14) Liu, Z., & Lee, E. C. (2015). Solvent engineering of the electron transport layer using 1, 8-diiodooctane for improving the performance of perovskite solar cells. *Organic Electronics*, *24*, 101-105.

15) Li, W., Zhou, Y., Andersson, B. V., Andersson, L. M., Thomann, Y., Veit, C., ... & Wuerfel, U. (2011). The Effect of additive on performance and shelf-stability of HSX-1/PCBM photovoltaic devices. *Organic electronics*, *12*(9), 1544-1551.

16) Chang, S. Y., Liao, H. C., Shao, Y. T., Sung, Y. M., Hsu, S. H., Ho, C. C., ... & Chen, Y. F. (2013). Enhancing the efficiency of low bandgap conducting polymer bulk heterojunction

solar cells using P3HT as a morphology control agent. *Journal of Materials Chemistry A*, *1*(7), 2447-2452.

17) McDowell, C., Abdelsamie, M., Zhao, K., Smilgies, D. M., Bazan, G. C., & Amassian, A. (2015). Synergistic impact of solvent and polymer additives on the film formation of small molecule blend films for bulk heterojunction solar cells. *Advanced Energy Materials*, *5*(18), 1501121.

18) Peng, J., Sun, Y., Chen, Y., Yao, Y., & Liang, Z. (2016). Light and thermally induced evolutional charge transport in CH3NH3PbI3 perovskite solar cells. *ACS Energy Letters*, *1*(5), 1000-1006.

19) Shimata, Y., & Saeki, A. (2017). Hole Relaxation in Polymer: Fullerene Solar Cells Examined by the Simultaneous Measurement of Time-of-Flight and Time-Resolved Microwave Conductivity. *The Journal of Physical Chemistry C*, *121*(34), 18351-18359.

20) Shintaku, N., Izawa, S., Takagi, K., Naito, H., & Hiramoto, M. (2017). Hole-and electron-only transport in ratio-controlled organic co-deposited films observed by impedance spectroscopy. *Organic Electronics*, *50*, 515-520.

21) Nogueira, A. F., Montanari, I., Nelson, J., Durrant, J. R., Winder, C., Sariciftci, N. S., & Brabec, C. (2003). Charge recombination in conjugated polymer/fullerene blended films studied by transient absorption spectroscopy. *The Journal of Physical Chemistry B*, *107*(7), 1567-1573.

22) Moritomo, Y., Yonezawa, K., & Yasuda, T. (2016). Carrier formation dynamics in prototypical organic solar cells as investigated by transient absorption spectroscopy. *International Journal of Photoenergy*, *2016*.

23) Peet, J., Kim, J. Y., Coates, N. E., Ma, W. L., Moses, D., Heeger, A. J., & Bazan, G. C.

(2007). Efficiency enhancement in low-bandgap polymer solar cells by processing with alkane dithiols. *Nature materials*, *6*(7), 497-500.

24) Zhao, J., Li, Y., Yang, G., Jiang, K., Lin, H., Ade, H., ... & Yan, H. (2016). Efficient organic solar cells processed from hydrocarbon solvents. *Nature Energy*, *1*(2), 1-7.

25) Huang, Y., Kramer, E. J., Heeger, A. J., & Bazan, G. C. (2014). Bulk heterojunction solar cells: morphology and performance relationships. *Chemical reviews*, *114*(14), 7006-7043.

26) Ye, L., Zhang, S., Ma, W., Fan, B., Guo, X., Huang, Y., ... & Hou, J. (2012). From binary to ternary solvent: morphology fine-tuning of D/A blends in PDPP3T-based polymer solar cells. *Advanced Materials*, *24*(47), 6335-6341.

27) Collins, B. A., Li, Z., Tumbleston, J. R., Gann, E., McNeill, C. R., & Ade, H. (2013). Absolute measurement of domain composition and nanoscale size distribution explains performance in PTB7: PC$_{71}$BM solar cells. *Advanced Energy Materials*, *3*(1), 65-74.

28) Liu, F., Zhao, W., Tumbleston, J. R., Wang, C., Gu, Y., Wang, D., ... & Russell, T. P. (2014). Understanding the morphology of PTB7: PCBM blends in organic photovoltaics. *Advanced Energy Materials*, *4*(5), 1301377.

29) Cheng, P., Ye, L., Zhao, X., Hou, J., Li, Y., & Zhan, X. (2014). Binary additives synergistically boost the efficiency of all-polymer solar cells up to 3.45%. *Energy & Environmental Science*, *7*(4), 1351-1356.

30) Yao, Y., Hou, J., Xu, Z., Li, G., & Yang, Y. (2008). Effects of solvent mixtures on the nanoscale phase separation in polymer solar cells. *Advanced Functional Materials*, *18*(12), 1783-1789.

31) Guo, X., Zhang, M., Ma, W., Ye, L., Zhang, S., Liu, S., ... & Hou, J. (2014). Enhanced Photovoltaic Performance by Modulating Surface Composition in Bulk Heterojunction

Polymer Solar Cells Based on PBDTTT-C-T/PC$_{71}$BM. *Advanced materials*, *26*(24), 4043-4049.

32) Ye, L., Jing, Y., Guo, X., Sun, H., Zhang, S., Zhang, M., ... & Hou, J. (2013). Remove the residual additives toward enhanced efficiency with higher reproducibility in polymer solar cells. *The Journal of Physical Chemistry C*, *117*(29), 14920-14928.

33) Tremolet de Villers, B. J., O'Hara, K. A., Ostrowski, D. P., Biddle, P. H., Shaheen, S. E., Chabinyc, M. L., ... & Kopidakis, N. (2016). Removal of residual diiodooctane improves photostability of high-performance organic solar cell polymers. *Chemistry of Materials*, *28*(3), 876-884.

34) Venkatesan, S., Chen, Q., Ngo, E. C., Adhikari, N., Nelson, K., Dubey, A., ... & Qiao, Q. (2014). Polymer solar cells processed using anisole as a relatively nontoxic solvent. *Energy Technology*, *2*(3), 269-274.

35) Li, S., Zhang, H., Zhao, W., Ye, L., Yao, H., Yang, B., ... & Hou, J. (2016). Green-solvent-processed all-polymer solar cells containing a perylene diimide-based acceptor with an efficiency over 6.5%. *Advanced Energy Materials*, *6*(5), 1501991.

36) Zhang, H., Yao, H., Zhao, W., Ye, L., & Hou, J. (2016). High-efficiency polymer solar cells enabled by environment-friendly single-solvent processing. *Advanced Energy Materials*, *6*(6), 1502177.

37) Park, C. D., Fleetham, T. A., Li, J., & Vogt, B. D. (2011). High performance bulk-heterojunction organic solar cells fabricated with non-halogenated solvent processing. *Organic Electronics*, *12*(9), 1465-1470.

38) Chen, K. S., Yip, H. L., Schlenker, C. W., Ginger, D. S., & Jen, A. K. Y. (2012). Halogen-free solvent processing for sustainable development of high efficiency organic solar

cells. *Organic Electronics*, *13*(12), 2870-2878.

39) Chueh, C. C., Yao, K., Yip, H. L., Chang, C. Y., Xu, Y. X., Chen, K. S., ... & Chen, W. C. (2013). Non-halogenated solvents for environmentally friendly processing of high-performance bulk-heterojunction polymer solar cells. *Energy & Environmental Science*, *6*(11), 3241-3248.

40) Tsai, P. T., Tsai, C. Y., Wang, C. M., Chang, Y. F., Meng, H. F., Chen, Z. K., ... & Yu, P. (2014). High-efficiency polymer solar cells by blade coating in chlorine-free solvents. *Organic Electronics*, *15*(4), 893-903.

41) Sprau, C., Buss, F., Wagner, M., Landerer, D., Koppitz, M., Schulz, A., ... & Colsmann, A. (2015). Highly efficient polymer solar cells cast from non-halogenated xylene/anisaldehyde solution. *Energy & Environmental Science*, *8*(9), 2744-2752.

42) Guo, X., Zhang, M., Cui, C., Hou, J., & Li, Y. (2014). Efficient polymer solar cells based on poly (3-hexylthiophene) and indene–C60 bisadduct fabricated with non-halogenated solvents. *ACS applied materials & interfaces*, *6*(11), 8190-8198.

43) Zhao, W., Ye, L., Zhang, S., Sun, M., & Hou, J. (2015). A universal halogen-free solvent system for highly efficient polymer solar cells. *Journal of Materials Chemistry A*, *3*(24), 12723-12729.

44) Chen, X., Liu, X., Burgers, M. A., Huang, Y., & Bazan, G. C. (2014). Green-Solvent-Processed Molecular Solar Cells. *Angewandte Chemie*, *126*(52), 14606-14609.

45) Cai, W., Liu, P., Jin, Y., Xue, Q., Liu, F., Russell, T. P., ... & Cao, Y. (2015). Morphology Evolution in High-Performance Polymer Solar Cells Processed from Nonhalogenated Solvent. *Advanced Science*, *2*(8), 1500095.

46) Meng, B., Song, H., Chen, X., Xie, Z., Liu, J., & Wang, L. (2015). Replacing alkyl with

oligo (ethylene glycol) as side chains of conjugated polymers for close π–π stacking. *Macromolecules*, *48*(13), 4357-4363.

47) Lee, J. K., Ma, W. L., Brabec, C. J., Yuen, J., Moon, J. S., Kim, J. Y., ... & Heeger, A. J. (2008). Processing additives for improved efficiency from bulk heterojunction solar cells. *Journal of the American Chemical Society*, *130*(11), 3619-3623.

48) Ho, C. H. Y., Dong, Q., Yin, H., Leung, W. W. K., Yang, Q., Lee, H. K. H., ... & So, S. K. (2015). Impact of solvent additive on carrier transport in polymer: fullerene bulk heterojunction photovoltaic cells. *Advanced Materials Interfaces*, *2*(12), 1500166.

49) Huo, L., Liu, T., Sun, X., Cai, Y., Heeger, A. J., & Sun, Y. (2015). Single-junction organic solar cells based on a novel wide-bandgap polymer with efficiency of 9.7%. *Advanced Materials*, *27*(18), 2938-2944.

50) Taguchi, D., Sumiyoshi, R., Chen, X., Manaka, T., & Iwamoto, M. (2014). Study of interface layer effect in organic solar cells by electric-field-induced optical second-harmonic generation measurement. *Thin solid films*, *554*, 51-53.

51) Taguchi, D., Shino, T., Zhang, L., Li, J., Weis, M., Manaka, T., & Iwamoto, M. (2011). Direct probing of photovoltaic effect generated in double-layer organic solar cell by electric-field-induced optical second-harmonic generation. *Applied physics express*, *4*(2), 021602.

52) Chen, X., Taguchi, D., Manaka, T., & Iwamoto, M. (2014). Interfacial charging originated from the conductivity decrease of C60 layer in IZO/pentacene/C60/Al organic double-layer solar cells. *Organic Electronics*, *15*(1), 162-168.

53) Verbiest, T., Clays, K., & Rodriguez, V. (2009). *Second-order nonlinear optical characterization techniques: an introduction*. CRC press.

54) Ahmad, Z., Abdullah, S. M., Taguchi, D., Sulaiman, K., & Iwamoto, M. (2015). A way for studying the impact of PEDOT: PSS interface layer on carrier transport in PCDTBT: $PC_{71}BM$ bulk hetero junction solar cells by electric field induced optical second harmonic generation measurement. *Journal of Applied Physics*, *117*(16), 163101.

55) Chen, X., Taguchi, D., Shino, T., Manaka, T., & Iwamoto, M. (2011). Analysis of interface carrier accumulation and relaxation in pentacene/C60 double-layer organic solar cell by impedance spectroscopy and electric-field-induced optical second harmonic generation. *Journal of Applied Physics*, *110*(7), 074509.

56) Taguchi, D., Weis, M., Manaka, T., & Iwamoto, M. (2009). Probing of carrier behavior in organic electroluminescent diode using electric field induced optical second-harmonic generation measurement. *Applied Physics Letters*, *95*(26), 342.

57) Alrougy, I. M., Taguchi, D., & Manaka, T. (2019). Spectroscopic Study of Electric Field Induced Optical Second Harmonic Generation from PCPDTBT and PC 71 BM Thin Films. *IEICE Transactions on Electronics*, *102*(2), 119-124.

58) Lou, S. J., Zhou, N., Guo, X., Chang, R. P., Marks, T. J., & Chen, L. X. (2018). Effects of 1, 8-diiodooctane on domain nanostructure and charge separation dynamics in PC 71 BM-based bulk heterojunction solar cells. *Journal of Materials Chemistry A*, *6*(46), 23805-23818.

59) M. Pagliaro, R. Ciriminna, and G. Palmisano, *Flexible solar cells* (Wiley, Weinheim, 2008) Chapter 4.

60) Taguchi, D., Shino, T., Chen, X., Zhang, L., Li, J., Weis, M., ... & Iwamoto, M. (2011). Analyzing photovoltaic effect of double-layer organic solar cells as a Maxwell-Wagner effect system by optical electric-field-induced second-harmonic generation measurement. *Journal of Applied Physics*, *110*(10), 103717.

Chapter 5

5 Investigation of Z907 Additive Effect on Carrier Transport in BHJ by EFISHG

5.1 Introduction

This chapter aims to experimentally conduct the Z907 with BHJ in solar cell measurement using the electric-field-induced optical second harmonic generation (EFISHG) measurement via laser wavelength. The prepared nanoparticles were added to the Z907 dye in order to study their effect on the carrier transport of the fabricated BHJ solar cell. From EIS investigation, a decrease in resistance is noticed from 5400 to 4300 in Z907's device. This fall in resistance plays a role in improved photoelectrons which are formed in the BHJ layer indicating that the end of the electrode is reached without any loss. Occasionally, most results from EFISHG Measurement of the internal field, which is directed from Au to ITO electrode, have shown massive improvements. Moreover, this indicates that the improvement of the internal field is due to the Z907 additive. The enhanced performance is attributed to OSCs with Z907 which may scatter more photons to the substrate in comparison to the particle free solar cell. Thus, the carrier behavior in the solar cell is enhanced which subsequently results in efficiency enhancement of about 45%.

5.2 General background

A process that takes place in all plants and organisms that enables them to transform solar energy to chemical energy is known photosynthesis. This is where dyes and pigments are used for overall growth. As a result, research expertise decided to further study and focus on the photoexcitation of dye molecules where movement of charge takes place. This is especially in renewable energy applications which include all of the following areas: artificial photosynthesis,[1,2] water splitting

and fuel cells,[3−5] and photovoltaics (PVs).[6−9] Specifically in the field of photovoltaics, joining of dye molecules (also known as conjugated polymers) with inorganic electron accepting materials happens. This joining results in hybrid organic−inorganic materials which consist of solution-processability. This would be provided from an organic donor considering all of mechanical, environmental, and thermal stabilities of the inorganic acceptor. In fact, there are two forms of organic/metal oxide PV devices which are (1) "bulk hetero-junction" organic solar cells and (2) conjugated polymer/metal oxide devices. In the first type, excited electrons from both light absorbing active layer and hole-electron transport are accepted by a nanostructured porous metal oxide electrode. However, the second type differs because the polymer acts as both the light absorber and the hole conductor. When light is absorbed by a conjugated polymer, a bound electron−hole pair is generated which is called, an exciton. Moreover, in order to encourage exciton dissociation and electrons movement, great organic/inorganic interfacial areas are required for the excitonic origin of the photoexcited state. The electron flow would be from the conjugated polymer to the metal oxide [10-11]. In addition, transferring charges to individual electrodes must ensure every stage is continuous in the active layer.

In order to gain BHJ-type morphologies in conjugated polymer/metal oxide films, a nanostructured metal oxide layer is manufactured. Then, the conjugated polymer is penetrated [12-13] ensuring the conjugated polymer is mixed with metal oxide nanoparticles [14−16]. Possibly, if not this, there should be a joining section for the conjugated polymer with appropriate metal oxide precursors [17,18]. As up-to-date research indicates, highly ordered BHJ morphologies are accomplished via dye self-assembled monolayers (SAMs) using ITO. This way, a significantly ordered conjugated metal is gained which consists of a mesostructured SAMs film. Anyhow, by using judicious selection of the structure-directing agents (SDA), closeness between the

conjugated polymer and the ITO framework is directly managed. In return, charge generation efficiency is also controlled [19]. Usually, any BHJ hybrid films would have a thickness of ~200 nm which leads them to powerfully absorb in the clear area of the electromagnetic spectrum. So far, almost all studies outlined a substandard photovoltaic performance where power conversion efficiencies would be less than 2% [20]. According to some experiments, the reduced extent of electronic coupling between organic conjugated polymer and inorganic metal oxide is the major cause for small charge generation efficiency [21,22]. However, it is necessary to consider that via bridging coordination bonding, dyes can be powerfully coupled. As a result, quick coherent electron injection takes place from the dye's excited state to the ITO [10,24]. As well as this, there would be a methodical charge formation having a device efficacy of greater than 12%. As a matter of fact, when the conjugated polymer is used as the hole conductor, computations of incident photon-to-current efficiency for the solid-state OSCS prove that the major part of the photocurrent is produced as a result to dye excitation where the dye's efficient electron injection is reflected reliably [25−27].

Actually, in order to develop the device's performance, introducing dye molecules into conjugated polymer/metal oxide BHJ materials is the trick. This is because enhanced dye/metal oxide couple whilst ensuring the polymer-based device is simply evaluated and manufactured [28−30]. When it comes to gaining advantages from dye communication with the conjugated polymer/metal oxide BHJ materials, managing both dye's location and chemical interconnections is important. To be more certain that dye/metal oxide interactions produce the electronic coupling, the dye molecules have to be pointed towards the hybrid inorganic−organic surface. This electronic coupling is vital to gather any electrons linked to the dye's photoexcited state. The fact that dye molecules have an influence on the efficacy of a conjugated polymer/metal oxide device, was first outlined by Goh

et al. for bilayer devices [31]. To ensure improvement in both light harvesting and repression of charge recombination, depositing a monolayer of dye molecules has to take place between the ITO and the conjugated polymer. Thus, the devices' efficacy is maximized. Various methods of dye integration into the conjugated polymer have been outlined in many studies that focus on BHJ devices. One of these methods is known is dye grafting onto ITO [28−30, 32-35]. Despite the success in developing these devices where photocurrent was well formed, however there was a poor electron transfer taking place between nanoparticles (nanorods), which hinders the device's performance.

5.3   Metal complexes (Z907)

The metal Ruthenium was first found by a Russian scientist called Karl Ernst Claus in the year 1844. In today's world and even before, the maximum efficient cell performance for DSSC used Ruthenium complex dye derivatives. Primarily, Ruthenium is an infrequent transition metal which originates from the VIII group having a coordination number of 6. Moreover, it can form powerful bonds with immine group (-C=N-). Commonly, ruthenium complexes are known to bind to TiO2 via carboxylic group (-COOH) that is anchored to two 2-2' bipyridine as illustrated in Figure. 5.1.
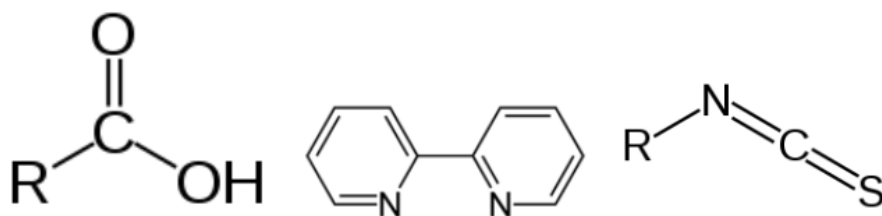
Figure 5.1. Carboxylic group, 2,2 bipyridine group and isothiocyanate group (starting from the left side)

Once examining the full compound, two isothiocyanate groups are located at the opposing side. Photoexcited electrons are noticed to move from the di-immine group all the way to the titanium substrate to the COOH group once the dye is added. For this scenario, titanium dioxide injection

occurs in a tiny period of time, femto (pico) seconds. In terms of charge, the positive charge density which is still found in the dye transfers to both Ru atom and isothiocyanate groups. This process takes place as a result to electrostatic repulsion. Thus, any recombination with the excited electrons is slowed due to the electrostatic forces. The commonly used types of ruthenium dyes include N719, N$_3$, and black dyes. In general, all these mentioned dyes demonstrate an acceptable absorbance spectrum, however a reduced extinction coefficient when contrasted to various dyes such as K19 and Z907.

For this study, a suitable dye for DSSC is referred to Z907 having the chemical name cisBis(isothiocyanato)(2,2'-bipyridyl4,4'-dicarboxylato)(4,4-di-nonyl-2-bipyridyl) ruthenium(II), as can be shown in Figure 5.2.
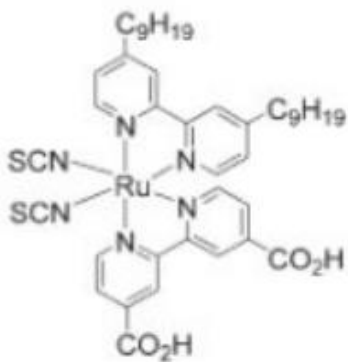

Figure 5.2. Z907 chemical structures

5.4 Sample fabrication

The electron transporting layer of this device, Z907, is prepared by mixing 5.22 mg with 30 ml of ethanol solvent. The solution is kept in an ultrasonic bath for more than an hour until it fully dissolves, and a red colour is seen. The sample for this investigation is dipped in the solution and left on a surface temperature of about 35 ˚C for minimum 12 hours as illustrated in Figure 5.3. Once that is accomplished, the sample is cleaned twice using ethanol and then placed in an oven at a temperature of 70 ˚C for approximately 3 hours. The next step is to ensure the precipitated

sample is Z907 via absorption as demonstrated in Figure 5.4. Two solutions of the active layer of this device are prepared which are PCPDTBT: PC$_{71}$BM. The first one is a concentrated solution made by mixing 10mg:15mg with 1 ml of chloroform solvent to produce 1:1.5 of PCPDTBT: PC$_{71}$BM solution. An estimate of 100 nm thick PCPDTBT: PC$_{71}$BM BHJ films were placed on top of PEDOT: PSS layers. Using thermal evaporation, the top gold (Au) electrode having a thickness of 100 nm was deposited as noted in Figure 5.5.

Figure 5.3. The sample fabrication
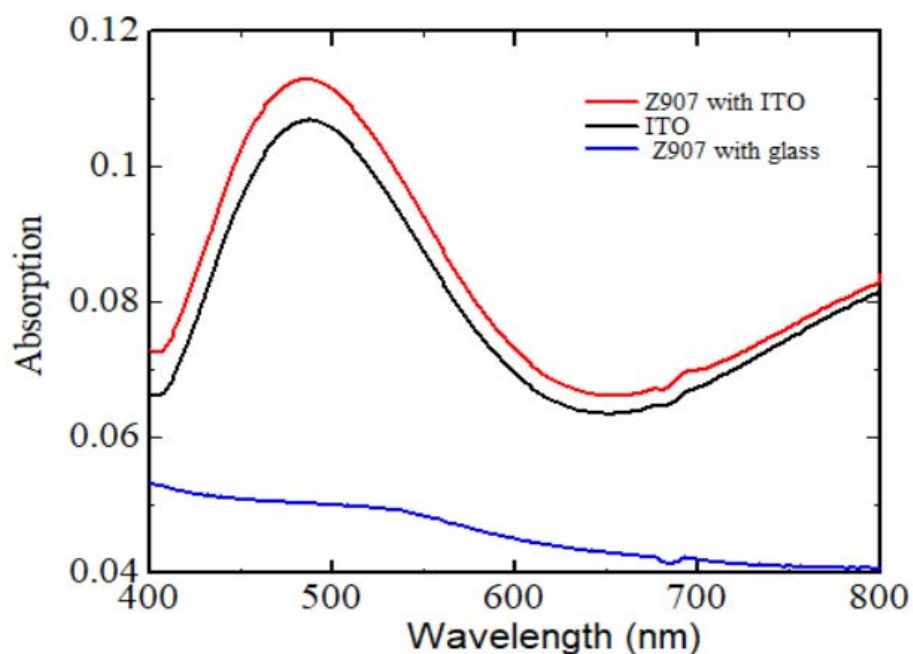
Figure 5.4. The absorption against the wavelength for three samples of Z907
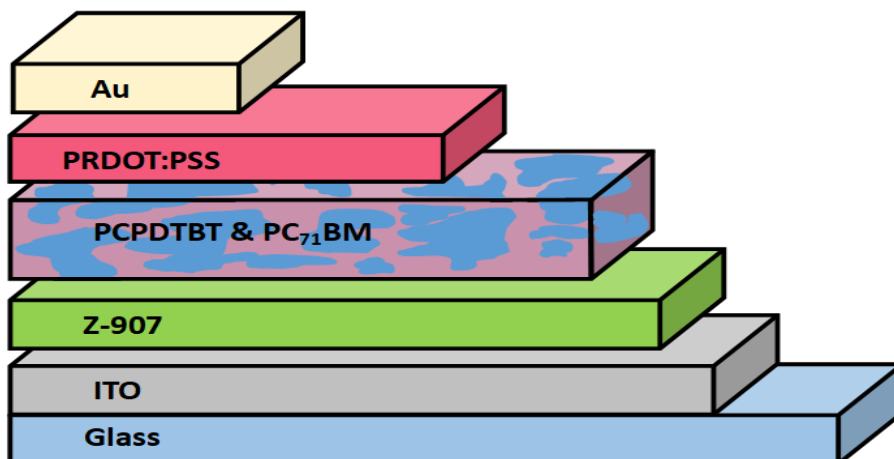
Figure 5.5. Schematic structure of BHJ solar cells with Z907.

5.5 I–V Characteristic

The current density-voltage characteristics of OSCs with Z907 are shown in Figure 5.6. In order to make reliable comparison, the current density-voltage characteristic of the reference OSCs without Z907 is also provided. Any data gained from J-V curve measurements regarding cell's performance are outlined in Table 5.1. The findings state that an increase in photocurrent density (JSC) is noted to be from 4.54 to 5.38. In addition, open-circuit voltage (VOC) also increases from 0.50 to 0.59 for OSCs with Z907. These results were compared to the OSCs that had no Z907. It is worth noting that as JSC increases, power conversion efficiency also increases directly. By using OSCs with Z907, an improved cell performance is obtained which enhances charge extraction to the substrate in comparison to the Z907 free solar cell. The efficiency achieved by the OSCs using Z907 was 0.98% with an efficiency enhancement of ~45 % compared to the OSCs without Z907.

Table 5.1. The cell's performance based on data gained from J-V curve measurements

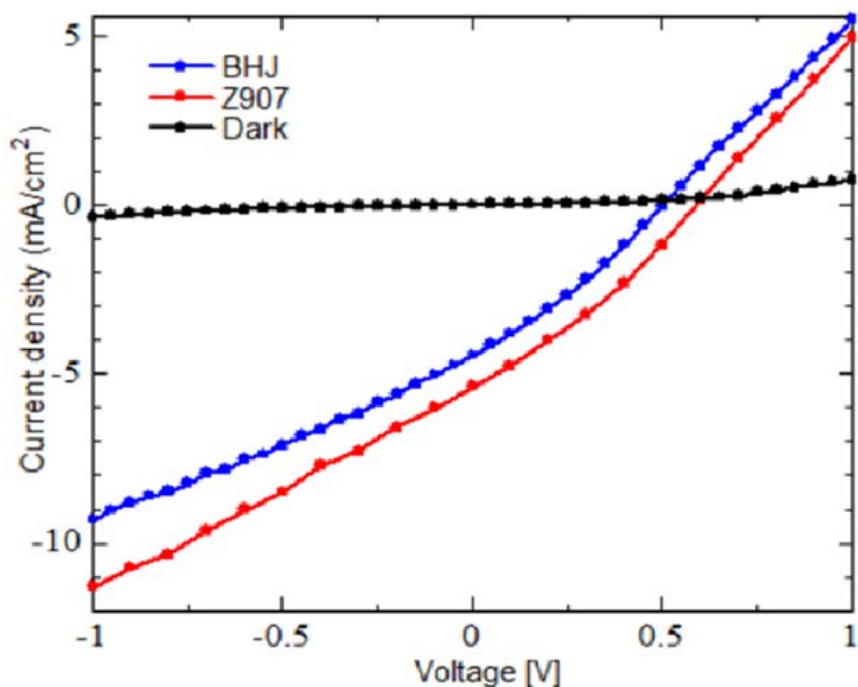| Inverted structure	Voc (V)	Jsc (mA/cm^2)	FF (%)	η (%)
BHJ	0.50	4.54	29	0.67
With Z-907	0.59	5.38	29	0.98

Figure 5.6. The relation between current density and supplied voltage of OSCs with Z907

5.6 IPCE spectra

In this work, the IPCE spectra is computed in order to analyse the impact of the device with and without the Z907 additive. Figure 5.7 presents that improvement of the IPCE device with Z907 additive had a wavelength range of 400-900 nm and AM 1.5G solar illumination which led to a developed efficiency of 45 %. Correspondingly, any improvements noticed in the IPCE indicate an improvement in light absorption and charge and exciton dissociation [36]. Moreover, Figure 5.7 declares that IPCE improvement is due to the Z907 additive. As well as this, a marginal influence on the absorption spectra is achieved as noticed in Figure 5.8. To sum up, the EFISHG was successfully used to discover the enhancement of IPCE due to the improvement of carrier behavior and charge extraction at both polymer/metal oxide BHJ materials and devices.
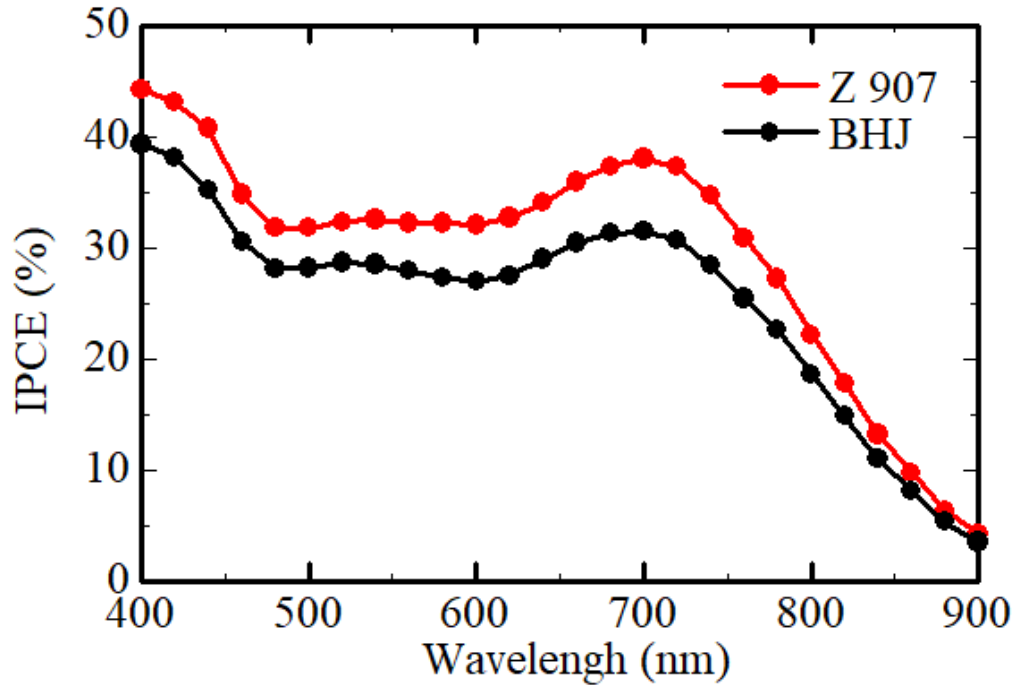
Figure 5.6. The relation between IPCE and wavelength of Z907 and BHJ

5.7 Absorption spectra

Analyzing the absorption spectrum of the active layer is significant in distinguishing the blend where the material type is correspondingly linked to the absorbed light. This was critically achieved by conducting the absorption spectrum for both with and without Z907 devices since the deposited material slows down the movement of photons to get the lower layer. Figure 5.8 illustrates the registered values of absorption spectra for with and without Z907 device. It is clearly noticed that there is no influence of adding Z907 additive on the absorption spectra. Furthermore, the thickness of active layer is not predominantly affected by the added Z907 additive.
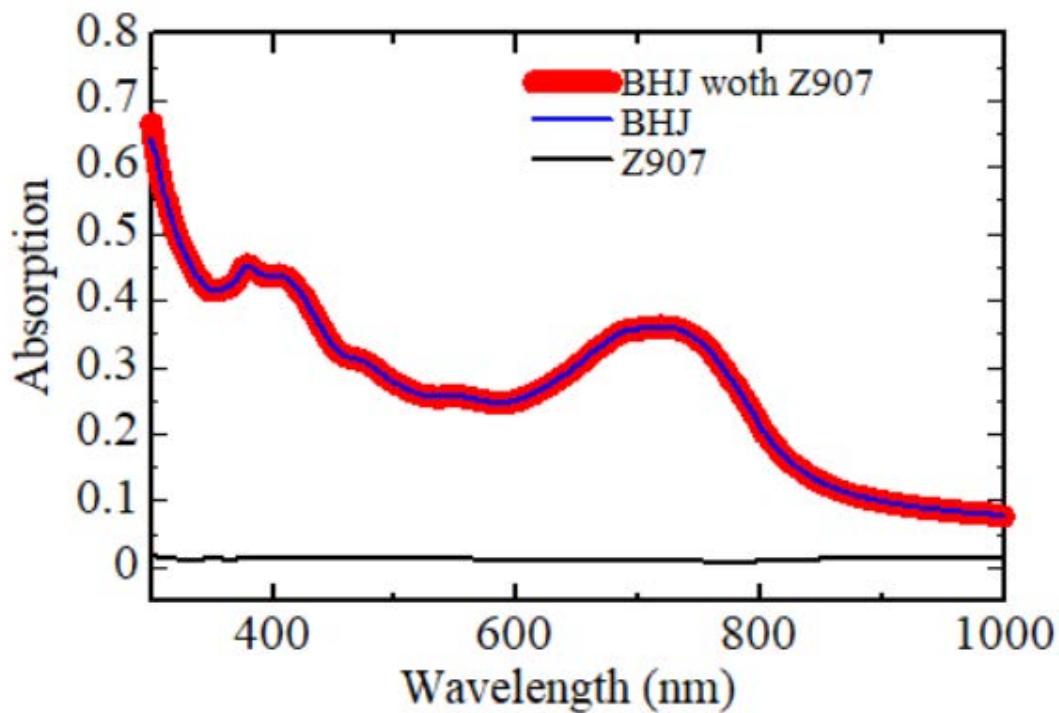
Figure 5.8. The variation of absorption vs wavelength for with and without adding Z907 to BHJ

5.8   Electrochemical impedance spectroscopy (EIS)

To gain a complete comprehension of the developed performance, impedance spectroscopic measurements were carried out to discover the device's resistance as illustrated in Figure 5.9. In general, the resistance is concluded from the diameter of the semicircle [37]. Using Z907, a fall in resistance is noted to be 5400 to 4300. Thus, both an enhanced photocurrent and FF are achieved as a result to developing transport properties which will be described later in this study.
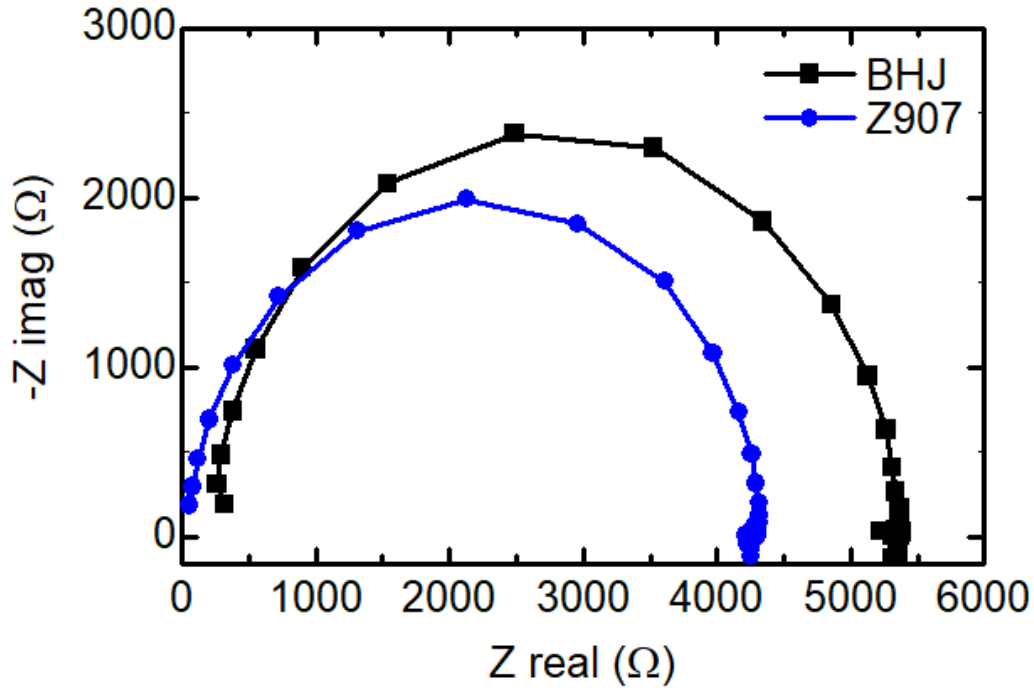
Figure 5.9. The impact of Z image on Z real for BHJ and Z907

As seen from Figure 5.10, the Randles cell is regarded as one of the uncomplicated and popular cell models. This cell consists of a double layer capacitor, a solution resistance, and a charge transfer (also known as polarization resistance). The Randles cell has proved to be a convenient cell where it is the initial point for complicated cell models. For this model, the following equations are used for both the real part of the impedance Z' and the imaginary part of the impedance Z''.

$$Z' = \frac{\frac{1}{R}}{\frac{1}{R^2} + \omega^2 C^2} \qquad (5.1)$$

$$Z'' = \frac{\omega\, C}{\frac{1}{R^2} + \omega^2 C^2} \qquad (5.2)$$

Furthermore, resistors for the cell were computed where series resistance was reduced from 300 to 500 after adding Z907.
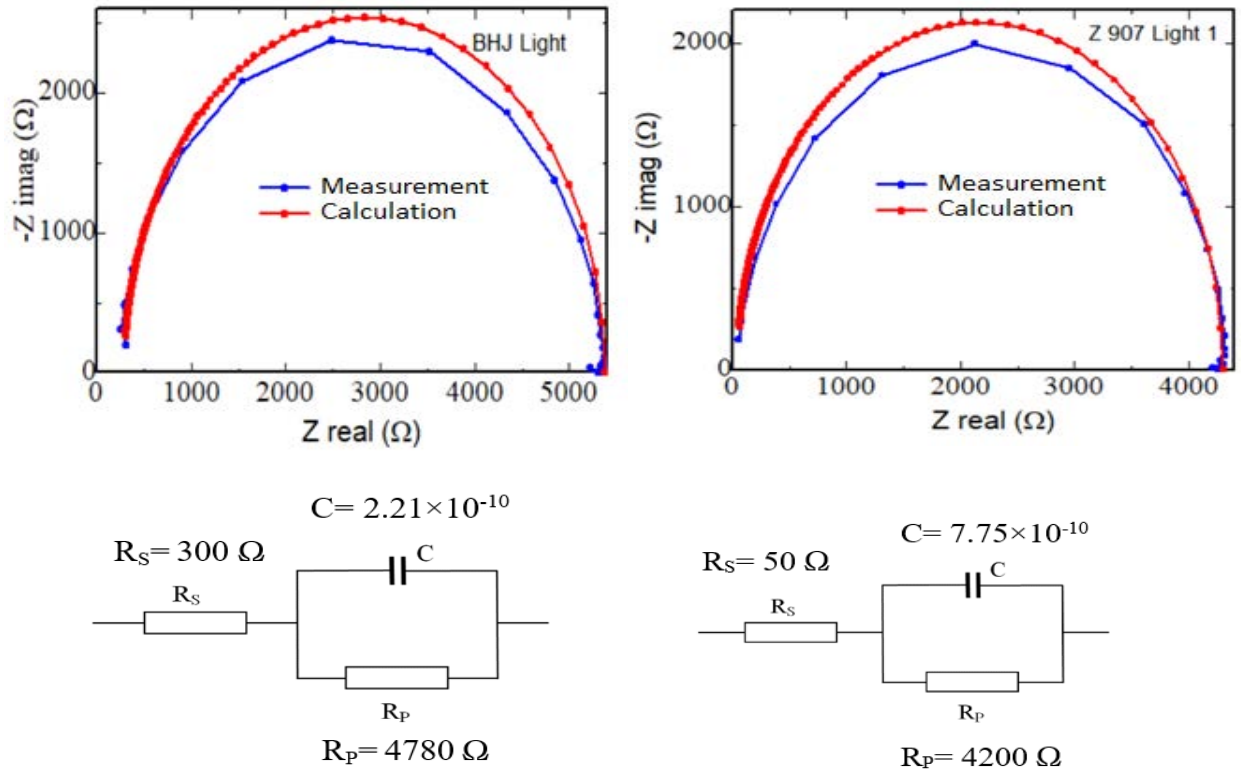
Figure 5.10. The consistency of Z image and Z real for BHJ and Z907 calculations towards the measurements

5.9   EFISHG Measurement

5.9.1   Internal Field

Basically, the internal field ($\vec{E}_P$) between PCPDTBT and PC$_{71}$BM stimulates the movements of holes where electrons generate in BHJ layer towards both Au and ITO electrode, respectively. However, applying an external voltage is required in order to generate internal electric field. Typically, it is known that the electric field $\vec{E}(0)$ in Z907 consists of three components: the external electric field ($\vec{E}_e$), the space-charge field ($\vec{E}_s$), and the internal electric field ($\vec{E}_P$). Regarding this, Figure 5.11 shows EFISHG intensity measurements for the two devices containing with and without Z907. The measurements were performed using a voltage range of +8 V to -8 V. Independently, an improvement in EFISHG is observed for both PCPDTBT and PC$_{71}$BM having

a wavelength of 500 nm and 540 nm, respectively. According to Eq. 1, the EFISHG intensity is proportional to the square of the local field ($I_{2\omega} \propto |\vec{E}_0|^2$). There is an applied minimum voltage of Ve= +1.8 V in each device in addition to the SH intensity of PCPDTBT using an SH wavelength of 500 nm. However, the SH intensity of $PC_{71}BM$ used an SH wavelength of 540 nm. It is notable to say that the minimum voltage has increased by Ve=+0.4V in Z907. Periodically, when voltage has a negative value, the process of internal field being directed from Au to ITO electrode has improved. Moreover, improvement in the internal field due to Z907 additive is clearly shown in Figure 5.11.
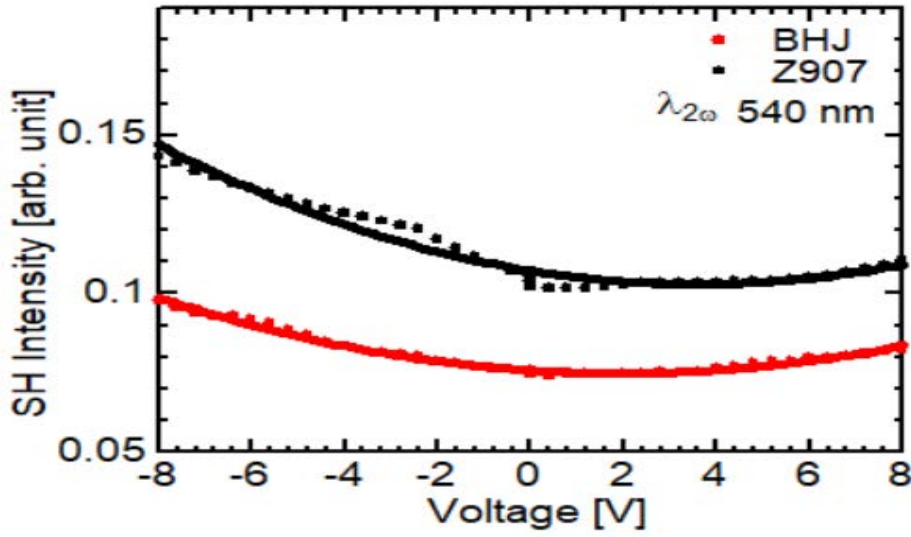

Figure 5.11. The SH intensity measurements of with and without Z907 against the voltage variation

5.9.2   Carrier Behavior

The alterations in SH intensity once EFISHG measurements were carried out against operational time are depicted in Figure 5.12. The conditions emphasized the use of OSCs devices both with and without Z907 additive for a voltage ranging from -3V and +3V. Specifically, the changes in SH intensity correspond greatly to the generated electrostatic field from electrode charges $\vec{E}_e$.

First, the findings from EFISHG measurements for the Z907 layer justify there is no alteration in SHG intensity when +3V was applied. This is because no impact was given by the donor layer. When examining Figure 5.12, the green color represents time from t = 0 to response time of the equivalent circuit t_{RC}. This is distinguished via igniting the electrostatic field in the BHJ layer. t_{RC} is dominantly linked to both the capacitance C of BHJ layer and resistance of ITO. Therefore, the generated SHG is agreed to be expressed as $|\vec{E}_P + \vec{E}_e(t)|^2$. Moreover, an interesting note is that experimental results from EFISHG measurements throughout time were compatible for both with and without Z907. On the other hand, the brown color represents the approximation of charge accumulation at both the donor and acceptor interface via an equivalent circuit model. It is important to consider that the charging process is also named as the Maxwell-Wagner effect. In this work, the emphasis is on modelling PCPDTBT (donor) as an electronic source with the two of conductance G_1 and capacitance C_1. Besides, modelling of PC$_{71}$BM (acceptor) was by using conductance G_2 and capacitance C_2. For this model, all charges provided by the donor have moved at time constant $t_1 = \frac{C_1}{G_1}$, and were gained in acceptor at time constant $t_2 = \frac{C_2}{G_2}$. These constants are classified as dielectric relaxation time. The measure in accumulated charge along the interfacial area of donor and acceptor is similar for both with and without the addition of Z907 layer. Further analysis of Figure 5.12 illustrates that the blue color is an indoor field in PC$_{71}$BM. This is where the Z907 has developed charge transport of electrons in the acceptor material. In terms of the yellow color, it points out the charge collection for the device. Normally, OSCs are popular for having a structure split into various sections: both of BHJ and the electrode linked together. When looking at the end of the acceptor material, basically there is an anchoring bound of BHJ to the ITO. The charge-transfer complex has unstable forces of attraction which are weaker than covalent forces. As a result, charge accumulation takes place between interface acceptor material and ITO.

This layer is agreed to have an engagement in electronic transition into ITO. As a carbon chain is formed, there is a bridge built between the acceptor and ITO. Therefore, this reduces charge recombination and elevates up charge collection for the device.
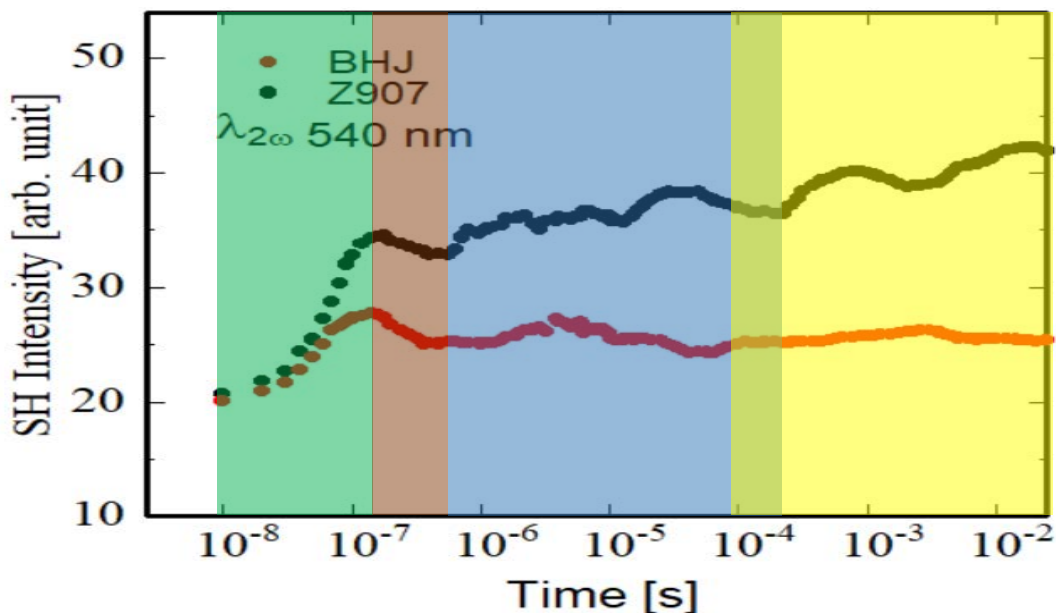

Figure 5.12. The influence of SH intensity with the time for BHJ and Z907

5.10 Conclusions

The electric-field-induced optical second harmonic generation (EFISHG) measurement via laser wavelength was used in this chapter to experimentally conduct the measurements of Z907 with BHJ in solar cell. This enables to study the influence of adding the nanoparticles to the Z907 dye on the carrier transport of the fabricated BHJ solar cell. The results of EFISHG measurement showed a drop in the resistance due to adding the Z907. This in turn has improved photoelectrons which are formed in the BHJ layer and internal field that instructed from Au to ITO electrode. Statistically, the efficiency of solar cell was enhanced by 45% due to the enhancement of the carrier behavior in the solar cell.

5.11 Bibliography

1. Eisele, D. M.; Cone, C. W.; Bloemsma, E. A.; Vlaming, S. M.; van der Kwaak, C. G. F.; Silbey, R. J.; Bawendi, M. G.; Knoester, J.; Rabe, J. P.; Vanden Bout, D. A. Utilizing Redox-Chemistry to Elucidate the Nature of Exciton Transitions in Supramolecular Dye Nanotubes. Nat. Chem. 2012, 4, 655−662.

2. Frischmann, P. D.; Mahata, K.; Wurthner, F. Powering the Future of Molecular Artificial Photosynthesis with Light-Harvesting Metallosupramolecular Dye Assemblies. Chem. Soc. Rev. 2013, 42, 1847− 1870.

3. Abe, R.; Shinmei, K.; Koumura, N.; Hara, K.; Ohtani, B. VisibleLight-Induced Water Splitting Based on Two-Step Photoexcitation between Dye-Sensitized Layered Niobate and Tungsten Oxide Photocatalysts in the Presence of a Triiodide/Iodide Shuttle Redox Mediator. J. Am. Chem. Soc. 2013, 135, 16872−16884.

4.) Brillet, J.; Yum, J. H.; Cornuz, M.; Hisatomi, T.; Solarska, R.; Augustynski, J.; Graetzel, M.; Sivula, K. Highly Efficient Water Splitting by a Dual-Absorber Tandem Cell. Nat. Photonics 2012, 6, 823−827.

5. Youngblood, W. J.; Lee, S. H. A.; Kobayashi, Y.; HernandezPagan, E. A.; Hoertz, P. G.; Moore, T. A.; Moore, A. L.; Gust, D.; Mallouk, T. E. Photoassisted Overall Water Splitting in a Visible LightAbsorbing Dye-Sensitized Photoelectrochemical Cell. J. Am. Chem. Soc. 2009, 131, 926−927.

6. Chung, I.; Lee, B.; He, J.; Chang, R. P. H.; Kanatzidis, M. G. AllSolid-State Dye-Sensitized Solar Cells with High Efficiency. Nature 2012, 485, 486−499.

7. Graetzel, M.; Janssen, R. A. J.; Mitzi, D. B.; Sargent, E. H. Materials Interface Engineering for Solution-Processed Photovoltaics. Nature 2012, 488, 304−312.

8. Yella, A.; Lee, H.-W.; Tsao, H. N.; Yi, C.; Chandiran, A. K.; Nazeeruddin, M. K.; Diau, E. W.-G.; Yeh, C.-Y.; Zakeeruddin, S. M.; Gratzel, M. Porphyrin-Sensitized Solar Cells with Cobalt(II/III)-Based¨Redox Electrolyte Exceed 12% Efficiency. Science 2011, 334, 629−634.

9. Kamat, P. V. Boosting the Efficiency of Quantum Dot Sensitized Solar Cells through Modulation of Interfacial Charge Transfer. Acc. Chem. Res. 2012, 45, 1906−1915.

10. Coakley, K. M.; Liu, Y.; McGehee, M. D.; Frindell, K. L.; Stucky, G. D. Infiltrating Semiconducting Polymers into Self-Assembled Mesoporous Titania Films for Photovoltaic Applications. Adv. Funct. Mater. 2003, 13, 301−306.

11. Qiao, Q.; McLeskey, J. J. T. Water-Soluble Polythiophene/ Nanocrystalline TiO2 Solar Cells. Appl. Phys. Lett. 2005, 86, 153501− 3.

12. Kuo, C. Y.; Tang, W. C.; Gau, C.; Guo, T. F.; Jeng, D. Z. Ordered Bulk Heterojunction Solar Cells with Vertically Aligned TiO2 Nanorods Embedded in a Conjugated Polymer. Appl. Phys. Lett. 2008, 93, 033307−3.

13. Williams, S. S.; Hampton, M. J.; Gowrishankar, V.; Ding, I. K.; Templeton, J. L.; Samulski, E. T.; DeSimone, J. M.; McGehee, M. D. Nanostructured Titania-Polymer Photovoltaic Devices Made Using PFPE-Based Nanomolding Techniques. Chem. Mater. 2008, 20, 5229− 5234.

14. Van Hal, P. A.; Wienk, M. M.; Kroon, J. M.; Verhees, W. J. H.; Slooff, L. H.; Van Gennip, W. J. H.; Jonkheijm, P.; Janssen, R. A. J. Photoinduced Electron Transfer and Photovoltaic Response of a Mdmo-Ppv:TiO2 Bulk-Heterojunction. Adv. Mater. 2003, 15, 118− 121.

15. Chang, C.-H.; Huang, T.-K.; Lin, Y.-T.; Lin, Y.-Y.; Chen, C.-W.; Chu, T.-H.; Su, W.-F. Improved Charge Separation and Transport Efficiency in Poly(3-Hexylthiophene)-TiO2 Nanorod Bulk Heterojunction Solar Cells. J. Mater. Chem. 2008, 18, 2201−2207.

16. Kwong, C. Y.; et al. Poly(3-Hexylthiophene):TiO2 Nanocomposites for Solar Cell Applications. Nanotechnology 2004, 15, 1156−1161.

17. Oosterhout, S. D.; et al. Controlling the Morphology and Efficiency of Hybrid Zno:Polythiophene Solar Cells via Side Chain Functionalization. Adv. Eng. Mater. 2011, 1, 90−96.

18. Oosterhout, S. D.; Wienk, M. M.; van Bavel, S. S.; Thiedmann, R.; Jan Anton Koster, L.; Gilot, J.; Loos, J.; Schmidt, V.; Janssen, R. A. J. The Effect of Three-Dimensional Morphology on the Efficiency of Hybrid Polymer Solar Cells. Nat. Mater. 2009, 8, 818−824.

19. Neyshtadt, S.; Jahnke, J. P.; Messinger, R. J.; Rawal, A.; Segal Peretz, T.; Huppert, D.; Chmelka, B. F.; Frey, G. L. Understanding and Controlling Organic−Inorganic Interfaces in Mesostructured Hybrid Photovoltaic Materials. J. Am. Chem. Soc. 2011, 133, 10119−10133.

20. Boucle, J.; Ackermann, J. Solid-State Dye-Sensitized and Bulk´ Heterojunction Solar Cells Using TiO2 and ZnO Nanostructures: Recent Progress and New Concepts at the Borderline. Polym. Int. 2012, 61, 355−373.

21. Segal-Peretz, T.; Leman, O.; Nardes, A. M.; Frey, G. L. On the Origin of Charge Generation in Hybrid Tiox/Conjugated Polymer Photovoltaic Devices. J. Phys. Chem. C 2011, 116, 2024−2032.

22. Piris, J.; Ferguson, A. J.; Blackburn, J. L.; Norman, A. G.; Rumbles, G.; Selmarten, D. C.; Kopidakis, N. Efficient Photoinduced Charge Injection from Chemical Bath Deposited CdS into Mesoporous TiO2 Probed with Time-Resolved Microwave Conductivity. J. Phys. Chem. C 2008, 112, 7742−7749.

23. Segal-Peretz, T.; Leman, O.; Nardes, A. M.; Frey, G. L. On the Origin of Charge Generation in Hybrid Tiox/Conjugated Polymer Photovoltaic Devices. J. Phys. Chem. C 2011, 116, 2024−2032.

24. Nazeeruddin, M. K.; Humphry-Baker, R.; Liska, P.; Gratzel, M. ¨Investigation of Sensitizer Adsorption and the Influence of Protons on Current and Voltage of a Dye-Sensitized Nanocrystalline TiO2 Solar Cell. J. Phys. Chem. B 2003, 107, 8981−8987.

25. Abrusci, A.; Ding, I. K.; Al-Hashimi, M.; Segal-Peretz, T.; McGehee, M. D.; Heeney, M.; Frey, G. L.; Snaith, H. J. Facile Infiltration of Semiconducting Polymer into Mesoporous Electrodes for Hybrid Solar Cells. Energy Environ. Sci. 2011, 4, 3051−3058.

26. Zhang, W.; Zhu, R.; Ke, L.; Liu, X.; Liu, B.; Ramakrishna, S. Anatase Mesoporous TiO2 Nanofibers with High Surface Area for Solid-State Dye-Sensitized Solar Cells. Small 2010, 6, 2176−2182.

27. Zhang, W.; Zhu, R.; Li, F.; Wang, Q.; Liu, B. High-Performance Solid-State Organic Dye Sensitized Solar Cells with P3HT as Hole Transporter. J. Phys. Chem. C 2011, 115, 7038−7043.

28. Liao, W.-P.; Hsu, S.-C.; Lin, W.-H.; Wu, J.-J. Hierarchical TiO2 Nanostructured Array/P3HT Hybrid Solar Cells with Interfacial Modification. J. Phys. Chem. C 2012, 116, 15938−15945.

29. Lin, Y.-Y.; Chu, T.-H.; Li, S.-S.; Chuang, C.-H.; Chang, C.-H.; Su, W.-F.; Chang, C.-P.; Chu, M.-W.; Chen, C.-W. Interfacial Nanostructuring on the Performance of Polymer/TiO2 Nanorod Bulk Heterojunction Solar Cells. J. Am. Chem. Soc. 2009, 131, 3644− 3649.

30. Mor, G. K.; Kim, S.; Paulose, M.; Varghese, O. K.; Shankar, K.; Basham, J.; Grimes, C. A. Visible to Near-Infrared Light Harvesting in TiO2 Nanotube Array-P3HT Based Heterojunction Solar Cells. Nano Lett. 2009, 9, 4250−4257.

31. Goh, C.; Scully, S. R.; McGehee, M. D. Effects of Molecular Interface Modification in Hybrid Organic-Inorganic Photovoltaic Cells. J. Appl. Phys. 2007, 101, 114503−12.

32. Boucle, J.; Chyla, S.; Shaffer, M. S. P.; Durrant, J. R.; Bradley, D. ́ D. C.; Nelson, J. Hybrid Solar Cells from a Blend of Poly(3- Hexylthiophene) and Ligand-Capped TiO2 Nanorods. Adv. Funct. Mater. 2008, 18, 622−633.

33. Said, A. J.; et al. Hybrid Bulk Heterojunction Solar Cells Based on P3HT and Porphyrin-Modified ZnO Nanorods. J. Phys. Chem. C 2010, 114, 11273−11278.

34. Suresh, P.; Balaraju, P.; Sharma, S. K.; Roy, M. S.; Sharma, G. D. Photovoltaic Devices Based on PPHT:ZnO and Dye-Sensitized PPHT:Zno Thin Films. Sol. Energy Mater. Sol. Cells 2008, 92, 900− 908.

35. Mawyin, J.; et al. Hybrid Heterojunction Nanorods for Nanoscale Controlled Morphology in Bulk Heterojunction Solar Cells. J. Phys. Chem. C 2011, 115, 10881−10888.

36. M. Pagliaro, R. Ciriminna, and G. Palmisano, *Flexible solar cells* (Wiley, Weinheim, 2008) Chapter 4.

37. Kuwabara, T., Kawahara, Y., Yamaguchi, T., & Takahashi, K. (2009). Characterization of inverted-type organic solar cells with a ZnO layer as the electron collection electrode by ac impedance spectroscopy. *ACS applied materials & interfaces*, *1*(10), 2107-2110.

Chapter 6

6 General conclusions

6.1 Summary

Throughout this study, the main aim was to build a specialized model which enables the analysis of carrier behaviors in BHJ to take place. The overall focus was on enhancing the performance of OSCs. Specifically, the research uses the optical measurements of EFISHG which probe carrier behaviors in materials instantly. The main conclusions that can be drawn from this dissertation are as follow.

Chapter 1 includes a good summary on background information regarding OSCs. Besides this, literature reviews and operational mechanisms of OSCs in materials were included ensuring they were based accurate information from the photovoltaic field. Once examining the first chapter of this study, the major intention is understood. When it comes to the structure of OSCs, although massive growth is noticed in power conversion efficiency of photovoltaic cells, a major gap is still present in comprehending some behaviors like carrier injection and transport process. According to, this work aims to solve some of these mysteries.

The second chapter presents the required information regarding the most suitable materials used for processing each layer of the OPV device. In addition, thorough information were provided for experimental deposition techniques, as well as measurement computations. To fully understand and select a systematic measurement technique, this chapter critically evaluates a technique called; electric field induced second-harmonic generation (EFISHG). At last, this chapter benefits from the Maxwell-Wagner model which is associated with physical actions for charge accumulation occurring in the interface.

Chapter 3 explores carrier behaviors in BHJ OSCs using EFISHG measurements. It is concluded that circuit response time between positive and negative voltages is approximately identical. However, for Maxwell–Wagner-type interfacial charging taking place between positive and negative voltages, a notable variation was noted for response time. In particular, this illustrated electrons accumulation (Qs) in the interfacial area between the donor and the acceptor. Consequently, it was found that accumulated electrons in the donor side (PCPDTBT) were lesser than electrons at the acceptor (PC71BM). In return, total efficacy of the bulk heterojunction OSCs was significantly impacted.

The fourth chapter emphasizes on the EFISHG measurement application in order to analyze the impact of adding 3 wt% DIO solvent to PCPDTBT: $PC_{71}BM$ (BHJ). From this chapter, it is agreed on that altering the size of domains vitally enhances BHJ layer performance. To be more precise, BHJ's efficiency has increased by approximately 25%. In fact, by using SHG measurement, managing both electrons transportation and holes at donor and acceptor is possible. Thus, examining the associated electric field is feasible. However, it is necessary to justify laser wavelength. Furthermore, no influence was noticed in the internal electric field when DIO was added. In general, DIO additive is known to decrease all of relaxation time, interface charge and space charge field. Therefore, it is agreed on that optimizing domain size of the interface would affect the reduction of accumulated charge. Overall, the performance of the PCPDTBT: $PC_{71}BM$ based BHJ film was massively improved.

Chapter 5 points out some experimental work where the Z907 was tested with BHJ in solar cells. The measurements were carried out using electric-field-induced optical second harmonic generation (EFISHG) at laser wavelength. To study the influence of nanoparticles on carrier transport in fabricated BHJ solar cells, few prepared nanoparticles were added to Z907 dye. From

EIS investigation, a drop in resistance was clearly observed to be from 5400 to 4300 in the device using the Z907. It is most likely that this fall in resistance has improved photoelectrons which are produced in the BHJ layer. Specifically, they reached the end of the electrode without any loss taking place. Occasionally, the findings from EFISHG measurements of the internal field, which was directed from Au to ITO electrode, have developed majorly. Besides, the internal field has also been improved due to Z907 additive. The enhanced performance of the OSCs when Z907 is used, a greater number of photons were scattered to the substrate in comparison to particle free solar cells. In conclusion, an improvement in carrier behavior in solar cells is perceived. This subsequently results in an enhancement of efficiency of about 45 %.

Eventually, below are several conclusions that are fully delivered from this thesis:

➢ EFISHG methods were utilized in order to investigate BHJ OSCs.

➢ The chosen probed SHG measurement is beneficial in examining both electrons and holes behaviors in BHJ OSCs.

➢ A clear picture for both carrier behaviors and interfacial charging of OSCs were established according to the field of dielectric physics.

➢ DIO alters the morphology of BHJ and causes balanced hole and electron transport in solar cells (efficiency higher by 25%).

➢ Adding metal complexes such as Z-907 contributes to enhance the charge extraction (efficiency higher by 45%).

6.2 Further work

The future work plan is to study the interfacial properties and carrier behavior in OSCs with complicated structure and other optimized treatment. The main content of my proposed research is consisting of part:

Design new experimental methods for direct observing carrier relaxation inside tandem (multijunction) OSCs based on SHG technique. Study the carrier behavior inside tandem OSCs, including current path across the blended film, carrier relaxation and accumulation inside the multijunction layer, trapping mechanism and so on. Investigate the quenching behavior happened on the interface between blended film and metal electrodes by using SHG technique and also study the contribution of blocking layer taking into account of dielectric performance of the organic layer. Study the probable influence of evaporation speed and composition ratio of blended film on the carrier relaxation and transport.

Acknowledgements

List of Publications and conference presentations

Lists of publication.

1. Alrougy, Ibrahim M., Dai Taguchi, and Takaaki Manaka. "Spectroscopic Study of Electric Field Induced Optical Second Harmonic Generation from PCPDTBT and PC 71 BM Thin Films." IEICE Transactions on Electronics 102.2 (2019): 119-124.

2. Alrougy, Ibrahim M., Dai Taguchi, and Takaaki Manaka. " Effect of 1,8-Diiodooctance additive on the charge carriers behavior in the PCPDTBT:PC71BM BHJ films investigated by using electric-field-induced optical second-harmonic generation measurement." Journal of Materials Science: Materials in Electronics 32.3 (2021): 2845-2852.

Conference Papers

1. Alrougy, Ibrahim M., Dai Taguchi, and Takaaki Manaka. " Investigation of PEDOT: PSS Insertion Effect on Carrier Transport in PCPDTBT: PC71BM Bulk Heterojunction Organic Solar Cell by EFISHG." 2018 International Conference on Solid State Devices and Materials (SSDM), 2018.

2. Alrougy, Ibrahim M., Dai Taguchi, and Takaaki Manaka. " Investigation on Carrier Transport in PCPDTBT: PC71BM Bulk Heterojunction Organic Solar Cell by EFISHG." 10th Multidisciplinary International Student Workshop (MISW), 2018.

3. Alrougy, Ibrahim M., Dai Taguchi, and Takaaki Manaka. " Spectroscopic study of electric field induced optical second harmonic generation from PCPDTBT and PC71BM thin films. " 10th International Symposium on Organic Molecular Electronics (ISOME), 2018.

4. Alrougy, Ibrahim M., Dai Taguchi, and Takaaki Manaka. "Investigation of 1, 8-Diiodooctane (DIO) Additive Effect on Carrier Transport in Bulk Heterojunction Organic Solar Cell by EFISHG." 2019 Compound Semiconductor Week (CSW). IEEE, 2019.